Spring 2024

Maneuverability of Cuttlefish and Squid: An Integrated Kinematic and Hydrodynamic Analysis

Alissa Marie Ganley
Old Dominion University, alissaganley@yahoo.com

MANEUVERABILITY OF CUTTLEFISH AND SQUID:

AN INTEGRATED KINEMATIC AND HYDRODYNAMIC ANALYSIS

by

Alissa Marie Ganley
B.S. March 2016, University of California, Santa Cruz

A Dissertation Submitted to the Faculty of
Old Dominion University in Partial Fulfilment of the
Requirements for the Degree of

DOCTOR OF PHILOSOPHY

ECOLOGICAL SCIENCES

OLD DOMINION UNIVERSITY
May 2024

Approved by:

Ian K. Bartol (Director)

Daniel J. Barshis (Member)

Michael Vecchione (Member)

John P. Whiteman (Member)

Paul S. Krueger (Member)

ABSTRACT

MANEUVERABILITY OF CUTTLEFISH AND SQUID:
AN INTEGRATED KINEMATIC AND HYDRODYNAMIC ANALYSIS

Alissa Marie Ganley
Old Dominion University, 2024
Director: Dr. Ian K. Bartol

Turning is important for life underwater, playing roles in predator avoidance, prey capture, locomotion, and communication. While turning abilities have been explored in many taxa, little is known about maneuverability of cephalopods, such as cuttlefishes and squids. The objectives of this dissertation include: (1) quantifying the turning abilities of cuttlefish hatchlings and determining whether there are species-specific differences; (2) examining the turning capabilities of adult cuttlefishes, with the goal of comparing adult performance with that of conspecific hatchlings; and (3) quantifying how adult neritic squids perform turns to provide a broader context of maneuvering strategies in cephalopods. To investigate turning, swimming behaviors of hatchling/adult cuttlefishes (*Sepia officinalis* and *Sepia bandensis*) and adult squids (*Doryteuthis pealeii* and *Illex illecebrosus*) were recorded using high-speed videography, and kinematic parameters were analyzed. For cuttlefish studies, particle image velocimetry (hatchlings) and defocusing digital particle tracking velocimetry (adults) data were also collected along with video. Hatchling *S. officinalis* turned faster than hatchling *S. bandensis*, but both species completed equally tight turns. Orientation (arms-first or tail-first) did not have a significant effect on turning performance. Cuttlefish hatchlings consistently used multiple short jets for controlled turning, with *jet mode I* (isolated vortex rings) being 3-4 times more common than *jet mode II* (elongated jets with leading rings). Adult *Sepia bandensis* turned tightly but

relatively slowly, relying primarily on short vortex ring jets, and adults outperformed conspecific hatchlings in angular velocity and turning radii. As with hatchlings, orientation did not have a significant effect on kinematic or hydrodynamic properties in adult cuttlefishes, and most turns were performed arms-first. Squid *Illex illecebrosus* completed faster but broader turns than *D. pealeii*. Both species were able to complete tighter turns when oriented arms-first versus tail-first, and *I. illecebrosus* curled its arms more in the arms-first mode, which likely increased angular velocity through a reduction in moment of inertia. The neritic squids considered here exhibited similar overall turning performance to cuttlefishes, although cuttlefishes relied on shorter jets and demonstrated no orientation differences. This study advances our understanding of turning capabilities of cuttlefishes throughout ontogeny and broadens our understanding of turning performance of squids.

This thesis is dedicated to myself, not because I did this alone, but because it is important to recognize one's own achievements and celebrate them.

"Either write things worth reading or do things worth the writing" -Benjamin Franklin.

I have done both.

ACKNOWLEDGEMENTS

I am lucky to have so many people to thank for their love and support:

First, to my advisor: Dr. Ian Bartol, for the incredible amount of support I received. For being an exemplary teacher and mentor and treating me like family. Graduate school is challenging, and I am forever grateful to have had a wonderful professor to look up to. I cannot thank you enough.

To my family. First my parents: June and Michael, without whom I would never have been in a position to succeed. You both taught me perseverance, advocacy, tenacity, drive, and strength of mind. I am here because of your hard work and support. I am proud to be your daughter. And to my sister, Katie: for being the best cuddler around, bar none. Your giggles light up my life.

To the friends I made during my time here: Mollie, Cate, Christina, Zack, Davis, James, Abbey, Fred, Kody, Mel, and Amanda: you kept me sane and cheered me on when I was down. Each of you has been instrumental in my success and made my time here some of the best in my life.

To the friends who remained from before: Erin, Parker, Jules, and Darius. I am so lucky to continue to have you in my life. Your guidance, support, and comfort mean the world to me. I am so excited for the next chapter in our lives.

Finally, to my partner, Josh, who came into my life relatively recently, and yet has been one of my biggest cheerleaders. Thank you for taking a chance on me. I love you.

"Love all, trust a few, do wrong to none"

-William Shakespeare; All's Well That Ends Well

NOMENCLATURE

A	angular impulse of jet, Kg m^3 s^{-1}
A_{fin}	maximum range of amplitude of fin beats standardized by animal length (No Units)
COR	center of rotation (No Units)
D_ω	diameter of the jet based on vorticity, cm
F	formation number (No Units)
F_{ave}	average frequency of fin beats between both fins, Hz
F_{in}	frequency of fin beats for inside fin, Hz
F_{mantle}	frequency of mantle contractions, Hz
F_{out}	frequency of fin beats for outside fin, Hz
I	impulse of jet, m^4 s^{-1}
L_ω	length of jet based on vorticity, cm
L_ω/D_ω	length to diameter ratio of a jet (No Units)
ML	mantle length, cm
Re	Reynolds number of squid based on L (No Units)
R_{mean}	average radius of turn, cm
R_{min}	minimum radius achieved during turn, cm
$(R/L)_{mean}$	average length-specific turning radius of a turn (No Units)
$(R/L)_{min}$	minimum length-specific turning radius of a turn (No Units)
L	total length of animal, cm
U_{jave}	average jet velocity, cm s^{-1}
U_{jmax}	maximum jet velocity, cm s^{-1}

θ_{arms}	degree of arm curling, deg
θ_{total}	total angular displacement of the turn, deg
ρ	density of water, kg m^{-3}
ω_{ave}	average angular velocity, deg s^{-1}
ω_{max}	maximum angular velocity achieved during turn, deg s^{-1}

TABLE OF CONTENTS

Page

LIST OF TABLES

LIST OF FIGURES

CHAPTER 1

INTRODUCTION

1.1 TURNING AND JET PROPULSION

Turning is fundamental for navigating complex underwater habitats, hunting, predator avoidance, and communication (Bartol et al., 2022; Hanlon and Messenger, 1996; Hanlon et al., 2018). Many researchers have studied turning behaviors in fishes (Domenici, 2001; Domenici and Blake, 1997; Walker, 2000; Webb and Fairchild, 2001), marine mammals (Blanchet et al., 2016; Fish, 1993; Fish, 1996; Fish, 1998; Fish and Hui, 1991; Fish and Rohr, 1999; Fish et al., 1988; Fish et al., 2008), elasmobranchs (Fish et al., 2018; Lowe, 1996; Parson et al., 2011; Porter et al., 2011), and various other taxa (Fish and Nicastro, 2003; Gatto and Reina, 2020; Jones and Trueman, 1970; Mayerl et al., 2019; Rivera et al., 2006; Stevens et al., 2018). Swimmers that employ jet propulsion, such as jellyfishes, siphonophores, and squids, have also been studied, further expanding our understanding of turning diversity within the aquatic realm (Bartol et al., 2002; Colin et al., 2020; Gemmell et al., 2015; Gemmell et al., 2019).

Many of the turning studies above have demonstrated that an increase in body flexibility contributes to greater turning capacity for most animals, although some rigid-bodied animals can also achieve high turning performance under certain conditions (Fish, 1999; Fish and Nicastro, 2003; Rivera et al., 2006, Walker, 2000). Two important concepts associated with evaluating turning performance are maneuverability and agility. Maneuverability is the ability of an animal to turn in a small area, and agility is the speed of the turning behavior (Bartol et al., 2016; Norberg and Rayner, 1987; Walker, 2000; Webb, 1994). Maneuverability is often reported in terms of length-specific turning radius (*R/L*), where *R* is the radius of curvature of the center of rotation (*COR*; point in the domain of the animal that moves the least during the turn) through

the turning path and L is the length of the animal. The dimensionless R/L metric allows for comparisons of turn tightness across taxa and ontogenetic stage. Agility is measured in terms of angular velocity (ω), which is defined by the rate at which the angle of the animal (measured in the plane of the turn) changes during a turn.

For animals that rely on jet propulsion, the physics associated with the jet is important and may be useful for identifying organizing principles for turning performance. Two important components of pulsed jetting are: (1) impulse per pulse supplied by the jet momentum flux ($\mathbf{I_u}$) - and (2) impulse per pulse supplied by the nozzle exit over-pressure ($\mathbf{I_p}$), i.e., the transient increase in pressure behind the animal as the jet is initiated. They relate to time averaged thrust ($\mathbf{F_t}$) as follows (Krueger and Gharib, 2003):

$$(1)\ F_t = \frac{I_u + I_p}{t}$$

where t is the period between successive jets. The $\mathbf{I_p}$ component adds as much as 42% to overall impulse relative to a steady, non-pulsatile jet (Krueger, 2001; Krueger and Gharib, 2003), yet is often ignored in many of the biological jet flow models, which assume steady flow (e.g., Daniel 1983). Given the importance of pulsed jetting in squids and cuttlefishes, thrust augmentation through $\mathbf{I_p}$ likely plays an important role during turning maneuvers.

To fully realize the benefits of $\mathbf{I_p}$, the concept of formation number (F) is important. Formation number represents the physical limit of a pulsed vortex ring. In mechanical studies of pulsatile jets, the formation number occurs when the ratio between the length of the stroke of the pulse generator and its diameter approach 4 (Gharib et al., 1998). When jets are produced near F, fluid rolls up into a well-developed vortex ring that provides optimal per-pulse-averaged thrust, given $\mathbf{I_p}$ is maximized (Gharib et al., 1998; Krueger and Gharib, 2003). When L/D exceeds F, the vortex ring stops entraining circulation, impulse, and energy, separates from the jet, and extra

fluid creates a tail behind the vortex ring. While the leading-edge vortex ring in these longer jets still provides the $\mathbf{I_p}$ augmentation benefit, the trailing jet does not, producing only $\mathbf{I_u}$. Through manipulation of the jet aperture, some jet-propelled animals can produce F as high as 8-11 (Bartol et al., 2009a; Dabiri et al., 2007), suggesting that some jetters may produce jets of higher pulse-averaged thrust than those produced in mechanical studies. Indeed, Bartol et al. (2009b, 2016) has shown that isolated vortex rings with L_ω/D_ω <3 (a proxy for pulse generator characteristics in Gharib et al., 1998 defined by length of vorticity extent to diameter of vortex cores) have higher propulsive efficiency than longer jets with L_ω/D_ω >3. While a number of jet patterns involving interconnected vortex rings, long jets with ring elements, and turbulent jets have been observed during rectilinear swimming (Bartol et al., 2016; Bartol et al., 2019), two modes are especially prominent: *jet mode I*, where ejected fluid rolls up into an isolated vortex ring and *jet mode II*, where a leading vortex ring together with a trailing jet are produced (Bartol et al., 2008, 2009b, 2016). The transition between these modes occurs at L_ω/D_ω ~3-4 for most animals measured. Considering squids employ both jet modes, there appears to be a tradeoff during rectilinear swimming between *jet mode I*, which maximizes propulsive efficiency, and *jet mode II*, which produces greater overall force (Bartol et al. 2008, 2009b, 2016, 2019). However, it is unclear at this stage, whether F and L_ω/D_ω are important parameters for categorization of turns or whether vortex-wake patterns deviate from those observed during steady swimming.

1.2 CEPHALOPODS ARE UNIQUE

Cephalopods are an abundant, ecologically important, understudied class of marine organisms that maneuver using a unique combination of pulsed jetting and finning movements. Comprised of greater than 800 species (Sanchez et al., 2018), cephalopods exhibit a wide

diversity of turning behaviors, ranging from rapid turns during escape responses to controlled precise maneuvers when navigating complex habitats. Many cephalopods can hover, change direction rapidly, ascend and descend vertically, and swim forward and backward (Bartol et al., 2001a; Hanlon et al., 1983; Vecchione and Roper, 1991). Cephalopods are both predator and prey, thereby executing turns for both prey capture and predator avoidance, both of which are integral for survival. All cephalopods use jet propulsion at some level to move through the water, with many cephalopods, such as squids and cuttlefishes, augmenting the jet with complex motions of their fins (Anderson and DeMont, 2005; Bartol et al., 2001a; Bartol et al., 2009a; Bartol et al., 2016; Bartol et al., 2019; Hoar et al., 1994; Jastrebsky et al., 2016).

Squids exhibit greater morphological diversity than cuttlefishes. Squids have fins that span 10-90% of their mantle length, with fin shape and locomotive contributions varying widely (Hanlon et al., 2018; Hoar et al., 1994; O'Dor, 2013; Sfakiotakis et al., 1999). Conversely, cuttlefishes primarily have skirt-like fins that surround the entirety of their mantle, and the shape of the fins are less variable. Using a combination of pulsed jetting and fin movements, some squids and cuttlefishes show exceptional maneuvering abilities with turning rates that exceed 700 deg s^{-1} and turning radii that are among the lowest recorded for any aquatic taxa (Bartol et al., 2022; Bartol et al., 2023; Jastrebsky et al., 2016). Moreover, squids and cuttlefishes do not fall neatly into current body categories considered in turning studies, i.e., rigid versus flexible, but rather represent a hybrid group with prominent flexible (e.g., arms, fins) and rigid/stiff (e.g., cuttlebone or chitinous pen) features.

From an ecological perspective, squids and cuttlefishes have different lifestyles. Squids are ecologically more diverse, living in shallow in-shore waters, travelling vast distances in the open ocean as pelagic dwellers, and residing in the dim, cold waters of the deep ocean.

Conversely, cuttlefishes are generally shallow-water reef animals that are more tied to the benthos, having to maneuver the complex structure of the reef (Hanlon and Messenger, 1996; Nesis, 1987). Cuttlefishes are neutrally buoyant, and squids are often negatively buoyant, though deep-water squids can also be neutrally buoyant (Bartol et al., 2001a; Denton and Gilpin-Brown, 1961a; O'Dor and Webber, 1991). Squids and cuttlefishes both exhibit a unique dual-mode (jet and fins) form of propulsion, but cuttlefishes generally have more fin muscle mass and devote more oxygen use to their fins, relying more heavily on fin propulsion than jet propulsion (O'Dor and Webber, 1991). Indeed, shallow water and pelagic squids devote ~35-40% of their body to mantle volume, while cuttlefishes allocate only 25% (O'Dor and Webber, 1991). In contrast to shallow-water and pelagic squids, many deep-sea squids (e.g., Mastigoteuthidae and Magnapinnidae) appear to rely almost exclusively on their fins for swimming (Hanlon et al., 2018).

Propulsion in squids and cuttlefishes is driven by muscular hydrostatic systems with tightly packed 3D arrays of obliquely striated muscle oriented in mutually perpendicular directions that create force and support for movement (Kier, 1989). The fins of both squids and cuttlefishes act hydrostatically by serially shortening or lengthening sets of muscles to perform complex movements. Squids and cuttlefishes have three main sets of muscles in their fins: (1) the dorsoventral muscles that connect the bottom and top of the fins to a median fascia, (2) longitudinal muscles that run parallel to the body and perpendicular to the dorsoventral muscles in bundles, and (3) the transverse muscles that run from the body out to the far edge of the fins perpendicular to the longitudinal bundles (Johnsen and Kier, 1993; Kier, 1989; Kier and Thompson, 2003). These three muscle groups together can produce the undulatory and flapping motions that generate forces and torques necessary for turning. Similarly, the mantle and the

funnel of squids and cuttlefishes act hydrostatically to produce strong jets. Two main sets of muscles control the movement of the mantle muscles: the circular and radial muscles. Circular muscles run in bundles circumferentially around the squids, while radial muscles connect the inner and outer walls of the mantle. The mantle of the squids and cuttlefishes cannot be shortened or lengthened due to the cartilaginous pen and cuttlebone respectively, so contraction of the circular muscles decreases the diameter of the mantle and forcefully expels water out of the funnel, as well as thickens the walls of the mantle. The radial muscles then contract to thin the mantle walls, thereby increasing the mantle volume for the refilling phase. Mantle expansion and refilling is also aided by elastic recoil of connective tissue in the mantle (Kier and Thompson, 2003; Shadwick, 1994). Within the funnel, circular muscles contract to decrease the aperture, while longitudinal muscles control length changes and the degree of bending. To re-expand the funnel following closure, radial muscles contract, thinning the funnel wall. These radial muscles are also important in preventing kinking during funnel bending (Kier and Thompson, 2003). The ability to control aperture diameter dynamically and to bend the funnel within a hemisphere below the body allow squids and cuttlefishes to regulate jet flow and swimming orientation. While squids and cuttlefishes are unique in their dual-mode propulsive system and muscular hydrostatic architecture, surprisingly little is known about their turning performance.

1.3 ONTOGENETIC CONSIDERATIONS

As swimmers develop, they experience different flow regimes and undergo vast morphological changes. Thus, understanding how turning capabilities change with ontogeny is critical for a comprehensive understanding of maneuverability. How an animal swims and

maneuvers in its environment is related to the Reynolds number (*Re*), the ratio of inertial forces to viscous forces, which is defined as follows:

$$(2)\ Re = \frac{\rho l v}{\mu}$$

where ρ is the density of the fluid, l is a body length term, v is the velocity of the flow, and μ is the dynamic viscosity of the water. The *Re* regime impacts how flow energy dissipates, the efficacy of propulsors, sinking rate, and the ability to glide. Animals must adapt to the physical constraints of the *Re* environment. At high *Re* ($>10^3$), inertial forces dominate and streamlined bodies help facilitate reduction of pressure drag forces while swimming. Oscillatory patterns of movement, including lift-based fin, flipper, and fluke propulsion work well, and most high-speed adult swimmers locomote within this range. At low *Re* (<1), viscosity dominates, and streamlined bodies are less advantageous since pressure drag resulting from flow separation is minimal relative to skin friction drag. Many animals minimize their surface area to reduce skin friction drag at low *Re*, leading to spherical or cylindrical body shapes. Additionally, oscillatory flow does not work well at low *Re* due to the reversibility of flow. Rather, animals in these ranges rely on drag-based rowing and asymmetric propulsion, including metachronal patterns of cilia beating, corkscrew-type movement of flagella, and jetting with check valves to prevent reversal of flow during refilling (Colin et al., 2020; Gemmell et al., 2019; Kiorboe et al., 2014; Vogel, 2013). In the intermediate *Re* range (*Re*= 10^0-10^3), both inertial and viscous forces play prominent roles (Bartol et al., 2009b; Daniel et al., 1992; McHenry and Jed, 2003). Within this range, drag-based propulsion appears to be the most dominant form of propulsion with lift-based circulatory propulsion being less common. However, little is known overall about animal movement within the intermediate flow regime.

All cephalopods undergo a drastic change in morphology and size during their lifetime, with locomotion occurring over a wide range of *Re*. Most cephalopods hatch out at about 1-5% of their adult body length (Boletzky, 1987; Domingues et al., 2001; Goff and Daguzan, 1991). Hatchling cuttlefishes usually experience Reynolds numbers of around 100-1300, and throughout their lifetime, they can experience a 10,000-fold increase in *Re* (adult *Re* ~10^5; see Chapter 2). Squids experience a similar range from *Re* ~25-100 in early development to *Re* of 10^3-10^6 as adults (Bartol et al., 2008; Bartol et al., 2009b). Both size and body morphology are important for movement across *Re* regimes, especially when turning. Body width to length ratios, propulsor location, and body rigidity are all significant factors for maneuverability (Bartol et al., 2002; Colin et al., 2020; Gemmell et al., 2015; Gemmell et al., 2019; Parson et al., 2011; Rivera et al., 2006; Stevens et al., 2018; Walker, 2000). Hatchling cuttlefishes have a larger body width to length ratio than squid paralarvae, as well as greater body rigidity due to the early development of the cuttlebone (Bettencourt and Guerra, 2001; Denton and Gilpin-Brown, 1961a). Furthermore, paralarval squids have a larger funnel relative to their mantle length than adult squids (Thompson and Kier, 2001). How these differences in morphology affect cephalopod turning capabilities over a broad range of *Re* are not known.

While funnel location is similar in both squids and cuttlefishes, fin morphology at the different life stages is quite different. Similar to adult cuttlefishes, hatchlings have a skirt-like fin that partially surrounds the mantle of the cuttlefishes, whereas squid paralarvae have more underdeveloped fins that are restricted to the posterior tip of their mantle. It is thought that the fins of paralarvae play a limited role in propulsion relative to the jet in shallow water squids (Bartol et al., 2008; Bartol et al., 2009b). Thus, it is reasonable to assume that the fins also play a

reduced role (relative to the jet) for turning in paralarvae. This may not be the case in hatchling cuttlefishes, however, given the larger morphology of the fins.

At low *Re*, wake patterns around swimmers differ in some notable ways. In zebrafish, larvae produce flows with wider vorticity cores with lower vorticity magnitude than those observed at later ontogenetic stages (Müller et al. 2000). This is due to greater relative viscosity at these low to intermediate *Re*, where viscous interactions lead to a thick boundary layer and a large drag wake (Müller et al. 2008). Despite these vortex differences, the overall qualitative wake patterns of both adult and larval zebrafish are similar when turning, with both adults and larvae producing pairs of vortex rings in the horizontal plane of the wake (Müller et al. 2008).

Jet-propelled swimmers are similarly impacted by high viscous forces in low *Re* regimes. Small hydromedusae, *Sarsia tubulosa*, produce elongated, less-defined vortex rings at $Re < 30$, whereas they produce distinct vortex rings with no discernible tail at $Re \sim 30\text{-}100$. At $Re > 100$ *S. tubulosa* generate distinct rings with tails and produce higher impulse and kinetic energy with increased bell diameter (Katija et al. 2015). Paralarval squid *Doryteuthis pealeii* ($Re \sim 5\text{-}90$) show a similar range of vortex patterns, from spherical vortex rings to elongated vortex rings with a tail but no discernible pinch-off from the leading ring (Bartol 2009a). Paralarvae also increase their speed during vertical station holding by producing longer rather than quicker jets. Bartol et al. (2009a) hypothesize that refill requirements may limit contraction frequencies, requiring them to employ longer jets to increase their speed during station holding. Interestingly, paralarvae were found to have relatively higher propulsive efficiency during the jet ejection phase than adult squids (Bartol et al. 2008). The high contraction phase efficiency at the paralarval stage was thought to be due to a combination of factors, including jets being more directly aligned with the direction of motion than in juvenile and adult squids (Bartol et al 2001, Anderson and

Grosenbaugh 2005, Bartol et al. 2009b); low slip values, which are a product of larger relative funnel apertures in paralarvae relative to adults (Packard 1969; Thompson and Kier 2001; Bartol et al. 2009b); and ejection of proportionally larger volumes of water in paralarvae, which have relatively larger mantle volumes than adults (Gilly et al. 1991; Preuss et al. 1997; Thompson and Kier 2001). Despite vast *Re* changes with development and the importance of turning for ecological success, nothing is currently known about turning performance across ontogeny for either cuttlefishes or squids.

1.4 STUDY OBJECTIVES

For this dissertation, several important knowledge gaps in the understanding of cephalopod turning performance were assessed. Chapters 2 and 3 focus on turning capabilities of cuttlefishes throughout ontogeny, from hatchlings (Chapter 2) to adults (Chapter 3), whereas Chapter 4 focuses on understanding turning performance in several squid species for which little is known. Three driving questions were posed that align with the chapters: (1) what are the turning capabilities of hatchling cuttlefishes, and are there species-specific differences in turning performance during early ontogeny (Chapter 2); (2) how do adult cuttlefishes perform turns and how does adult performance compare with that of conspecific hatchlings (Chapter 3); and (3) how effective are adult neritic squids at turning (Chapter 4)? To address the first of these questions, digital particle image velocity (DPIV) and high-speed videography were used to record routine turns in two species of hatchling cuttlefish, *Sepia bandensis* and *Sepia officinalis*. This integrated approach is useful in linking kinematic body movements with resulting wake flows. For the second question, Defocusing Digital Particle Tracking Velocimetry (DDPTV) together with high-speed videography were used to study turning in adult cuttlefish *Sepia*

bandensis. An integrated kinematic/hydrodynamic approach was used here as well, with the notable difference being volumetric (3D) flows were considered, which was not possible with the small fields of view used in the hatchling studies. For the final question, turns of two species of neritic squids, *Doryteuthis pealeii* and *Illex illecebrosus,* were recorded, and kinematic analyses were used to assess turning agility and maneuverability. Collectively, these chapters represent the most comprehensive study of turning in cuttlefishes throughout ontogeny and the only turning data of two ecologically and commercially important squids (*D. pealeii* and *I. illecebrosus*).

CHAPTER 2

BABY'S FIRST JETS:

A KINEMATIC AND HYDRODYNAMIC ANALYSIS OF TURNING IN CUTTLEFISH HATCHLINGS

2.1 BACKGROUND

A growing body of literature reports on turning in aquatic animals because turning is essential for hunting prey, avoiding predators, and interacting with conspecifics (Bartol et al., 2022; Bartol et al., 2023; Costello et al., 2015; Costello et al., 2021; Dabiri et al., 2020; Danos and Lauder, 2007; Fish and Holzman, 2019; Fish and Nicastro, 2003; Fish et al., 2003; Jastrebsky et al., 2016; Jastrebsky et al., 2017; Maresh et al., 2004; Parson et al., 2011; Porter et al., 2011; Rivera et al., 2006; Thandiackal and Lauder, 2020). However, little is known about turning at early life stages, where animals may face unique challenges, including movement in intermediate Reynolds number (*Re*) regimes, increased predation risk, muscular system constraints, and neural control limitations (Bartol et al., 2008; Bartol et al., 2009a; Boyle, 1996; Martínez and Moltschaniwskyj, 1999; Preuss et al., 1997; Robin et al., 2014; Thompson and Kier, 2001; Thompson and Kier, 2006; York et al., 2016; York et al., 2020). How young swimmers adjust to these challenges and develop turning strategies is central to their survival.

Research on zebrafish, *Danio rerio*, has provided valuable insights into turning capabilities across different life stages. Both larval and juvenile stages of *D. rerio* use two turning patterns, routine and escape turns, each with distinct kinematic signatures and neural control mechanisms (Budick and O'Malley, 2000). While both stages use similar turning modes, turning performance differs across ontogeny, with angular displacement and angular velocity decreasing throughout larval and early juvenile stages. Following the transition to the adult stage,

when the fins are fully developed, these turning capabilities improve (Danos and Lauder, 2007). Important flow control/hydrodynamic differences throughout ontogeny have relevance for turning performance. Control surfaces play a large role in turning, with the caudal fin being integral for turns in larval stages and other fins being more important in juvenile and adult stages (Danos and Lauder, 2007). In juvenile zebrafish, tail movements produce vortex rings with thicker boundary layers that dissipate more rapidly relative to adults, suggesting that viscous forces act strongly at intermediate *Re* (Müller et al., 2000; Müller et al., 2008). These vortex rings have wide cores with lower circulation relative to adult flows (Müller et al., 2000). Wide cores and low circulation result in slower jets, and presumably slower turns (Gharib et al., 1998; Nitsche, 2006; Wu et al., 2007).

Animals that use jet propulsion to swim and turn experience unique locomotive challenges throughout their lifetime. A common feature of jet propulsion is vortex ring formation, where the ejected flow forms a torus, or donut, of spinning water. Katija et al. (2015) found that the medusa, *Sarsia tubulosa*, exhibits different patterns of vortex ring formation according to *Re*. At lower intermediate *Re* (10-30), these jellies produce elongated vortex ring structures and more classical elliptical vortex rings, while at higher intermediate *Re* (30-100), jet pulses exhibit a longer jet structure consisting of vortex rings with a trailing jet component. This transition to longer jets increases the swimming speed of medusa, but results in lower propulsive efficiency with increased bell diameter and *Re* (Katija et al., 2015). This strategy is also seen in brief squid, *Lolliguncula brevis*, where shorter vortex ring jets predominate at early ontogenetic stages and longer jets become more common at later life stages (Bartol et al., 2008, 2009a, 2009b).

In cephalopods, jet pulse patterns that produce isolated vortex rings, as is often the case in early life stages, are referred to as *jet mode I*; jet behaviors that result in a leading vortex ring structure with a trailing jet flow component are known as *jet mode II* (Bartol et al., 2008; Bartol et al., 2009a; Bartol et al., 2009b). In squids, *jet mode I* is associated with greater propulsive efficiency, while *jet mode II* results in greater thrust and lift production (Bartol et al., 2008; Bartol et al., 2009a; Bartol et al., 2009b; Bartol et al., 2016; Bartol et al., 2022; Bartol et al., 2023; Stewart et al., 2010; York et al., 2020). Gladman and Askew (2023) found that hatchlings almost exclusively use *jet mode I* jets during rectilinear escape jetting, but Bartol et al. (2009b) found that paralarvae were more variable. These jet modes have relevance for not only straight swimming, but turning as well, as shorter jets offer more control and facilitate tighter turns, while longer jets power faster turns (Bartol et al., 2022; Bartol et al., 2023). For unsteady behaviors like turning, interconnected vortex flow jet structures beyond the two primary modes are also common (Bartol et al., 2023), suggesting that a diversity of jet flows are employed to achieve turns in some cephalopods.

In addition to the production of different flow modes, the jet can be directed in any angle below the animal via a flexible funnel (Bartol et al., 2001; Thompson and Kier, 2001; Thompson et al., 2010), which facilitates turning. Using a vectored pulsed jet, adult squids and cuttlefishes can swim in the arms-first (forward) or tail-first (backward) orientation, ascend vertically, and complete maneuvers that involve banking, rapid rotations, lateral movements, and trajectory reversals (Bartol et al., 2016; Bartol et al., 2019; Bartol et al., 2022; Bartol et al., 2023; Chapter 4). Like adults, young squids and cuttlefishes can rotate their funnels to direct jet flow and perform a variety of turning maneuvers, including arms-first/tail-first swimming, circular in-plane movements, spiral motions, and zig-zag jetting (York and Bartol, 2016).

To augment jet flows, many cephalopods employ fin movements to swim and turn. In squid *Doryteuthis opalescens* paralarvae, there is a distinct shift at around 6 mm mantle length (~35 days of age) where swimming performance and behavior change dramatically due to fin development, resulting in more directed swimming and schooling behavior (Vidal et al., 2018). Similar transitions are likely in other species of squids and cuttlefishes. Irrespective of when the transition occurs ontogenetically, fin development is probably important for turning during early ontogeny given that fins improve stability, provide thrust to augment the jet, and act as control surfaces in adult squids and likely cuttlefishes (Bartol et al., 2019; Bartol et al., 2023; Stewart et al., 2010).

Although squids and cuttlefishes share many behavioral, morphological, and locomotive characteristics, there are key differences in the taxa. Cuttlefishes generally live in complex reef systems and are “lie and wait” predators, whereas most squids reside in less structured habitats and are more active swimmers (Hanlon et al., 2018). Cuttlefishes have a more benthic lifestyle, and presumably produce lower jet flows than squids. Unlike most squids that are negatively buoyant, cuttlefishes are neutrally buoyant, which is achieved using a rigid, gas-filled, internal cuttlebone (Denton and Gilpin-Brown, 1961b; Walker, 2000). Because of their neutral buoyancy, the jet and fins are not needed to maintain vertical position, allowing for a greater percentage of propulsor-generated force/torque to be applied to swimming and turning than is possible in negatively buoyant squids, which need to direct flows downward for depth maintenance (Denton and Gilpin-Brown, 1961b; Hanlon and Messenger, 1996; Hanlon et al., 2018; O’Dor, 1988). In addition, the fin shapes of cuttlefishes are generally similar, with thin skirt-like fins that extend along the entirety of the mantle, whereas squids have a wide range of fin shapes (Hoar et al., 1994). Longer fins, like those in cuttlefishes, tend to have complex movements, including both

oscillations and multi-wave undulations (Hoar et al., 1994; Hanlon and Messenger, 1996; Hanlon et al., 2018). Lastly, while squids and cuttlefishes both emerge from eggs, hatching size is quite different, with most squids hatching out at ~0.5-1 mm mantle length, and cuttlefish hatching out at ~5-15 mm in mantle length with more developed fins than paralarvae (Hanlon and Messenger, 1996; Hanlon et al., 2018; Villanueva et al., 2016).

Currently, little is known quantitatively about turning in most cuttlefishes, especially during early ontogeny. Adult dwarf cuttlefish *Sepia bandensis* exhibit the lowest length-specific turning radii (high maneuverability) of any aquatic taxa measured to date but only achieve moderate angular velocities (intermediate agility; Jastrebsky et al., 2016). This tradeoff between maneuverability and agility is observed in many nektonic taxa (Fish, 1999; Fish et al., 2003; Parson et al., 2011; Rivera et al., 2006; Thandiackal and Lauder, 2020). Cuttlefishes may prioritize turning tightly because they often reside in complex structures, often with limited turning space, and rely heavily on crypsis and slow movements to blend into environments for predator avoidance rather than escape jetting (Bloor et al., 2013; Josef et al., 2015; Langridge, 2009; O'Brien et al., 2017). No studies focusing on turning behaviors of cuttlefishes during early ontogeny have been performed to date.

For this study three hypotheses related to the turning abilities of two species of cuttlefishes, *Sepia officinalis* and *Sepia bandensis,* during early ontogeny (1-30 days) were examined. (1) *Sepia officinalis* hatchlings will have higher angular velocities (agility) than *Sepia bandensis*, but larger length-specific turning radii, and turning performance will not be affected by orientation. This prediction was based on *S. officinalis* having a more active adult lifestyle than *S. bandensis*, where fast turns are important for prey capture and predator avoidance. The tradeoff for fast turns is larger turning radii, thus *S. officinalis* was expected to turn more broadly

than *S. bandensis*. Given that cuttlefishes live in complex habitats where swimming forward and backward are advantageous, equal proficiency at turning arms-first and tail-first was expected. (2) Both jet modes (*I* and *II*) will occur in turning hatchlings, but *jet mode 1* will be most prominent. Although *jet mode II* is rare in squid paralarvae, this mode should be more prevalent in this study because cuttlefish hatchlings are larger than squid paralarvae (higher *Re*) and this study considered a broader range of movements than station holding, which was the primary behavior studied in Bartol et al. (2009a). Like *D. pealeii* paralarvae, however, short jet pulses (*jet mode I*) were expected to be the preferred wake pattern, as short vortex ring flows provide more directed control during turning than longer jets. (3) Lastly, hatchling cuttlefishes will have greater angular velocities and larger length-specific turning radii than adults. This prediction was based on smaller animals having lower moments of inertia and less hydrodynamic resistance than larger animals, which should promote faster turns, but less developed control surfaces and musculature, which should contribute to broader turning.

2.2 METHODS

2.2.1 Study species

Two species of hatchling cuttlefish, *Sepia bandensis* Adam, 1939 (L = 0.92 ± 0.013 cm, n=30) and *Sepia officinalis* Linnaeus, 1758 (L = 0.96 ± 0.012 cm, n=49), ranging in age from 1-30 days, were used in this study. There was no significant difference in total length between these species (t-test, t_{135}=1.783, p=0.077). Eggs were purchased from the Marine Biological Laboratory in Woods Hole, Massachusetts and Consistent Sea in Gardena, California. Eggs were kept in floating 5-gallon buckets with mesh-lined holes to facilitate water flow. The rim of each bucket was suspended at the water surface with polypropylene foam, and the buckets were

housed in a 450-gallon seawater tank equipped with mechanical and biological filtration, aeration, and temperature control. The tank water was maintained at 35 ppt and 25.5-26.5°C. Once hatched, cuttlefishes were fed live or frozen mysids (*Mysidopsis* spp.) by hand. Separate mesh lined buckets were used to hold larger older hatchlings to reduce incidence of cannibalism.

2.2.2 Data collection

One to five hatchlings of a single species were placed in a 10 cm x 10 cm x 10 cm plexiglass viewing chamber filled with filtered seawater seeded with silver-coated, neutrally buoyant, light reflective glass particles (diameter: 14 μm, Potters Industries, Valley Forge, PA). The animals were allowed to acclimate for at least five minutes before data were recorded. Three Dalsa cameras (Teledyne Dalsa, Inc., Waterloo, ON, Canada; 1400×1024 pixels, 100 frames s^{-1}) were positioned around the chamber to collect kinematic data of the animals from multiple angles, and a Powerview 4MP-HS PIV camera (TSI, Inc., Shoreview, MN; 2048 x 2048, 32 frames s^{-1}) was placed above the tank to record the light-reflective glass particles from a dorsal perspective. The PIV camera was outfitted with a 50 mm Nikkor lens to achieve a field of view of 10 cm x 10 cm and synchronized with either a Quantel Brilliant B Twins laser (380 mJ/pulse, 532 nm wavelength, Lumibird, Inc., Bozeman, MT) or Evergreen HP PIV laser (340 mJ/pulse, 532 nm wavelength, Lumibird, Inc., Bozeman, MT), which were used to illuminate the light-reflective particles. Dual laser firing and paired frame capture occurred at 10-15 Hz, with a time separation between paired images (Δt) of 1,000 μs. A thin (1.0 - 1.5 mm) laser sheet was projected parallel to the bottom of the tank, as cuttlefish hatchlings most often turn in the yaw plane. Red light was used to illuminate the kinematic cameras. Spectral filters were used with the

kinematic cameras and PIV camera to prevent overexposure from green laser light and red light, respectively.

A data collection "run" consisted of ~30 seconds of recording (300-450 paired PIV images: 3,000 images for each of three Dalsa cameras = 9,000 images). Breaks between runs were at least three minutes, and runs were terminated when animals started to display fatigue or failed to swim reliably. After trials, hatchlings were returned to their holding containers within the larger seawater tanks and kept separate from non-tested individuals. All research was conducted under IACUC #21-002.

2.2.3 Kinematic analysis

Turns for analysis were selected following three criteria: (1) the hatchling was at least one body length from the wall of the viewing chamber, (2) the total angular displacement of the turn was ≥5 degrees, and (3) high-quality PIV data of the jet flow was visible in the sampling volume. Body landmarks were tracked in kinematic videos using image tracking software (Hedrick, 2008). Points in the dorsal view were (1) posterior end of the mantle, (2) point equidistant between the eyes, (3) distal tip of longest arm, (4) widest point of left side of mantle, and (5) widest point of right side of mantle (Fig 1A). For the lateral view, points were (1) posterior end of mantle, (2) center of eye, (3) distal tip of longest arm, (4) posterior opening of funnel, and (5) body edge halfway down the mantle (Fig 1B). In-house MATLAB routines (MathWorks, Inc., Natick, MA, USA) were then used to calculate center of rotation (*COR*), angular velocity (ω), and radius of curvature of the center of rotation (R). *COR* is defined as the point in the domain of the cuttlefishes body that moved the least during the turn; it was calculated using the approach described in Bartol et al. (2023). The radius of curvature of the

COR (*R*) was calculated using the following equation, as in Bartol et al. (2022, 2023), and Jastrebsky et al. (2016, 2017):

$$(3)\ \frac{1}{R} = \frac{y''}{[1 + (y')^2]^{3/2}}$$

where $y' = dy/dx = \dot{y}/\dot{x}\,, y'' = d^2y/dx^2 = (\dot{x}\ddot{y} - \dot{y}\ddot{x})/\dot{x}^3$, x and y are the coordinates of the *COR* in the dorsal view, t is time, the over dot represents time differentiation, and the derivatives were evaluated using fourth-order accurate finite difference equations (Fig 1C). These *R* values were measured between each image frame, then averaged across the turn to calculate R_{mean}. The minimum radius during the turn, R_{min}, was the 90th percentile minimum *R* (the lowest 10% of measurements were removed to control for errors in body tracking). To account for animal size, *R* was divided by total length of the individual (*R/L*) for both average [$(R/L)_{mean}$] and minimum [$(R/L)_{min}$] turning radius. Angular velocity (ω) was also measured frame-by-frame and an average angular velocity (ω_{ave}) was computed for the turn. Maximum angular velocity during the turn (ω_{max}) was the 90th percentile maximum ω, with the highest 10% of measurements being removed to control for any tracking errors that may have occurred.

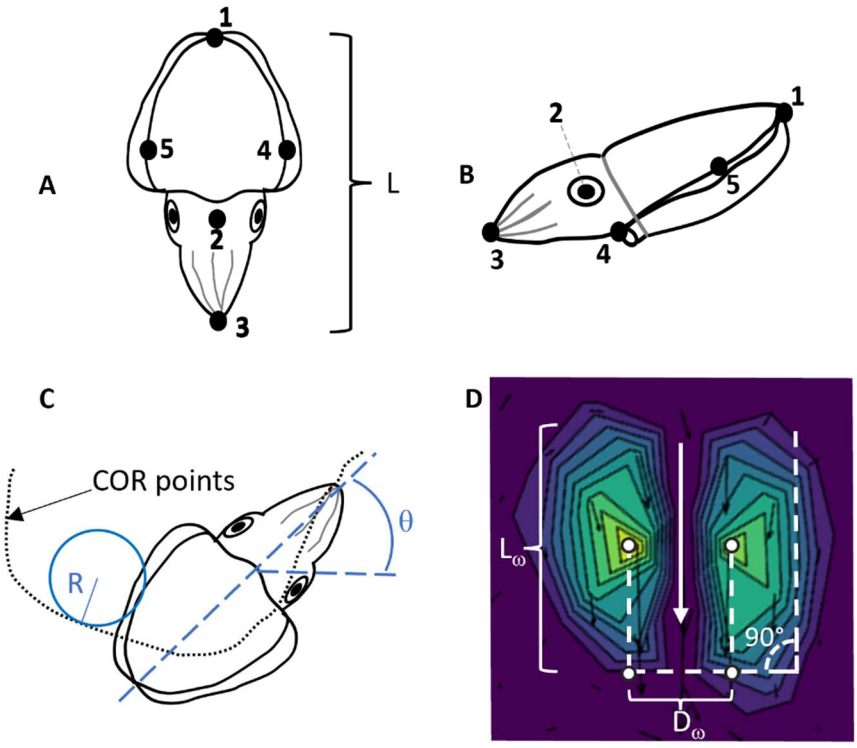

Fig 1. Illustrations of tracking points and vortex metrics used for analysis. (**A**) Dorsal view of a hatchling cuttlefishes with tracking points. (**B**) Lateral view of hatchling cuttlefishes with body tracking points and the total length of the animal (*L*). (**C**) Example of center of rotation (*COR*) points for a cuttlefishes turning counterclockwise (*COR* points are displayed per ~0.1 s). The radius (*R*) of the *COR* path is measured throughout the turn and divided by the total length of the animal to calculate length-specific radii of the turns (*R/L*). The numerical derivative of the animal angle of attack (θ) versus time was determined using a fourth-order finite difference formula. (**D**) Diagram of jet length (L_ω) and jet diameter (D_ω). D_ω is the distance between two vorticity cores (white circles) of a jet (white arrow). L_ω is the extent over which the jet vorticity field is above a specified threshold (20% of maximum vorticity).

2.2.4 Hydrodynamic analysis

Velocity vector and vorticity contour fields were calculated using Insight 4G software (TSI, Inc., Shoreview, MN). A recursive Nyquist grid engine and Fast Fourier Transform (FFT) correlator were used to determine particle displacements, with a first pass interrogation window size of 64 x 64 pixels and second pass interrogation window size of 32 x 32 pixels. Vector local validation was completed using the median test with a neighborhood of 5x5. Finally, vector field conditioning and smoothing was completed with recursive local mean filling and low pass filtering with a sigma = 0.8. Fin flows were not considered because they were of considerably lower magnitude than the dominant jet, and it was not possible to resolve flows around the small fins while also imaging the much larger jet flows. Following velocity vector field and vorticity contour field calculations, bulk wake properties were calculated in MATLAB (MathWorks, Inc., Natick, MA, USA) using routines developed in house. Bulk properties included average and maximum jet velocity (U_{jave}, U_{jmax}), jet length (L_ω), jet diameter (D_ω), impulse (**I**), and angular impulse (**A**). Jet diameter (D_ω) was the distance between vorticity cores as defined by the region of the highest 10% of vorticity (Fig. 1D). A line perpendicular to the line connecting the vorticity cores and extending along the jet vorticity field defined by a threshold (≥20% of maximum vorticity) was the jet length (L_ω; Fig. 1D). Impulse (**I**) was calculated using the following equation:

$$(4)\ \frac{\mathbf{I}}{\rho} = \pi\hat{\mathbf{z}} \int_{\text{jet}} \omega_\theta r^2 dr dz$$

where ω_θ is the azimuthal component of vorticity, r is the radial coordinate relative to the jet centerline, z is the longitudinal coordinate along the jet axis, and ρ is fluid density, and $\hat{\mathbf{z}}$ is a unit vector aligned with the jet centerline and oriented in the direction of the jet flow. By Newton's

third law, the impulse applied to the cuttlefishes is in the $-\hat{\mathbf{z}}$ direction. Angular impulse was computed from:

$$(5)\ \frac{\mathbf{A}_0}{\rho} = \frac{1}{3}\int \mathbf{x} \times \mathbf{x} \times \boldsymbol{\omega} \mathrm{dV}$$

where ρ is fluid density, $\mathbf{x}$ is the position vector relative to an arbitrary origin, $\boldsymbol{\omega} = \nabla \times \mathbf{u}$ is the vorticity vector, $\mathbf{u}$ is the fluid velocity vector, "×" is the vector cross product, and the integral is taken over the volume of the jet vorticity. For an axisymmetric jet with the jet centerline in the same plane as the cuttlefishes centroid, the angular impulse computed relative to the centroid of the cuttlefishes ($\mathbf{A}$) reduces to

$$(6)\ \frac{\mathbf{A}}{\rho} = \frac{r_0 I}{\rho}\hat{\mathbf{z}} \times \hat{\mathbf{r}}$$

where $\hat{\mathbf{r}}$ is the unit vector orthogonal to the jet centerline pointing in the direction of the cuttlefishes, r_0 is the distance between the jet centerline and the cuttlefishes centroid measured perpendicular to the jet centerline, and $I = |\mathbf{I}|$ is the magnitude of the impulse vector. By Newton's third law, the angular impulse applied to the cuttlefishes is opposite $\mathbf{A}$. The laser sheet thickness and funnel diameter were similar in size. Thus, to address underestimates of jet velocities and peak vorticity resulting from depth averaging across the laser sheet, a deconvolution routine was employed (see Bartol et al. 2009b for more detailed explanation of the deconvolution process).

2.2.5 Statistics

A two-way MANOVA was performed in SPSS (IBM SPSS v. 28.0.0.0) using species and orientation as the fixed factors, and both the kinematic and hydrodynamic metrics as dependent variables. Statistical significance was defined as $p \leq 0.05$ and the Pillai–Bartlett

statistic was used for determining significance, as recommended for unequal group sizes by Hand and Taylor (1987). When significance was detected, subsequent analyses of variance (ANOVA) tests were performed to determine which variables were significant. Dependent variables were transformed to fit assumptions of normality using the Tukey's ladder approach to identify appropriate alpha values. Linear regressions were calculated in SPSS on untransformed data with an equation of $y \propto x$. Averages are presented throughout with means ± standard error of the mean (s.e.m.).

2.3 RESULTS

A total of 136 turns (87 *Sepia officinalis* and 49 *Sepia bandensis*) was analyzed for this study. Of the 87 *S. officinalis* turns, 43.7% were oriented arms-first, and 56.3% were oriented tail-first; for the 49 *S. bandensis* turns, 38.8% were arms-first, and 61.2% were tail-first. Species identity had a significant effect on turning kinematics and hydrodynamic properties (MANOVA, $F_{8,125}$=15.328, $p<0.001$) while orientation did not (MANOVA, $F_{8,125}$=1.209, $p=0.299$), and no interaction effect was found (MANOVA, $F_{8,125}$=1.537, $p=0.151$). *Re* based on jet diameter and jet velocity (Re_{jet}) was ~0-30 and *Re* based on animal length and swimming velocity (Re_{animal}) was ~10-5500.

2.3.1 Kinematic analysis

$(R/L)_{mean}$ was 0.67±0.10 (range: 0.058-4.01) for *Sepia bandensis* and 0.64±0.06 (range: 0.058-2.30) for *Sepia officinalis*, while $(R/L)_{min}$ was 0.024±0.0049 (range: 0.0020-0.21) for *S. bandensis* and 0.024±0.0028 (range: 0.00019-0.16) for *S. officinalis*. For arms-first turns, $(R/L)_{mean}$ was 0.62 ± 0.091 (range: 0.027-4.01), whereas for tail-first turns, $(R/L)_{mean}$ was

0.68±0.061 (range: 0.057-2.31). Neither $(R/L)_{mean}$ nor $(R/L)_{min}$ was significantly different between species (ANOVA, $F_{1,132}$=0.221, p=0.639; $F_{1,132}$=0.348, p=0.556) or orientations (ANOVA, $F_{1,132}$=1.032, p=0.312; $F_{1,132}$=0.516, p=0.474). *Sepia officinalis* completed turns with higher average angular velocity (ω_{ave} = 85.23 ± 6.27 deg s^{-1}; ANOVA, $F_{1,132}$=56.442, p<0.001; Fig 2A) and higher maximum angular velocity (ω_{max} = 249.77 ± 16.69 deg s^{-1}; ANOVA, $F_{1,132}$=91.197, p<0.001; Fig 2B) than *S. bandensis* (ω_{ave} = 37.70 ± 3.21 and ω_{max} =88.85 ± 7.05 deg s^{-1}). The highest measured angular velocity was 215.50 deg s^{-1} for *S. bandensis* and 807.20 deg s^{-1} for *S. officinalis*. Orientation did not have a significant effect on angular velocity, with ω_{ave} and ω_{max} for arms-first turns = 72.93 ± 8.14 deg s^{-1} and 195.40 ± 20.50 deg s^{-1}, respectively, and ω_{ave} and ω_{max} for tail-first turns = 64.60 ± 5.33 deg s^{-1} and 189.19 ± 16.46 deg s^{-1}, respectively (ANOVA (ω_{ave}), $F_{1,132}$=0.954, p=0.330; ANOVA (ω_{max}), $F_{1,132}$=3.227 p=0.073). There was a significant positive relationship between ω_{ave} and $(R/L)_{mean}$ ($F_{1,135}$=11.23, p=0.001, R^2=0.077, Fig 2C) but the R^2 was relatively low. Regression of hatchling total length (L) versus ω_{ave} ($F_{1,135}$=1.130, p=0.290, R^2=0.008) was insignificant. Regression of hatchling total length (L) and $(R/L)_{mean}$ was significant, but the small R^2 demonstrates high variability within the data (F1,135=4.018, p=0.047, R^2=0.029). Due to poor resolution, fin beat frequencies were not determined reliably and thus were excluded from analyses. In some sequences, *Sepia bandensis* used their arms to “walk” across the bottom of the tank. However, these turns were excluded from analysis since jet-based turns were the primary focus.

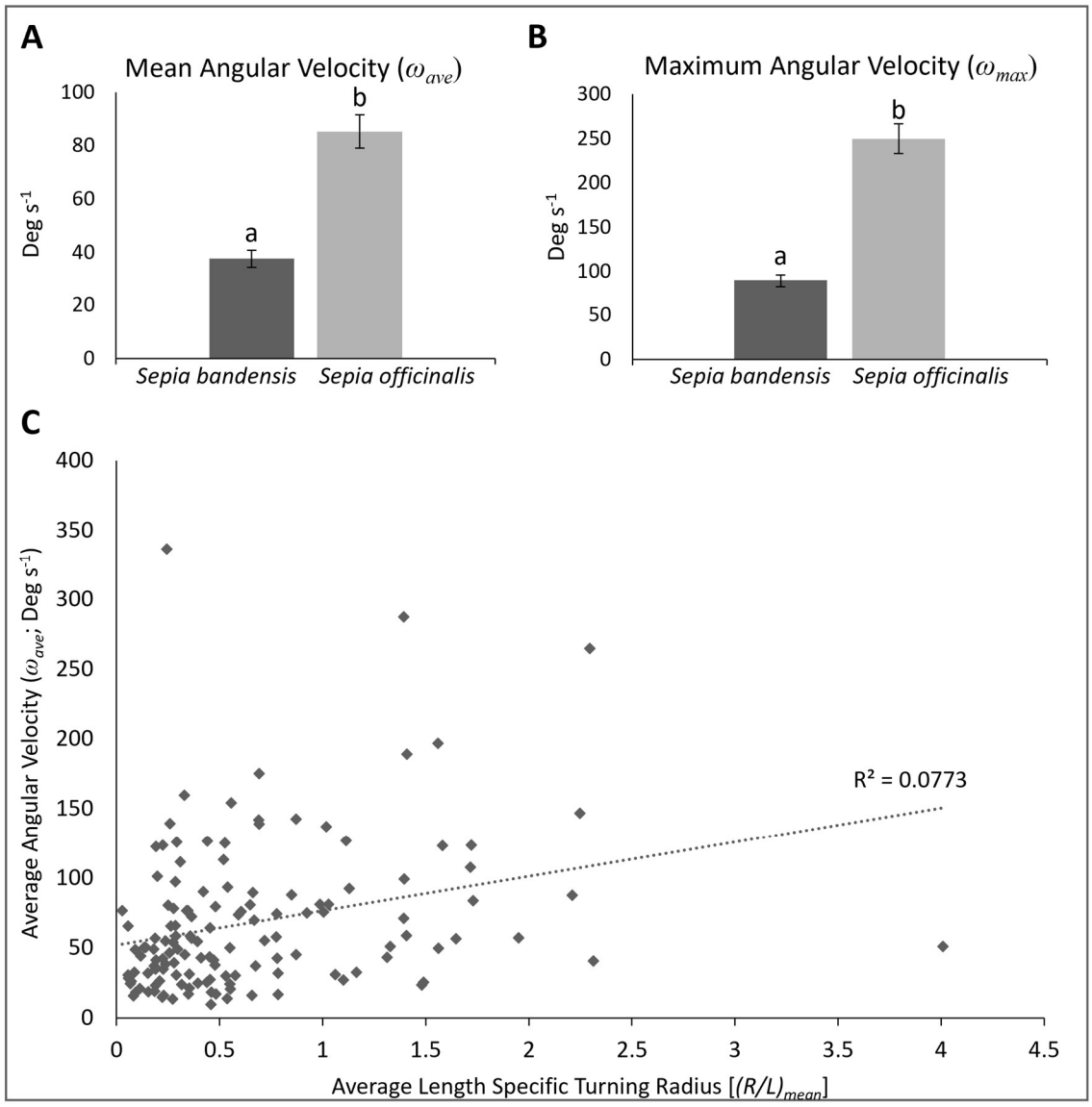

Fig 2. Kinematic measures of turning abilities for *Sepia bandensis* and *Sepia officinalis* hatchlings. (**A**) Mean angular velocity (ω_{ave}) and (**B**) maximum angular velocity (ω_{max}) during turns for both *S. bandensis* and *S. officinalis*. (**C**) Regression of pooled mean angular velocity (ω_{ave}) versus pooled length-specific turning radius [$(R/L)_{mean}$]. Significance is denoted by different letters in bar plots and significant regression relationship is denoted with dotted lines. All error bars presented are standard error of the mean.

2.3.2 Hydrodynamic analysis

During turns, both species produced the two principal jet patterns, as reported by Bartol et al., (2009a) for squids: *jet mode I*, where isolated vortex rings occur with each jet pulse, and *jet mode II*, where leading vortex rings with trailing tails are generated with each jet pulse (Figs 3, 4). *Sepia bandensis* had significantly larger L_ω/D_ω (4.14 ± 0.25) than *S. officinalis* (2.63 ± 0.13; ANOVA, $F_{1,132}$=30.849, p<0.001; Fig 5A). The formation number (*F*), i.e., the transition L_ω/D_ω between the two jet modes, for *S. officinalis* and *S. bandensis* was ~3-4, although in some rare cases, vortex rings with trailing jets were observed at L_ω/D_ω as low as 2. *Sepia bandensis* also exhibited lower angular impulse ($|\mathbf{A}|$=3.89x10^{-9} ± 8.30x10^{-10} Nms) compared to *S. officinalis* ($|\mathbf{A}|$ = 1.20x10^{-8} ± 2.54x10^{-9} Nms; ANOVA, $F_{1,132}$=10.672, p=0.001; Fig 5B). During turns, *S. bandensis* had significantly lower U_{jave} (0.629 ± 0.040 cm s^{-1}) and U_{jmax} (1.113 ± 0.077 cm s^{-1}) than *Sepia officinalis* (U_{jave} = 0.850 ± 0.035 cm s^{-1}; U_{jmax} = 1.432 ± 0.057 cm s^{-1}; ANOVA (U_{jave}), $F_{1,132}$=20.816, p<0.001; ANOVA (U_{jmax}), $F_{1,132}$=14.933, p<0.001, respectively; Fig 5C,D). The highest recorded *S. officinalis* jet velocity was 3.005 cm s^{-1}, while *S. bandensis*' maximum jet velocity was 2.582 cm s^{-1}.

U_{jave} and U_{jmax} were also positively related to the total length (*L*) of the individual (U_{jave}: $F_{1,135}$=11.018, p=0.001, R^2=0.076, Fig 5E; U_{jmax}: $F_{1,135}$=8.099, p=0.005, R^2=0.057, Fig 5F). Positive linear relationships between U_{jave} and ω_{ave} ($F_{1,135}$=12.859, p<0.001, R^2=0.088; Fig 6A) and U_{jmax} and ω_{max} ($F_{1,135}$=4.058, p=0.046, R^2=0.029; Fig 6B) were observed.

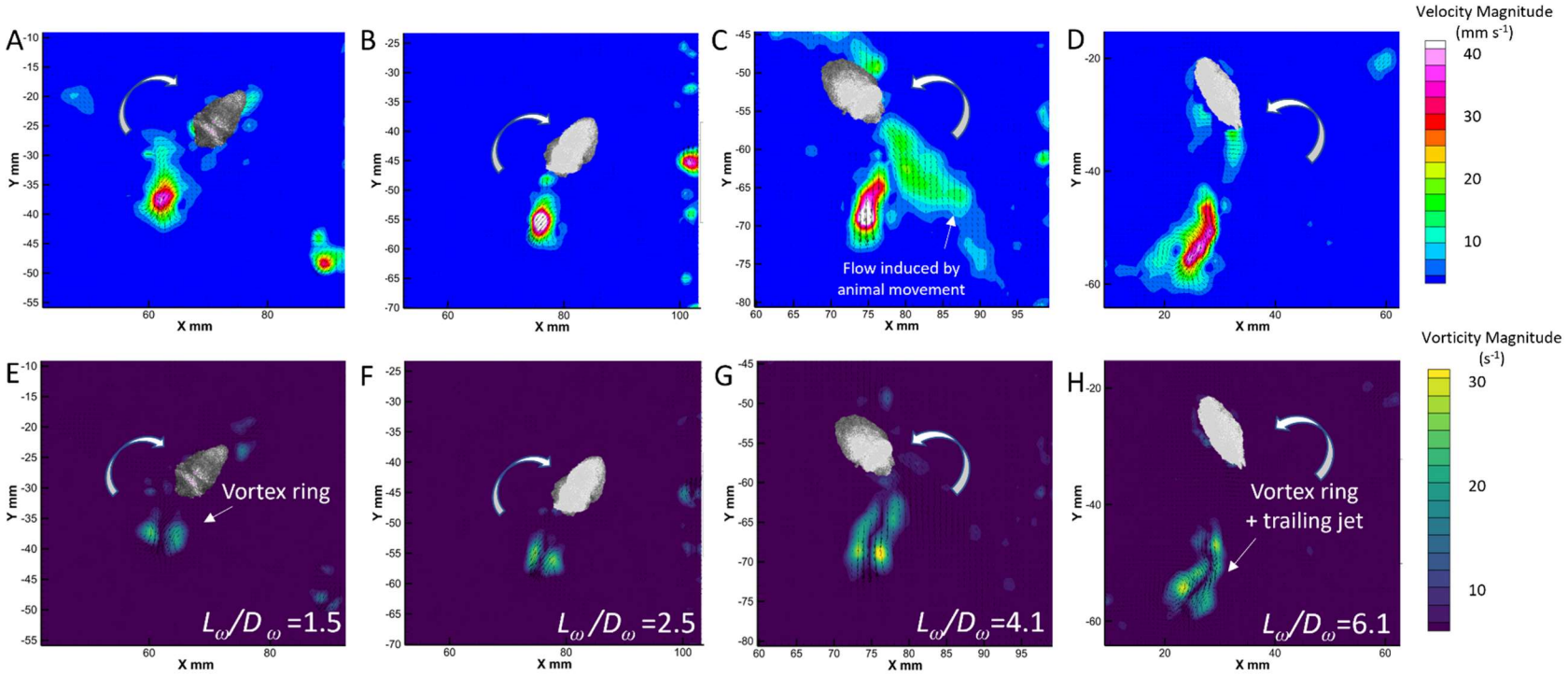

Fig 3. Digital particle image velocimetry plots for *Sepia officinalis* hatchlings. Velocity vector magnitude is depicted on the top row, while corresponding vorticity magnitude is shown on the bottom row. Turning path direction is shown with arrows and the length to diameter ratio of jet flows based on vorticity (L_ω/D_ω) are included on the lower right-hand corner, with L_ω/D_ω increasing moving left to right. Plots **A, B, E**, and **F** are representative of *jet mode I*, and plots **C, D, G,** and **H** are representative of *jet mode II*.

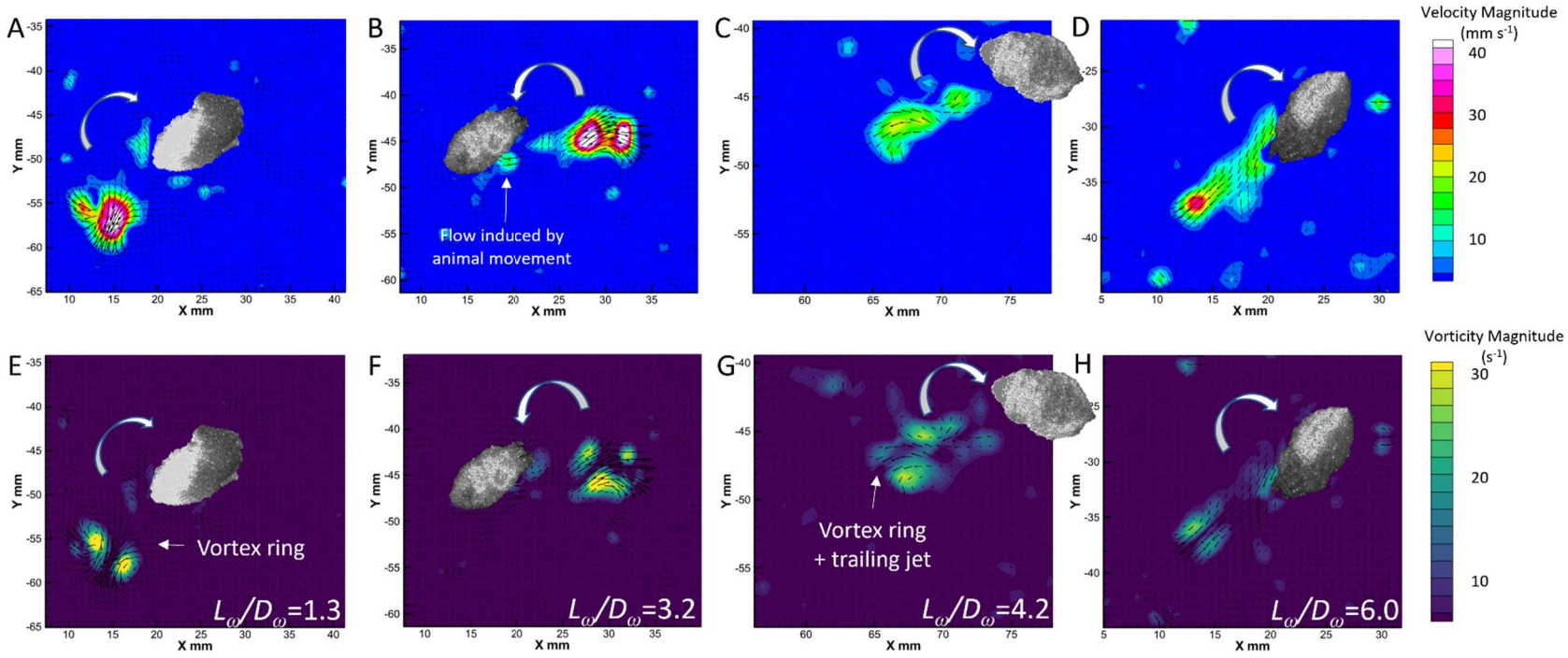

Fig 4. Digital particle image velocimetry plots for *Sepia bandensis* hatchlings. Velocity vector magnitude is depicted on the top row, while corresponding vorticity magnitude is shown on the bottom row. Turning path direction is shown with arrows and the length to diameter ratio of jet flows based on vorticity (L_ω/D_ω) are included on the lower right-hand corner, with L_ω/D_ω increasing moving left to right. Plots **A, B, E**, and **F** are representative of *jet mode I*, and plots **C, D, G**, and **H** are representative of *jet mode II*.

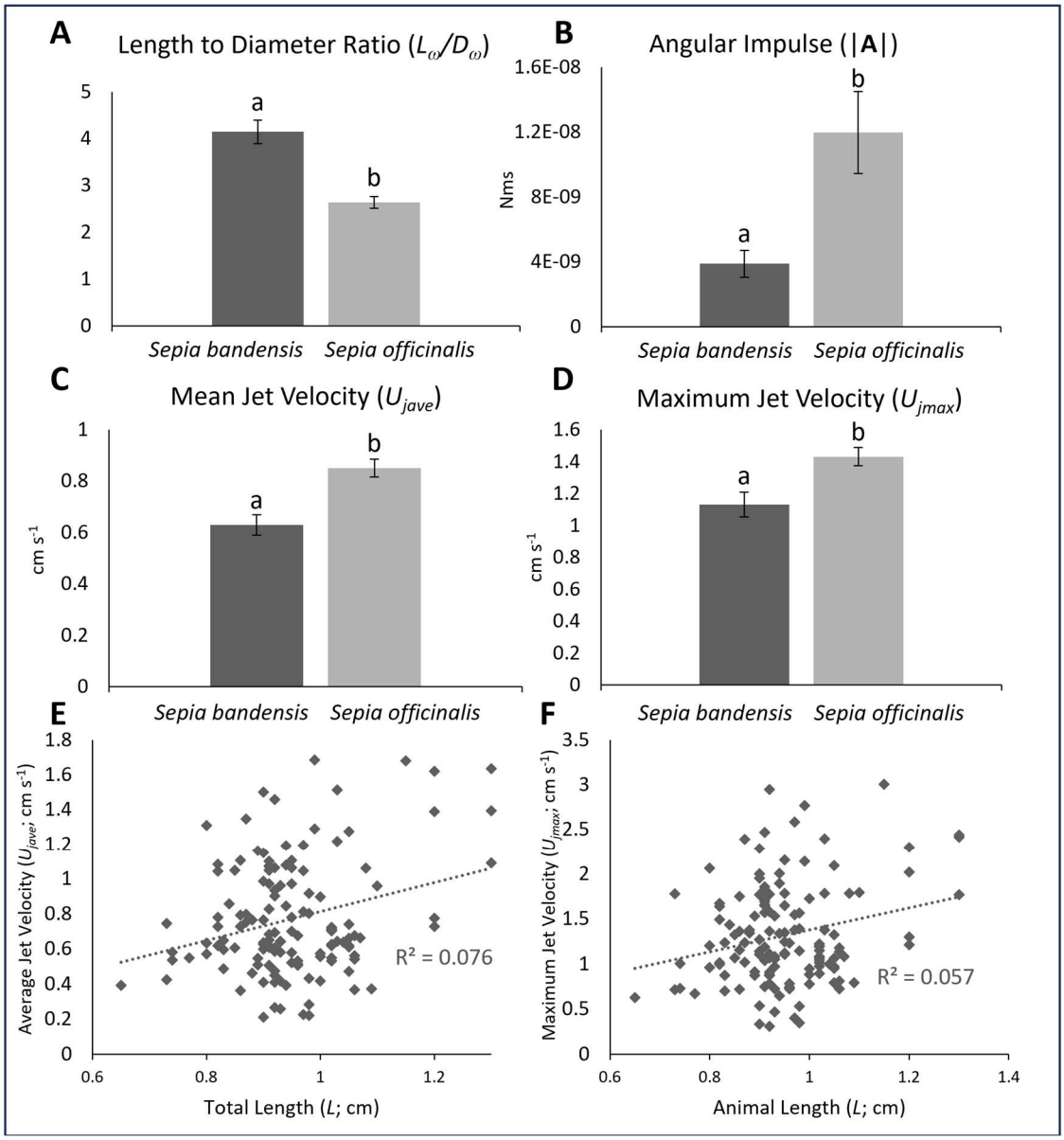

Fig 5. Hydrodynamic metrics of turning for both *Sepia bandensis* and *Sepia officinalis.* (**A**) Mean jet length to diameter ratio (L_ω/D_ω), (**B**) mean jet angular impulse (|**A**|), (**C**) mean jet velocity (U_{jave}), and (**D**) maximum jet velocity (U_{jmax}) for turning hatchlings. (**E**) Linear regression of average jet velocity (U_{jave}) versus hatchling total length (L). (**F**) Linear regression of maximum jet velocity (U_{jmax}) versus hatchling total length (L). For bar graphs, significance is noted with different letters and significant regression relationships are denoted with dotted lines. All error bars are standard error of the mean.

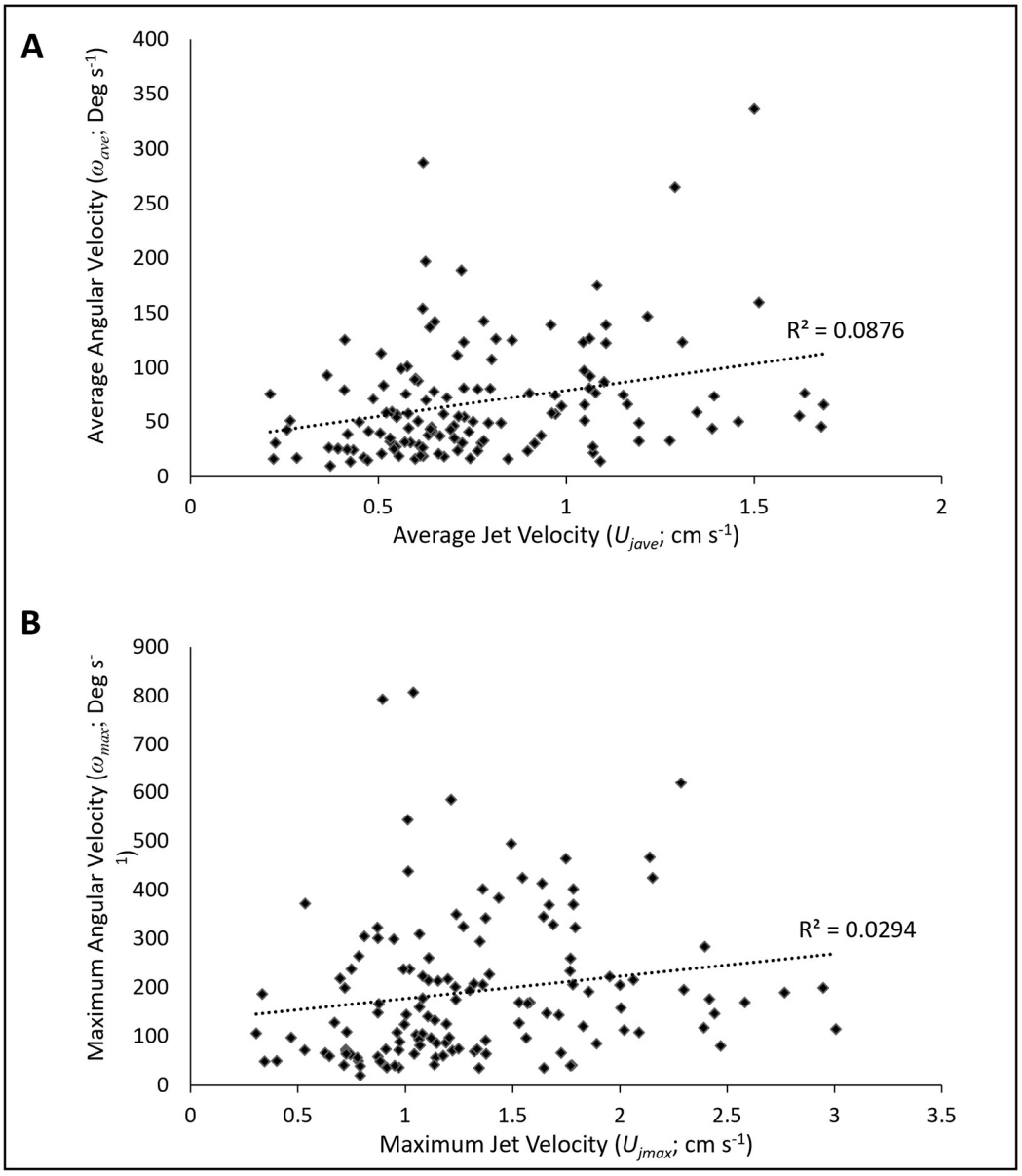

Fig 6. Linear regressions of jet velocity and angular velocity. (**A**) Linear regression of average angular velocity (ω_{ave}) and average jet velocity (U_{jave}). (**B**) Linear regression of maximum angular velocity (ω_{max}) and maximum jet velocity (U_{jmax}). Significant regressions are shown with a dotted line, and corresponding R^2 values are included on plots.

2.4 DISCUSSION

2.4.1 Kinematics

In this study, the turning abilities of two cuttlefishes species, *Sepia bandensis* and *Sepia officinalis*, during early ontogeny were examined. While both species performed turns of similar tightness (*R/L*), *S. officinalis* completed significantly faster turns (higher ω_{ave} and ω_{max}) than *S. bandensis*. This difference in turning agility is consistent with their lifestyles. *Sepia bandensis* is less energetic with a more benthic lifestyle even as hatchlings, relying heavily on crypsis as its first line of defense rather than escape jetting, while *S. officinalis* is more active, spends more time in the water column, and exhibits more escape jetting (Hanlon and Messenger, 1996; Hanlon et al., 2018; Norman, 2003). Thus, high angular velocities are less critical for *S. bandensis*. Indeed, *S. bandensis* was less active than *S. officinalis* during experimental trials and in holding tanks, with spontaneous turns being less frequent. Given the observed positive relationship between ω and *R/L*, *S. officinalis* was expected to have higher *R/L* than *S. bandensis.* However, the data did not support this prediction. The reason for this may relate to *S. officinalis'* greater reliance on short jets during turns, allowing for high turn control and lower-than-expected *R/L* (see hydrodynamics section).

Both species of hatchlings completed turns in the arms-first and tail-first orientation with equal proficiency. This finding differs from data on adult squids, where orientation can have a major effect on turning performance and jet dynamics (Bartol et al., 2022, 2023; Chapter 4). The lack of a significant orientation effect may be a product of several factors. First, during early ontogeny, the fins are less developed (Bartol et al., 2008; Kier and Thompson, 2003; Thompson and Kier, 2001; Thompson and Kier, 2006; Thompson et al., 2010; Vidal et al., 2018) and consequently their positioning anterior or posterior has less of an impact on propulsion, stability,

and lift production – properties that play important roles in orientation differences. Second, turning with similar adeptness in either orientation is central to survival during a critical developmental stage. Arms-first turning is important for hunting and food acquisition as the tentacles and arms must be oriented towards prey for strike and capture. Given energy reserves are limited at early life stages, it is essential for hatchlings to be highly proficient at turning to align with targets (Boucaud-Camou et al., 1985; Bouchaud, 1991; Hanlon and Messenger, 1996; Nixon, 1985). Equally important, however, is the ability to escape and evade predators, which is often achieved by turning and jetting quickly in the tail-first orientation. These tail-first evasion maneuvers are important given high predation rates on hatchlings (Boyle and Rodhouse, 2005; Hanlon and Messenger, 1996; O'Brien et al., 2017). While catching prey and hunting are important for adult animals as well, high predation coupled with limited energy reserves during early ontogeny likely places greater pressure on hatchlings to perform well in either orientation (Boyle and Rodhouse, 2005; Hanlon and Messenger, 1996; O'Brien et al., 2017). Third, at intermediate *Re* when viscous forces play a substantial role, the flow gradients near the animal are more diffuse and less dependent on shape or orientation (see Fig 3C, 4B), which would tend to mitigate orientation-based performance differences (Vogel, 2013; Yagi and Kawahara, 2005). Finally, because cuttlefishes are neutrally buoyant and do not need to direct their jet downward, orientation differences are likely less pronounced than in negatively buoyant squids, which need to generate jet flows for depth control throughout turns (often with significantly different funnel curvature depending on turn orientation).

Hatchling size did not affect turning performance (i.e., R/L or ω) indicating that cuttlefish hatchlings are similarly proficient throughout early development (1-30 days post-hatching). In squid paralarvae a transition in swimming performance occurs ~35 days old with the

development of fins (Vidal et al., 2018). Although this study did not examine hatchlings beyond 30 days old, a similar transition may occur in cuttlefishes (Boletzky, 2003; Hanlon et al., 2018; Young and Harman, 1988). Research on turning abilities of older hatchlings and adults would be helpful in determining whether a performance transition exists.

2.4.2 Hydrodynamics

Sepia officinalis had higher jet velocities (U_{jave}, U_{jmax}) than *Sepia bandensis*, which contributed to greater angular velocities (ω) based on the observed positive relationship between U and ω. In addition to higher jet velocities, *S. officinalis* exhibited higher angular impulses ($|\mathbf{A}|$) than *S. bandensis*, which is also consistent with the observed higher ω. Although little is known about the muscle mechanics of young cuttlefishes, these findings suggest that the mantle and funnel of *S. officinalis* are structured to generate more powerful, shorter (see below) jets than those of *S. bandensis*. Greater power/shorter pulses could be achieved by differences in contraction force and/or frequency, or differences in muscle composition (Kier and Thompson, 2003; Thompson and Kier, 2001; Thompson and Kier, 2006; Thompson et al., 2010). However, no analysis has yet been done on cuttlefishes mantle/funnel musculature during early ontogeny.

Based on the data, *S. bandensis* exhibited greater L_ω/D_ω despite lower jet velocities and angular impulses than *S. officinalis*. This finding differs from patterns observed in adult squids, where higher jet velocity and angular impulse generally occur with greater L_ω/D_ω (Bartol et al. 2022, 2023). In squids, short (low L_ω/D_ω) and long (high L_ω/D_ω) jets both have advantages for turning, as repeated short jet bursts provide more directed control within the turn, allowing for high agility, but longer jets provide more impulse, which facilitates higher angular velocity (Bartol et al. 2022, 2023). *Sepia officinalis'* strategy of using high-velocity, short jets combines

both of these two benefits, allowing for the production of powerful but controlled pulses throughout the turning path. Indeed, this approach allowed *S. officinalis* to achieve higher ω, but similar *R/L* compared to *S. bandensis*. The use of short jets in cuttlefishes has been reported by Helmer et al. (2017), who describe multiple, discrete, jet-driven rotations in adult *Sepia officinalis* during body reorientation, which are known as "saccades". These saccades can produce turns of 343 deg s^{-1} (Helmer et al., 2017). This behavior may be driven by multiple *jet mode I* jets, as seen in this study. Both species favored *jet mode I* jets rather than longer jets with tails during turns, with *Sepia bandensis* performing *jet mode I* jets 75.5% of the time, and *Sepia officinalis* performed *jet mode I* turns 81.4% of the time. This greater reliance on isolated vortex ring jets (*jet mode I*) not only likely contributes to improved turning performance by offering greater control of pulsed impulse as mentioned above, but it may also improve energy use, as *jet mode I* has higher propulsive efficiency than *jet mode II* during steady swimming in adult squids (Bartol et al., 2009a, 2016). The formation number (*F*) of ~3-4 recorded in the present study for both cuttlefishes species is similar to *F* reported for squids in Bartol et al. (2009b, 2022, 2023). However, although rare, some vortex rings with tails were observed at lower L_ω/D_ω (~2). This lower-than-expected *F* occurred because of widely spaced vortex cores, which can arise at low and intermediate *Re,* where vortex rings become thicker (Palacios-Morales and Zenit, 2013).

The observed positive relationship between jet velocity and total length was expected because larger, more developed animals have more powerful mantle musculature (Kier and Thompson, 2003; Thompson and Kier, 2001; Thompson and Kier, 2006; Thompson et al., 2010). However, there was large variation within animal size, demonstrating that while this trend holds true, smaller hatchlings do have the ability to produce relatively fast jets at small sizes, and larger hatchlings do not always produce jets of maximum speed.

2.4.3 Ontogenetic comparisons

This study is the first to examine turning performance in cuttlefishes during early ontogeny, and no quantitative studies focusing on turning in squid paralarvae have been performed to date. Squid paralarvae are capable of high rectilinear velocities (Vidal et al., 2018). For example, paralarval *Doryteuthis opalescens* can reach speeds of over 55.0 cm s^{-1} at around one month of age, as well as form small schools, which requires the ability to turn in unison (Vidal et al., 2018). Paralarval *Doryteuthis pealeii* employ escape jets at random angles, resulting in unpredictable trajectories and frequent turns that make it difficult for predators to track their positions (York et al., 2016).

While turning studies of cephalopods during early ontogeny are lacking, several turning performance studies of adult squids and cuttlefishes have been conducted. The brief squid, *Lolliguncula brevis*, and the dwarf cuttlefish, *Sepia bandensis*, are capable of very tight turns, with $(R/L)_{min}$ of ~0.003 and ~0.001, respectively (Jastrebsky et al., 2016). Mean ω_{max} for these cephalopods ranges from 160 deg s^{-1} (*S. bandensis*) to 269 deg s^{-1} *(L. brevis*; Jastrebsky et al., 2016), though *L. brevis* can reach ω_{max} >700 deg s^{-1} in some high-performance turns (Bartol et al., 2022; Jastrebsky et al., 2017). *Doryteuthis pealeii* and *Illex illecebrosus*, two neritic squids species, complete turns of slightly lower angular velocities (*D. pealeii*: ω_{max} = 82 deg s^{-1}, *I. illecebrosus:* ω_{max} = 109 deg s^{-1}) and slightly larger length-specific turning radii (*D. pealeii*: $(R/L)_{min}$ = 0.0097, *I. illecebrosus* $(R/L)_{min}$ = 0.012) than *L. brevis* and *S. bandensis* adults (Chapter 4). Given that cuttlefish hatchlings in the present study had $(R/L)_{min}$ = 0.024, adult cephalopods can clearly turn more tightly. However, hatchling *S. officinalis* had higher ω_{max} (~250 deg s^{-1}) than most of the adult cephalopods above (*L. brevis* being the exception), which was expected given smaller animals tend to have reduced moments of inertia and lower hydrodynamic

resistance (Fish and Nicastro, 2003). Surprisingly, *S. bandensis* hatchlings exhibited lower mean ω_{max} (~88 deg s^{-1}) than most of the adult cephalopods examined above (*D. pealeii* being the exception), including adult *S. bandensis*. The reason for this is unclear. Future studies that examine neuromuscular mechanics throughout ontogeny in this species may provide insights on this unexpected finding.

2.4.4 Comparisons with other taxa

Squids and cuttlefishes are not the only animals that use jet propulsion for turning. The colonial siphonophore *Nanomia bijuga* uses a series of individual nectophores that jet sequentially to move the colony. These small jetters experience *Re* similar to the lower end of hatchling cuttlefishes (*Re* ~100) and can complete turns of slightly faster average angular velocities (104 deg s^{-1}; Sutherland et al., 2019). However, they cannot complete turns as tightly (R/L_{min} ~ 0.05) as either *S. bandensis* or *S. officinalis* (R/L_{min} ~ 0.02) hatchlings. In addition, *N. bijuga* has a similar maximum angular velocity to *S. bandensis* (~215 deg s^{-1}; Sutherland et al., 2019) while *S. officinalis* in the present study reached a maximum angular velocity of 807 deg s^{-1}. Jellies also use jet propulsion to swim, contracting their bell asynchronously to produce turns. While the mechanisms of jellyfish turning are known (see Costello et al., 2021), detailed kinematic measurements of *R/L* and ω are not yet available (although *Aurelia aurita* is estimated to reach maximum angular velocities of ~400 deg s^{-1}; Dabiri et al., 2020). For slow turns, jellies produce multiple, asymmetric jets, but for more extreme turns, they employ more asymmetric bell movements, both in terms of jet pulsing and shape changes (Costello et al., 2021; Dabiri et al., 2020; Gemmell et al., 2015). This is different than cuttlefishes turns, which involve more vectored jet flows and higher pulsing frequencies. In addition, jellies produce only *jet mode I* jets

with low L_ω/D_ω (wide jets) during turns, while cuttlefishes hatchlings produce both *jet mode I* and *II*. This difference is likely due to the medusa jellies having wider jet apertures relative to plenum volume (cuttlefishes funnel diameter = ~1 mm, jellyfish bell diameter 0.5-14 cm; Costello et al., 2021; Dabiri et al., 2020; Gemmell et al., 2015).

Compared to non-jetters, *S. bandensis* and *S. officinalis* hatchlings turn slowly but rather tightly. Whirligig beetles (*Dineutes horni*) experience similar *Re* (~400-2050), and can produce extremely fast turns averaging around 1790 deg s^{-1}, but have an average length specific turning radius of 0.86 (Fish and Nicastro, 2003; Xu et al., 2012), more than an order of magnitude wider than those reported in the present study for hatchling cuttlefishes. Yellowfin tuna *Thunnus albacares* [$(R/L)_{min}$=0.20], California sea lions *Zalophus californianus* [$(R/L)_{min}$=0.09], bottlenose dolphins *Tursiops truncates* [$(R/L)_{min}$=0.08], angelfish *Pterophyllum eimekei* [$(R/L)_{min}$=0.07], and spotted boxfish *Ostracion meleagris* [$(R/L)_{min}$ = 0.03] all have minimum turning radii larger than *S. officinalis* and *S. bandensis* hatchlings, but leopard sharks *Triakis semifasciata* [$(R/L)_{min}$=0.006] and painted turtles *Chrysemys picta* [$(R/L)_{min}$=0.0018] are capable of tighter turns (Blake et al., 1995; Domenici and Blake, 1991; Fish et al., 2003; Maresh et al., 2004; Porter et al., 2011; Rivera et al., 2006; Walker, 2000). These larger bodied animals are capable of extremely tight turns with comparable angular velocities to hatchling cuttlefishes. Although smaller animals generally achieve higher angular velocities, the benefits of small size in hatchling cuttlefishes may be countered somewhat by the greater relative effect of viscous forces at intermediate *Re*, where body movements move large volumes of water that can slow down rotation (e.g., see Fig 3C, 4B). In addition, in adult animals, propulsors tend to be farther from the center of mass, providing greater torque.

2.4.5 Conclusions

Little is known about the turning abilities of swimmers during early ontogeny, especially jet-propelled animals. In this study, turning kinematics and flow dynamics of two species of cuttlefish hatchlings, *S. officinalis* and *S. bandensis*, were examined. *Sepia officinalis* turned more quickly than *S. bandensis* using higher velocity/impulse jets. While *S. officinalis'* jets were higher in velocity and angular impulse, they were also shorter (low L_{ω}/D_{ω}) than those of *S. bandensis*, which allowed *S. officinalis* to produce controlled jet flows and achieve comparable length-specific turning radii. Both species completed turns in either arms-first or tail-first orientations upon hatching through their first 30 days of life, with no difference in turning performance detected across the two orientations. Although both species produced short and long jets, hatchlings generally relied more heavily on short jets, which presumably allowed for greater control throughout the turning path. Relative to adults, cuttlefish hatchlings turned more broadly, but *S. officinalis* hatchlings turned more quickly; relative to other taxa, *S. officinalis* and *S. bandensis* turned slowly but relatively tightly.

CHAPTER 3

CUTTLEFISH TURN SLOWLY BUT TIGHTLY WITH DIRECTIONAL FLEXIBILITY USING SHORT VORTEX RING JETS

3.1 BACKGROUND

Turning is an important part of life in the oceans, necessary for capturing prey, avoiding predators, navigating complex habitats, and communicating with conspecifics (Bartol et al., 2022; Hanlon and Messenger, 1996; Hanlon et al., 2018). Turning performance has been examined in a range of taxa, including fishes, beetles, squids, and turtles (Bartol et al., 2022; Bartol et al., 2023; Blake et al., 1995; Budick and O'Malley, 2000; Danos and Lauder, 2007; Drucker and Lauder, 2001a; Fish and Nicastro, 2003; Fish et al., 2003; Fuiman and Webb, 1988; Jastrebsky et al., 2016; Jastrebsky et al., 2017; Müller and Lentink, 2004; Porter et al., 2011; Rivera et al., 2006; Walker, 2000; Webb and Kostecki, 1984; Weihs, 1972, Chapter 4). Studies integrating kinematic data with flow quantification data have provided valuable insights for understanding turning. For example, Epps and Techet (2007) found that giant danios (*Danio aequipinnatus*) use both maneuvering (initial) and propulsive (secondary) vortices to achieve C-start turns. Sunfish (*Lepomis macrochirus*) modify impulse and the timing of shed vortex rings to produce turns of differing strength, speed, and tightness (Drucker and Lauder, 2001a). Müller et al., (2008) analyzed the flow around larval zebrafish (*Danio rerio*) during routine turns and found that two sets of vortex rings are shed in rows on either side of the body, similar to patterns observed in anguilliform swimmers. During these turns, the wake is large and vortex ring circulation is short-lived, as expected for flows at intermediate Reynolds numbers. Thandiackal and Lauder (2020) found that turns in *D. rerio* are powered mainly by positive work done on the water by the posterior body region. However, 10-20% of the total work performed during turning

is negative work (from the fluid onto the body), which occurs anteriorly. This pattern is different than steady swimming, where positive work is generated at the tail end of the animal (Coughlin, 2000; Coughlin and Rome, 1996; Ellerby et al., 2022; Jayne and Lauder, 1995; Johnson et al., 1994; Rome et al., 1993).

In addition to studies of fishes, dual (kinematics + hydrodynamics) analyses have been used to understand turning in jet propelled animals. In the moon jelly, *Aurelia aurita*, hydrodynamic and kinematic analyses revealed that non-uniform bell contractions produce asymmetric vortex rings to effect turns (Gemmell et al., 2015), which differ from the symmetric vortex structures produced during rectilinear swimming (Colin et al., 2013; Dabiri, 2009; Dabiri et al., 2005). The vortex rings produced on the inside of the turn are often interconnected, similar to flows produced by some fish (Lauder and Drucker, 2002; Linden and Turner, 2004) and squids (Bartol et al. 2019, 2022, 2023). Conversely, siphonophores employ the same jet patterns used during rectilinear swimming, except that nectophores towards the apex of the colony are positioned at an angle with respect to the rest of the nectosome, providing flows with sufficient torque for turning (Costello et al., 2015).

Jet-propelled cephalopods, such as squids, have flexible funnels that vector jet flows in different directions below the animal, allowing for swimming in either arms-first (forward) or tail-first (backward) orientations. When turning, orientation plays a significant role, with most squids completing tight but slow arms-first turns and fast but broad tail-first turns, although some species diverge from this general pattern (Bartol et al., 2022; Bartol et al., 2023, Chapter 4). Squids use two main "jet modes" while swimming: *jet mode I*, where a short plug of water is ejected from the funnel creating one discrete vortex ring and *jet mode II*, where a longer, more sustained jet is produced with a leading vortex ring structure and a trailing jet (Bartol et al.,

2009a). During turns, squids often use multiple *jet mode I* pulses, as shorter more controlled jets are beneficial for tight turning. This mode is frequently favored when moving arms-first (Bartol et al., 2022; Bartol et al., 2023). *Jet mode II* pulses are often higher in jet velocity and impulse and drive high angular velocity, broad turns (Bartol et al., 2009a; Bartol et al., 2022; Bartol et al., 2023). There is a predictable transition between the two jet modes that occurs when the length to diameter ratio of the jet vorticity field (L_ω/D_ω) is ~3-4 (Bartol et al., 2009a, 2022, 2023). In mechanical jet systems, this transition is known as the formation number (F) (Gharib et al., 1998; Krueger and Gharib, 2003).

In contrast to many jet-propelled animals, such as salps, sea jellies, and siphonophores, cuttlefishes (another cephalopod related to squids) have more rigid bodies, skirt-like fins, and benthic lifestyles. With an internal cuttlebone made of calcium carbonate, cuttlefishes are able to maintain neutral buoyancy, but are limited in body flexibility (Denton and Gilpin-Brown, 1961b; Hanlon and Messenger, 1996; Hanlon et al., 2018). In general, animals with flexible bodies are considered more maneuverable (smaller turning radii) than animals with rigid bodies because they achieve greater body curvature and have lower moments of inertia (Fish, 1999; Parson et al., 2011; Walker, 2000). However, some rigid bodied animals, such as beetles, cuttlefishes, and turtles, are notable exceptions and can turn with low length-specific turning radii (Fish and Nicastro, 2003; Jastrebsky et al., 2016; Rivera et al., 2006). In addition to their rigid body structure, cuttlefishes have long skirt-like fins surrounding the mantle that together with the jet contribute to propulsion, setting them apart from salps, sea jellies, and siphonophores that rely exclusively on jet propulsion (Guerra, 2006; Hanlon and Messenger, 1996; Hanlon et al., 2018; Jereb and Roper, 2005; Kier, 1989). In contrast to more pelagic jetters, cuttlefishes are also

relatively benthic animals, living in reef systems where precise, controlled movements are advantageous for navigating complex structure.

Little is known about the turning capabilities of most cuttlefishes. Based on kinematic measurements, adult dwarf cuttlefish (*Sepia bandensis*) are among the tightest turning animals in the oceans, outperforming both rigid and most soft-bodied animals (Jastrebsky et al., 2016). Agility (angular velocity) in *S. bandensis* is more moderate, with flexible bodied animals of similar size turning an order of magnitude faster (Jastrebsky et al., 2016). In hatchling cuttlefishes, there are species-specific differences in turning abilities. *Sepia officinalis* hatchlings turn faster (ω_{max}=250 deg s^{-1}) than *S. bandensis* hatchlings (ω_{max}=89 deg s^{-1}), but both species turn with similar tightness [$(R/L)_{min}$ ~ 0.024; Chapter 2]. Faster turns in *S. officinalis* hatchlings are driven by higher jet velocities and angular impulses but smaller L_ω/D_ω than *S. bandensis* (Chapter 2). Both species favor short, repetitive jets over longer jet flows to perform turns. Although kinematic data of adult cuttlefishes and flow quantification data of hatchling cuttlefishes are available, nothing is known about jet or fin flows during turning in adult cuttlefishes, or how different hydrodynamic properties in adult cuttlefishes correlate with kinematic parameters.

In this study, an integrated kinematic/hydrodynamic analysis was used to quantify the turning ability of adult *Sepia bandensis*. Three hypotheses were examined: (1) Adult *Sepia bandensis* will use shorter, lower velocity jets for tight turns and longer, higher velocity jets for fast turns. Although jet length and jet velocity ranges of adult cuttlefishes were expected to be lower than those reported for adult squids, a trend toward longer, higher velocity jets for high angular velocity turns, similar to patterns reported in squids, was predicted. (2) Orientation will play a more reduced role in turning than observed in squids. This prediction was based on a

greater need (relative to more pelagic squids) to turn with similar proficiency across orientations when navigating complex reef environments, where forward/backward movements are common (Hanlon and Messenger, 1996; Hanlon et al., 2018). (3) *Sepia bandensis* will rely more heavily on *jet mode I* and lower jet velocities than squids do to achieve turns. This prediction was based on cuttlefish's preference for slower overall swimming speeds and residence in more benthic, complex habitats where short, low velocity pulses are useful for maneuvering in tight spaces (Hanlon and Messenger, 1996; Hanlon et al., 2018).

3.2 METHODS

3.2.1 Study animal

Eight juvenile/adult *Sepia bandensis* [Adam, 1939; total length (L) = 7.38 ± 1.48 cm] were purchased from the Marine Biological Laboratory in Woods Hole, Massachusetts. Individuals were kept in mesh-lined 5-gallon buckets suspended within a 450-gallon recirculating tank (30 ppt, 26.5°C). Holes were drilled in the 5-gallon buckets to facilitate water flow through the mesh lining, and pool noodles were affixed to the bucket rims to provide buoyancy. Animals were fed fresh and frozen mysid *spp*. as well as live *Palaemonetes spp*. All research was conducted under IACUC #21-002.

3.2.2 Data collection

For experimental trials, an animal was placed in a 10-gallon glass aquarium filled with filtered seawater matching the salinity and temperature of the holding tanks and seeded with light reflective neutrally buoyant particles (polyamide, 50 μm, Dantec Dynamics, Skövlunde, Denmark). A TSI V3V-8000 probe (three 2048 × 2048-pixel cameras, 14 × 14 × 10 cm sampling

volume, TSI, Inc., Shoreview, Minnesota, USA) was used to capture images of particles in 3-dimensions for flow field measurements. A dual-pulsed laser (EverGreen HP, 340 mJ, 532 nm, 15 Hz, Δt=2000 μs; Lumibird, Bozeman, MT, USA) synchronized to the probe using TSI hardware and V3V 4G software was used to illuminate a cylindrical volume of particles. In addition to the flow quantification camera, three Falcon cameras (1400 × 1024 pixels, 100 frames s^{-1}, Teledyne Dalsa, Inc., Waterloo, Ontario, CA) were positioned around the tank to capture dorsal (1 camera) and lateral (2 cameras) views of the cuttlefishes turning in the tank. Halogen lights with red (>600 nm) filters were used for illumination of video frames captured from the Falcon cameras. Additional filters were used with the Falcon cameras and TSI probe to eliminate cross illumination from the different light sources, i.e., green-wavelength laser, red-wavelength halogens.

Prior to data collection, individuals were allowed to acclimate in the viewing tank for 5-10 minutes. A data collection "run" lasted ~40 seconds, with 300 paired images from the V3V-8000 probe and ~4000 images from each Falcon camera being collected over the run. To reduce stress on the animals, 3–10-minute breaks were provided between runs, and a maximum of 35 runs were performed in a day.

3.2.3 Kinematic analysis

Turns were identified using three criteria: (1) the animal had to exhibit a change in heading of >9 degrees, (2) the cuttlefishes had to turn primarily in the x-z plane, and (3) the turn had to be visible in both the dorsal view and at least one of the lateral views. Landmarks on the animal's body (7 points in dorsal view, 6 points in lateral view; Fig 7A,B) were then digitized using motion tracking software (Hedrick, 2008). Cross-validation-criteria or mean squared error

techniques were used to smooth data before kinematic measures were calculated (Walker, 1998). The tracked points were used to calculate the mean angular velocity throughout the turn (ω_{ave}) and maximum angular velocity during the turn (ω_{max}). To control for outliers and tracking error, the top 10% of values of angular velocity were removed to determine ω_{max} for each turn.

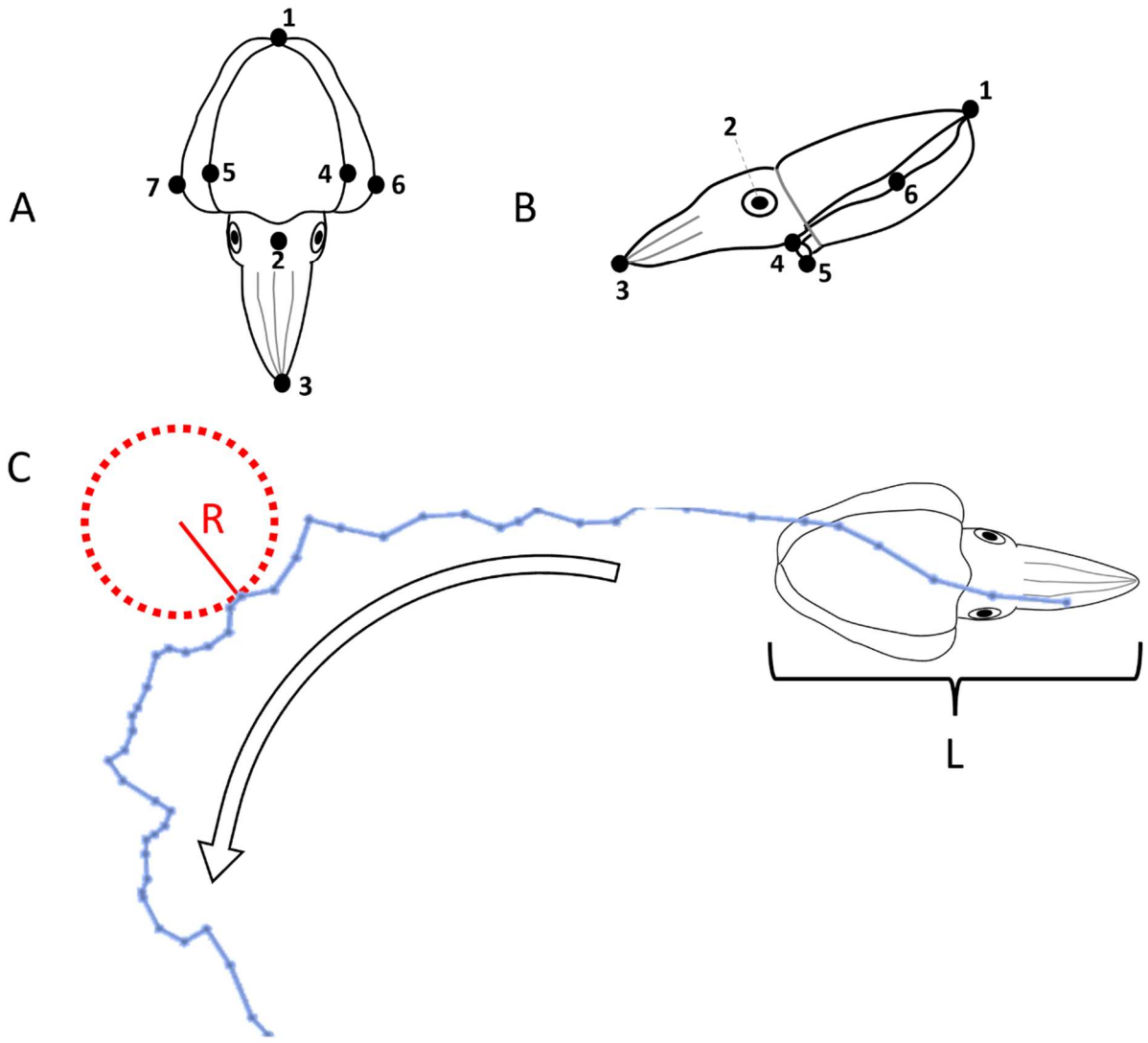

Fig 7. Illustration of adult *Sepia bandensis* kinematic measurement methods. (A) Points for body tracking in the dorsal view. **(B)** Points for body tracking in the lateral view. **(C)** Illustration from a turn in which the center of rotation (COR) points are overlayed in blue. The radius (*R*) of the COR path was measured throughout the turn, averaged, and divided by total length of the animal (*L*) to compute a length-specific radius (*R/L*). The white arrow depicts the direction of the turn.

The center of rotation (*COR*) was calculated between each frame using tracked points, where the *COR* was defined as the point in the dorsal view that moved the least during the turn. The radius of curvature of the *COR* (*R*) was calculated using:

$$(7)\ \frac{1}{\mathrm{R}} = \frac{\mathrm{z}''}{[1 + (\mathrm{z}')^2]^{3/2}}$$

where $z' = dz/dx = \dot{z}/\dot{x}\,, z'' = d^2z/dx^2 = (\dot{x}\ddot{z} - \dot{z}\ddot{x})/\dot{x}^3$, x and z are the coordinates of the COR in the dorsal view, t is time, the over dot represents time differentiation, and the derivatives were evaluated using fourth-order accurate finite difference equations (Fig 1C). Mean *R* for each turn sequence was calculated. To control for outliers and errors in tracking, the bottom 10% of *R* values were removed for each sequence to determine R_{min}. All *R* were standardized for animal length (*L*) to control for size differences, resulting in measures of average length-specific turning radius [$(R/L)_{mean}$] and minimum length-specific turning radius [$(R/L)_{min}$].

3.2.4 Hydrodynamic analysis

Defocusing Digital Particle Tracking Velocimetry (DDPTV) was used to quantify flow fields around turning cuttlefishes. Details on processing parameters can be found in Bartol et al. (2016; 2019; 2022; 2023). In general, 10,000-25,000 (some up to 70,000) velocity vectors were found per image using a 16 mm voxel, 75% voxel overlap, and smoothing factor of 1. For a given turn sequence, the frame where vorticity had completely separated from the cuttlefishes body and where impulse was maximal was processed. For sequences with more than one jet pulse, the first jet pulse was analyzed, as it was the primary driver of the turn, and it did not include interaction effects from secondary vortices. Not all turns meeting the kinematic criteria above included resolvable propulsive flows, as vortex structures were sometimes out of or near the edge of the sampling volume. The body of the animal was removed with the mask feature in

TSI's V3V 4G software to reduce erroneous vectors associated with the illuminated body. All velocity/vorticity figures were produced in Tecplot 360 (Tecplot, Bellevue, WA, USA). Average jet velocity (U_{jave}), maximum jet velocity (U_{jmax}), jet length (L_ω), jet diameter (D_ω), jet impulse (**I**), and jet angular impulse (**A**) were calculated using an in-house MATLAB routine. Jet diameter (D_ω) was the average diameter of the vorticity core (defined as regions >90% of peak jet vorticity) of the leading vortex ring, measured perpendicular to the jet centerline. Jet length (L_ω) was the extent over which the jet vorticity field (perpendicular to D_ω) was over a specified threshold (20% of the maximum vorticity). Linear impulse (**I**) was calculated using the following equation:

$$(8)\ \frac{\boldsymbol{I}}{\rho} = \frac{1}{2}\int_{jet} \mathbf{x} \times \boldsymbol{\omega} dV$$

where **x** is the position vector and **ω** is the vorticity vector ($\omega = \nabla \times \mathbf{u}$ where **u** is the velocity vector and the partial derivatives were calculated using central differences), ρ is the fluid density, and the integral was computed over the volume of the vortex, V, where the vorticity is non-zero (Saffman, 1995). Angular impulse (**A**) was calculated using the following equation derived from Wu et al., (2007):

$$(9)\ \frac{\mathbf{A}}{\rho} = -\frac{1}{2}\int |\mathbf{x}|^2 \boldsymbol{\omega} dV$$

By default, **A** associated with a vortex selected for analysis was computed with respect to the centroid of the vorticity magnitude of the vortex using the above equation. To determine **A** about the center of mass of the cuttlefishes, the origin of the calculated impulse was shifted (by moving the origin of **x**) to the cuttlefishes center of mass using the distance between the center of mass of the animal and the centroid of the vortex (determined from the custom MATLAB routines) in

accordance with Eq. 9. Given that cuttlefishes were primarily turning in the x–z plane, $\mathbf{A_{yaw}}$ was the focus of this study, although $\mathbf{A_{pitch}}$ and $\mathbf{A_{roll}}$ were also measured.

3.2.5 Statistics

Statistics were done in SPSS (IBM, v 28.0.0). All variables failed the Shapiro-Wilks normality test and required transformation. Most variables were log10 transformed to fit assumptions. However, maximum angular velocity (ω_{max}) and L_ω/D_ω failed normality testing with log10 transformations and were instead transformed using appropriate lambda from Tukey's ladder transformations. The absolute value of angular impulses for yaw, roll, and pitch were used for analysis, as magnitude, regardless of direction, was of interest. A three-way MANOVA was performed on transformed kinematic data to test for differences in test animal, turn orientation, and dataset. Dataset denotes whether the turn had associated high-quality hydrodynamic data or not. This variable was considered to test for bias in kinematic metrics when the added requirement of high-quality flow data is used. A separate two-way MANOVA was completed on transformed flow field data to test for differences in test animal and turn orientation. The Pillai's Trace statistic was used to determine significance as suggested for uneven group sizes. Follow-up ANOVAs and Tukey Post-Hoc tests were performed when necessary (e.g., test subjects) to determine where significance occurred. Linear regressions were performed on untransformed data. All means are reported ± standard error of the mean (s.e.m) unless otherwise stated. Significance was determined using $\alpha \leq 0.05$.

3.3 RESULTS

A total of 186 turns from all 8 individuals was considered for kinematic analysis; 47 of these turns included high-quality 3D velocimetry data and were considered further for hydrodynamic analysis. One cuttlefish (L =5.2 cm) did not produce high-quality 3D velocimetry data, and thus was only considered for kinematic analyses. Of the 186 total turns, 72.6% were performed in an arms-first orientation, and 27.4% were performed in a tail-first orientation.

3.3.1 Kinematic variables

The mean length specific turning radius [$(R/L)_{mean}$] across all cuttlefishes was 0.14 ± 0.013, with a range of 0.0107-1.16; the mean minimum length specific turning radius [$(R/L)_{min}$] was 0.013 ± 0.002, with a range of 0.00036 - 0.20. The average angular velocity (ω_{ave}) of turns was 45.85 ± 2.70 deg s^{-1}, with a range of 5.53 - 254.77 deg s^{-1}. The mean maximum angular velocity (ω_{max}) reached during turning was 110.34 ± 7.09 deg s^{-1}, with a range of 24.97 - 910.49 deg s^{-1}. In addition, there was a significant positive relationship between ω_{ave} and $(R/L)_{mean}$ (linear regression, $F_{1,185}$=24.61, $p<0.001$, R^2=0.118, Fig 8A), as well as a significant positive relationship between ω_{max} and $(R/L)_{min}$ for all turns (linear regression, $F_{1,185}$=115.97, $p<0.001$, R^2=0.387, Fig 8B).

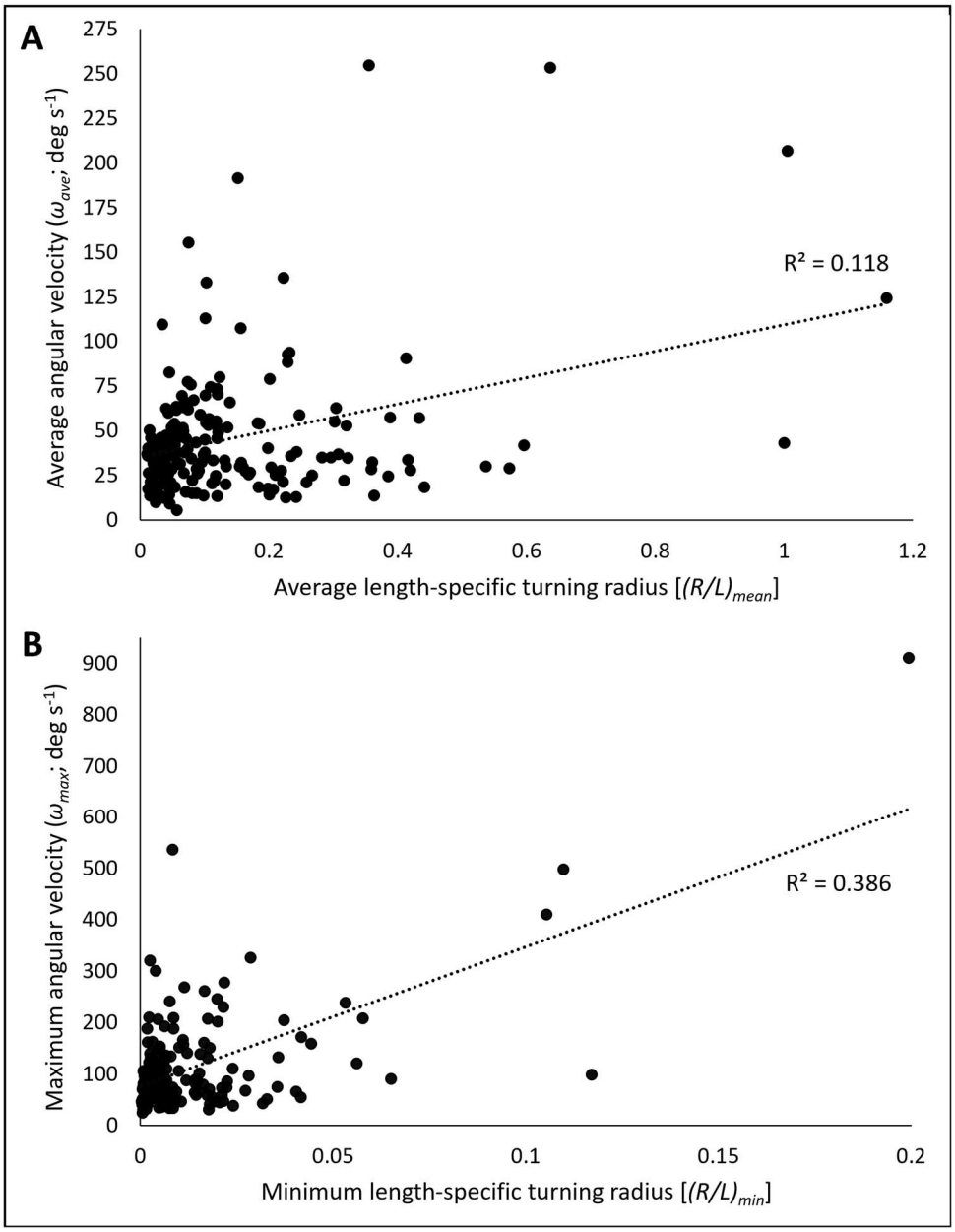

Fig 8. Regressions between angular velocity and turn radius. (A) The linear relationship between average angular velocity (ω_{ave}) and average length specific turning radius [$(R/L)_{mean}$]. **(B)** The linear relationship between maximum angular velocity (ω_{max}) and minimum length specific turning radius [$(R/L)_{min}$]. Significant regressions include trendlines and R^2 values.

When kinematic variables were analyzed, both test animal (MANOVA, $F_{28,632}$=1.838, p=0.006) and dataset type (i.e., kinematic only vs kinematic + hydrodynamic) were significant (MANOVA, $F_{4,155}$=3.547, p=0.008). Orientation was not significant (MANOVA, $F_{4,155}$=1.190, p=0.318), and there were no significant interaction factors (Table 1). Follow-up ANOVAs on test animal showed that individuals had significantly different $(R/L)_{mean}$ (ANOVA, $F_{7,186}$=5.770, p<0.001) and $(R/L)_{min}$ (ANOVA, $F_{7,186}$=5.155, p<0.001). When individuals were examined more closely, four cuttlefishes turned more tightly than the other four cuttlefishes (Fig. 9A,B). While not significant, it is interesting that the cuttlefishes that turned the fastest (ID #8, ω_{ave} =72.23, ω_{max} = 193.31 deg s^{-1}) also produced the widest turns ($(R/L)_{mean}$ = 0.381 $(R/L)_{min}$= 0.042; Fig 9). No significant difference in ω_{ave} (ANOVA, $F_{7,186}$=0.994, p=0.438) or ω_{max} (ANOVA, $F_{7,186}$=0.994, p=0.438) was detected among individuals (Fig 9C,D). Interestingly, ω_{ave} (ANOVA, $F_{1,186}$=10.360, p=0.002) and ω_{max} (ANOVA, $F_{1,186}$=9.238, p=0.003) were significantly lower for sequences with accompanying flow fields than those without, but no differences were detected for either $(R/L)_{mean}$ (ANOVA, $F_{1,186}$=0.091, p=0.400) or $(R/L)_{min}$ (ANOVA, $F_{1,186}$=0.012, p=0.817). For sequences with flow fields, ω_{ave} and ω_{max} were 32.34 ± 2.27 deg s^{-1} and 82.42 ± 5.79 deg s^{-1}, respectively; ω_{ave} and ω_{max} for sequences without high-quality flow fields were 50.55 ± 3.47 deg s^{-1} and 120.1 ± 9.21 deg s^{-1}, respectively (Fig 10A,B).

Table 1. MANOVA results for kinematic data. The symbol × indicates interaction effects and asterisks denote statistical significance.

Variable	**F**	**df**	**p**
Orientation	1.190	4,155	0.318
Individual	1.838	28,632	0.006*
Dataset	3.547	4,155	0.008*
Orientation × Individual	1.303	28,632	0.138
Orientation × Dataset	2.135	4,155	0.079
Individual × Dataset	1.465	24,632	0.071
Orientation × Individual × Dataset	1.352	16,632	0.160

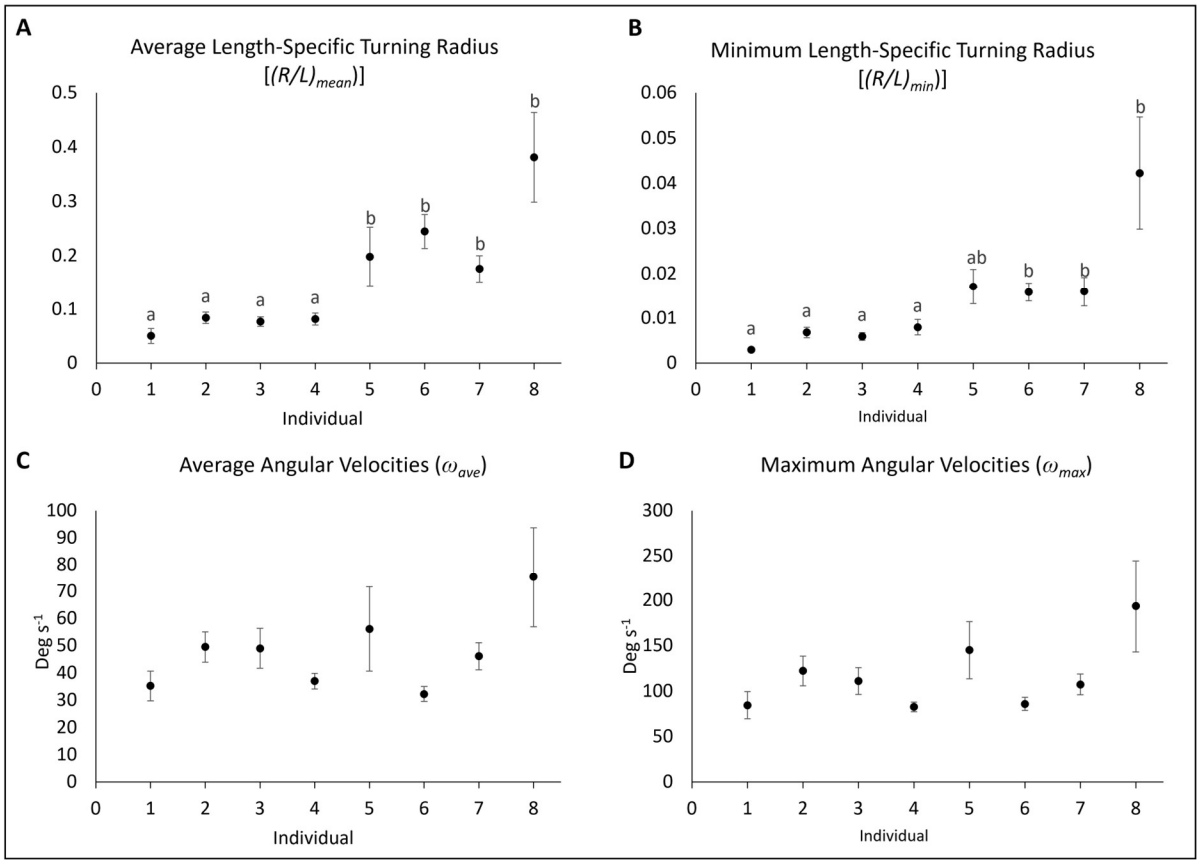

Fig 9. Individual-level difference in kinematic turning measures for *Sepia bandensis*. (A) The average length-specific turning radius $(R/L)_{mean}$ for each individual cuttlefish. **(B)** The average minimum length-specific turning radius $(R/L)_{min}$ for each individual cuttlefish. **(C)** The average angular velocity (ω_{ave}) of turns performed by individuals. **(D)** The average maximum angular velocity (ω_{max}) performed by individuals. Individual ID number is consistent throughout the figure and across figures (e.g., Fig 7), and all error bars are s.e.m. Significance is denoted by different letters, no significance was found in **C,D**.

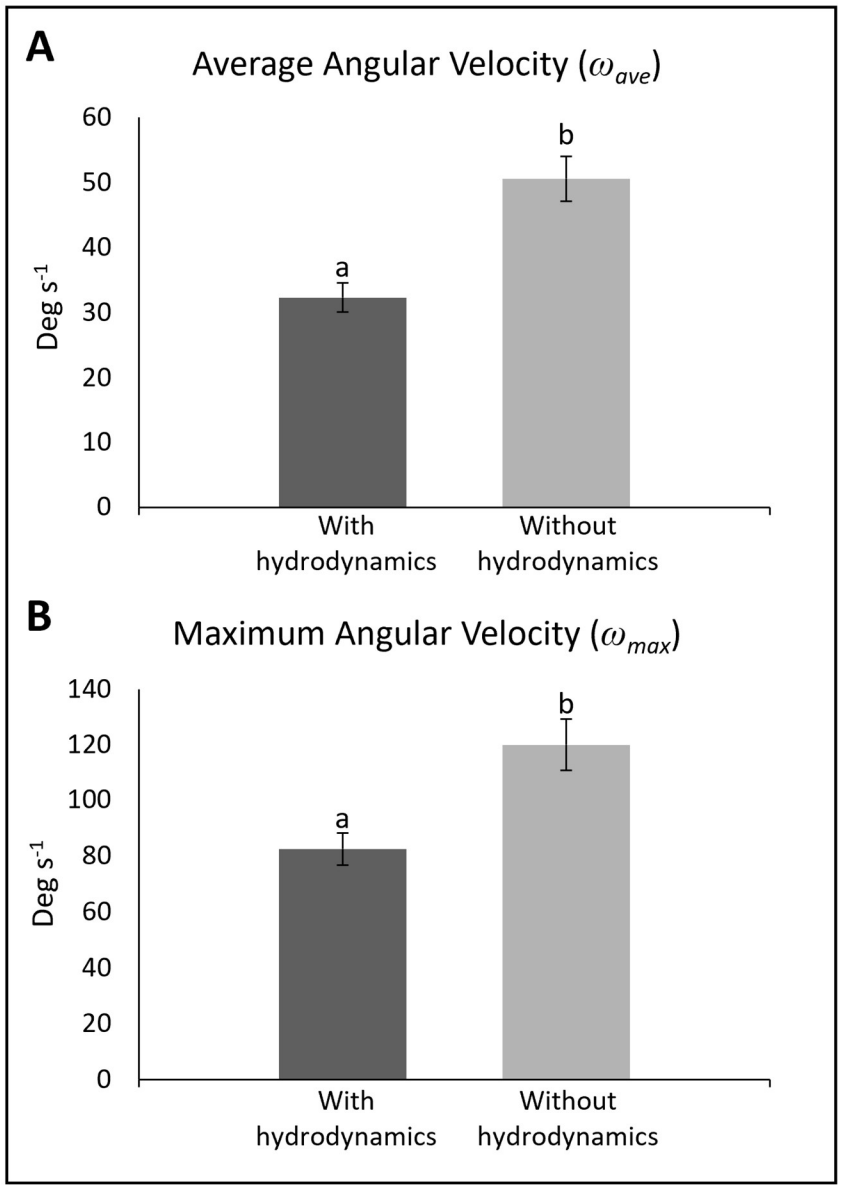

Fig 10. Kinematic measures between data sets. (A) The average angular velocity (ω_{ave}) of sequences with accompanying high-quality hydrodynamic data and without. **(B)** The average maximum angular velocity (ω_{max}) of sequences with accompanying high-quality hydrodynamic data and without. Error bars are standard error of the mean, and significance is denoted with different letters.

3.3.2 Hydrodynamic variables

Adult *Sepia bandensis* produced jets with a wide range of hydrodynamic signatures, including both *jet mode I* and *jet mode II*. Some jets had complex vorticity fields, such as multiple discrete rings, interconnected vortex rings, and elongated vorticity structures with vortex ring elements (Fig. 11). Although *jet mode II* and other modes were observed in some turning sequences, *jet mode I* was most prevalent, with short vortex rings often being produced in succession (Fig. 12). The average jet velocity (U_{jave}) was 14.11 ± 1.81 cm s^{-1} (range = 1.90 - 66.84 cm s^{-1}) and average maximum jet velocity (U_{jmax}) was 21.92 ± 2.57 cm s^{-1} (range of 3.28 – 91.75 cm s^{-1}). The average L_{ω}/D_{ω} for turning jets was 2.47 ± 0.18, with a range of 1.09-6.56.

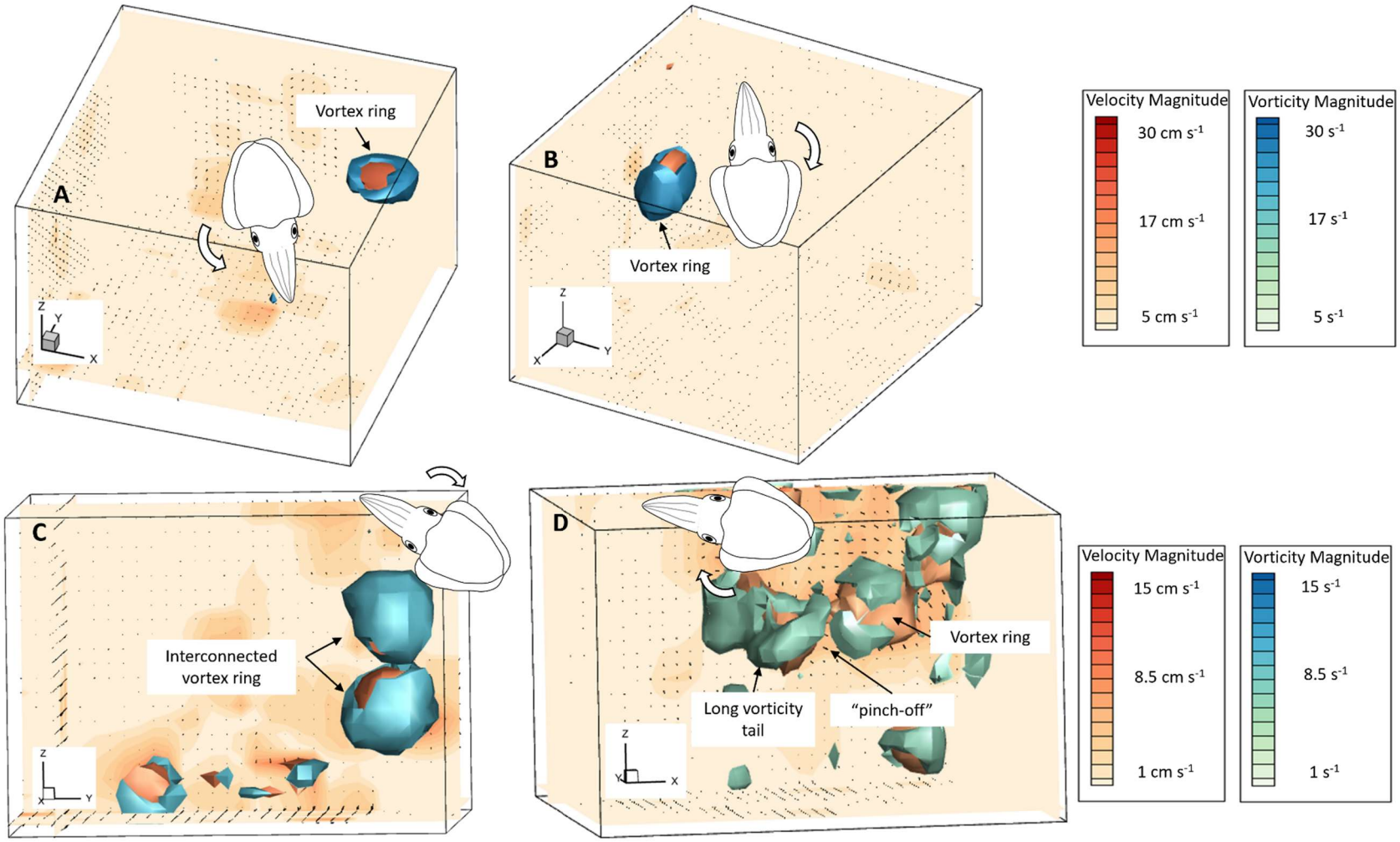

Fig 11. Examples of 3D velocity and 3D vorticity fluid flow produced by *Sepia bandensis* during turning. Velocity isosurfaces are shown in warm colors (orange/red), and vorticity isosurfaces are shown in cool colors (blue/green).

Fig 11. Continued. Note changes in vorticity and velocity scales among graphics. The cartoon illustrates the approximate location of the cuttlefish during the turn (not to scale). **(A)** An arms-first counterclockwise turn with a resulting single vortex ring. **(B)** A tail-first clockwise turn with a resulting single, slightly elongated vortex ring. **(C)** A tail-first clockwise turn with interconnected vortex rings. **(D)** An arms-first clockwise turn with a leading vortex ring and vorticity tail, which is pinched-off from the ring. **A** and **B** are considered *jet mode I*, and **C** and **D** are *jet mode II*.

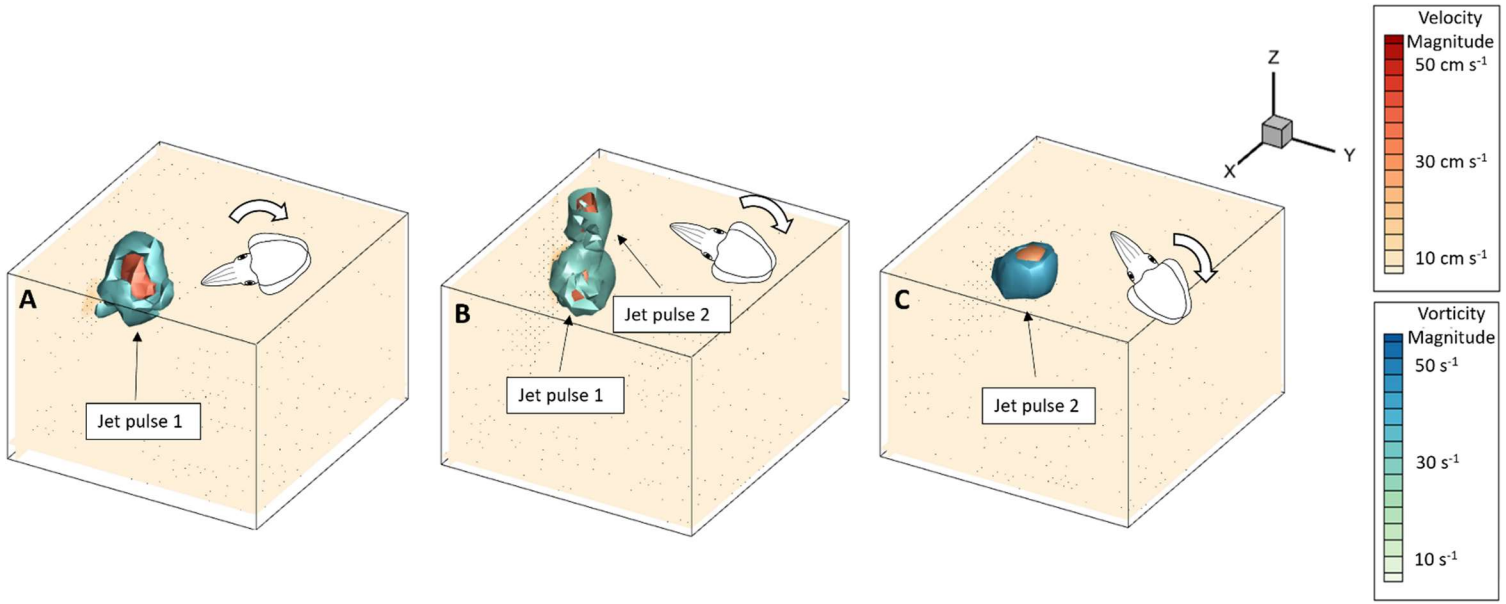

Fig 12. 3D Velocity and vorticity isosurfaces produced by *Sepia bandensis* during a turn. Velocity isosurfaces are shown in warm colors (orange/red), and vorticity isosurfaces are shown in cool colors (blue/green). The cartoon illustrates the approximate location of the cuttlefish during the turn (not to scale). This turn was completed with an average angular velocity of ~50 deg s^{-1} and an average length-specific radius of 0.02. **(A)** t=0 sec. The first jet pulse in the turn produces an isolated vortex ring that powers the beginning of the clockwise tail-first turn. **(B)** t=0.07 sec. A second jet pulse produces another vortex ring to further rotate the animal. **(C)** t=0.14 sec. The first jet pulse moves out of the sampling volume, and the second jet pulse is visible.

When hydrodynamic variables were analyzed, differences among test animals were significant (MANOVA, $F_{60,186}$=1.663, p=0.005), but turning orientation (MANOVA, $F_{10,26}$=1.220, p=0.324) and the interaction factor (MANOVA, $F_{40,116}$=0.875, p=0.680) were not. Follow-up ANOVAs indicated that there were significant differences in jet velocity (U_{jave}; ANOVA, $F_{6,186}$=6.237, p<0.001) and maximum jet velocity (U_{jmax}; ANOVA, $F_{6,186}$=5.376, p<0.001) among individuals (Fig 13A,B). The cuttlefish with the tightest turning capacity [ID #1, $(R/L)_{min}$ = 0.0013] produced some of the lowest jet velocities (U_{jave} = 2.74 cm s^{-1}, U_{jmax} = 4.80 cm s^{-1}) and angular velocities (ω_{ave} = 35.15, ω_{max} = 84.33 deg s^{-1}; Figs 9 and 13). One cuttlefish (ID #3) produced the highest U_{jave} (~32 cm s^{-1}) and a trend toward the highest U_{jmax} (~48 cm s^{-1}; Fig 13). There was no significant difference in the L_ω/D_ω across individuals (ANOVA, $F_{6,186}$=0.940, p=0.479). Linear regressions of L_ω/D_ω and angular velocity (ω_{ave}: $F_{1,46}$=0.0176, p=0.677; ω_{max}: $F_{1,46}$=1.606, p=0.212) and L_ω/D_ω and turning radius [$(R/L)_{mean}$: $F_{1,46}$=0.655, p=0.423; $(R/L)_{min}$: $F_{1,46}$=0.360, p=0.552] were not significant. Furthermore, linear regressions of jet velocity and turn tightness were insignificant for both average [U_{jave} vs $(R/L)_{mean}$: $F_{1,46}$=2.127, p=0.152] and extreme values [U_{jmax} vs $(R/L)_{min}$: $F_{1,46}$=0.687, p=0.412]. Jet velocity and angular velocity were also insignificant (U_{jave} vs ω_{ave}; $F_{1,46}$=1.597, p=0.213, R^2=0.034).

There were no significant differences in $\mathbf{A_{yaw}}$ (ANOVA, $F_{6,186}$=0.706, p=0.647), $\mathbf{A_{roll}}$ (ANOVA, $F_{6,186}$=1.403, p=0.241), and $\mathbf{A_{pitch}}$ (ANOVA, $F_{6,186}$=0.584, p=0.741) between individuals. The average $\mathbf{A_{yaw}}$ for all turns was $4.88 \times 10^{-3} \pm 1.02 \times 10^{-3}$ kg m^2 s^{-1} with a range of $2.55 \times 10^{-4} – 4.18 \times 10^{-2}$ kg m^2 s^{-1}. The average $\mathbf{A_{roll}}$ for all turns was $2.48 \times 10^{-3} \pm 4.08 \times 10^{-4}$ kg m^2 s^{-1} with a range of $8.44 \times 10^{-5} – 9.50 \times 10^{-3}$ kg m^2 s^{-1}. The average $\mathbf{A_{pitch}}$ for all turns was $2.98 \times 10^{-3} \pm 4.62 \times 10^{-4}$ kg m^2 s^{-1} with a range of $3.15 \times 10^{-5} – 1.35 \times 10^{-2}$ kg m^2 s^{-1}. $\mathbf{A_{yaw}}$ was 1.5-2 times higher than $\mathbf{A_{roll}}$ and $\mathbf{A_{pitch}}$, and there was a greater range of $\mathbf{A_{yaw}}$ than either $\mathbf{A_{roll}}$ or $\mathbf{A_{pitch}}$.

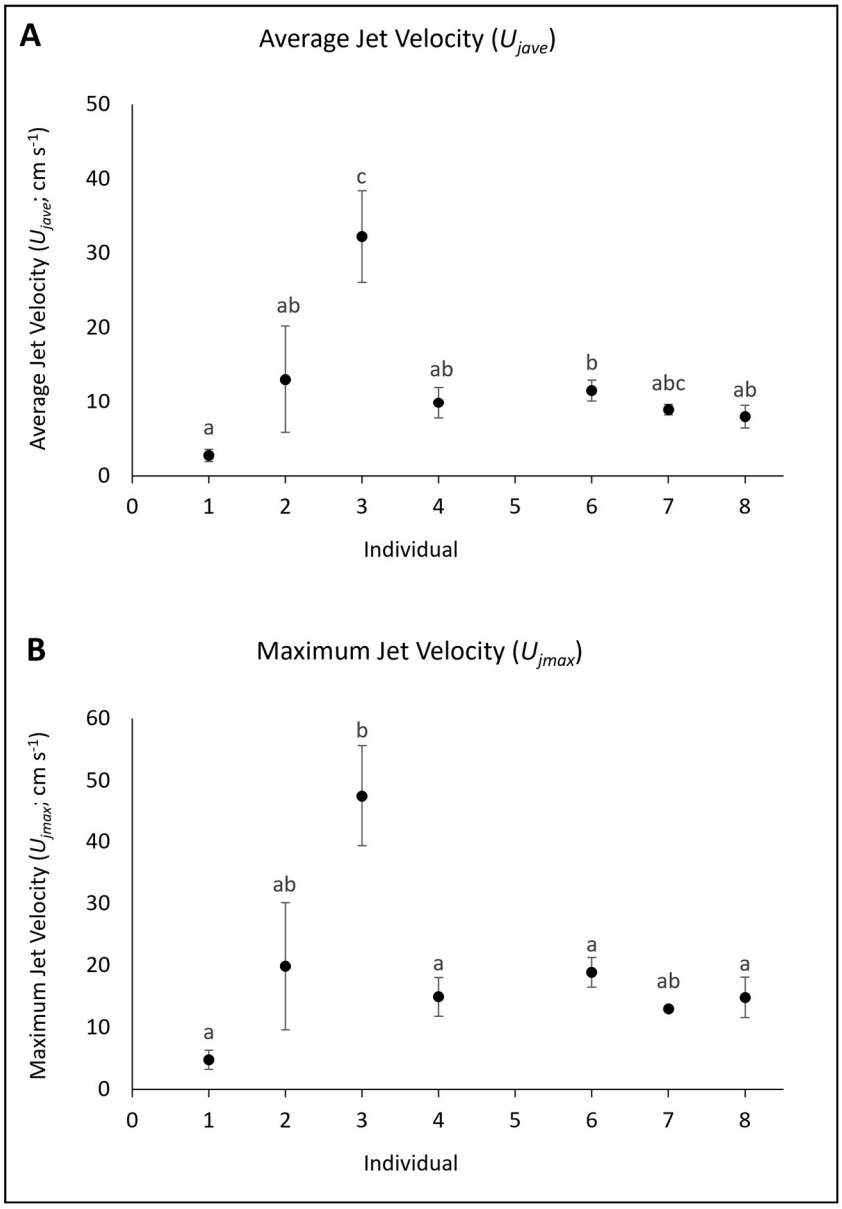

Fig 13. Jet velocities for individual *Sepia bandensis* during turns. (A) Average jet velocity (U_{jave}) for individuals. **(B)** Average maximum jet velocity (U_{jmax}) for individuals. Individual ID number is consistent throughout the figure and across figures. Note individual ID#5 did not produce wakes of sufficient quality to be included in the hydrodynamic analysis and was excluded. All error bars shown are s.e.m., and significance is denoted by different letters above points.

3.4 DISCUSSION

3.4.1 Relationships between turning kinematics and jet flows

In this study, an integrated kinematic and hydrodynamic analysis was used to quantify the turning ability of adult *Sepia bandensis*. The observed turning radii of *S. bandensis* [$(R/L)_{mean}$ ~0.14, $(R/L)_{min}$ ~0.013] are similar to tight turning squids [$(R/L)_{mean}$ ~0.15-0.20, $(R/L)_{min}$ ~0.006-0.020 (Bartol et al., 2022, 2023, Chapter 4)]. While Jastrebsky et al. (2016) reported lower turning radii [$(R/L)_{mean}$ ~0.09, $(R/L)_{min}$ ~0.001] for *S. bandensis*, this may be a product of turns being induced by prey targets, which potentially promotes tighter turns as animals maintain alignment with moving prey. Interestingly, the lowest $(R/L)_{min}$ value was similar across both studies [Jastrebsky et al (2016) = 0.00013, present study = 0.00036]. Tight turning is important for navigation in complex environments, such as reef systems where *S. bandensis* often resides, and for making fine adjustments for crypsis, which is critical for prey capture and predator avoidance (Hanlon and Messenger, 1996; Hanlon et al., 2018).

Sepia bandensis demonstrated angular velocities (ω_{ave} ~ 46 deg s^{-1}, ω_{max} ~110 deg s^{-1}) in reasonable agreement with those reported previously for this species (ω_{ave} ~ 55 deg s^{-1}, ω_{max} ~160 deg s^{-1}), and for longfin inshore squid *D. pealeii* (ω_{ave} ~ 27-38 deg s^{-1}, ω_{max} ~73-108 deg s^{-1}), and northern shortfin squid *I. illecebrosus* (ω_{ave} ~ 27-46 deg s^{-1}, ω_{max} ~70-82 deg s^{-1}), though ω for the present study are lower than for brief squid *Lolliguncula brevis* (ω_{ave} ~ 70-110 deg s^{-1}, ω_{max} ~140-268 deg s^{-1}; Jastrebsky et al., 2016; Bartol et al., 2022, 2023, Chapter 4). Given their small size (low rotational resistance) and heavy reliance on escape jetting, it seems reasonable that *L. brevis* would display high angular velocities (Finke et al., 1996; Good et al., 2023; Hanlon et al., 1983). Interestingly, the highest ω_{max} recorded in the present study (910.5 deg s^{-1}) was significantly larger than that recorded previously for cuttlefishes (485 deg s^{-1}; Jastrebsky et al.,

2016) or squids (726 deg s^{-1}; Bartol et al., 2022). Therefore, while *S. bandensis* does not routinely perform fast turns, it can reach high angular velocities when needed.

The first hypothesis of this study was not supported, as tighter turns were not associated with lower L_ω/D_ω and U_j, and faster turns were not linked to higher L_ω/D_ω and U_j. Indeed, neither L_ω/D_ω nor U_j, on their own, were reliable predictors of the turn type. Given that most jets were short ($L_\omega/D_\omega < 4$) and only one jet had an $L_\omega/D_\omega > 5$, it is not surprising that a strong relationship between L_ω/D_ω and either R/L or ω was found, as the spread of data was limited. However, the range of U_j was significant, and thus the absence of a relationship between U_j and ω or U_j and R/L was unexpected. One confounding factor may be jet frequency, which was not measured in the present study. In squids, ω increases with jet frequency, and ω is affected by multiple factors that include not only jet frequency, but U_j and L_ω/D_ω as well (Bartol et al., 2023). A similar combination of factors may be at work in the present study, making it difficult to isolate any one jet factor in turn performance.

3.4.2 Orientation

Although prior studies of squids have found differences in kinematic and hydrodynamic properties according to turn orientation (Bartol et al., 2022, 2023), a consistent orientation effect was not found in these cuttlefishes, providing support for the study's second hypothesis (that orientation will play a more reduced role in turning). In squids, such as *L. brevis* and *I. illecebrosus,* $\mathbf{I}$, $\mathbf{A_{yaw}}$, U_j, and L_ω/D_ω are greater during tail-first turns than arms-first turns, resulting in higher angular velocities but wider turning radii (Bartol et al., 2022; Bartol et al., 2023). Although R/L is lower for arms-first turns and $\mathbf{A_{yaw}}$ and L_ω/D_ω are generally higher during tail-first turns in the squid *D. pealeii* as well, ω_{ave} and ω_{max} can be greater during arms-first turns

when high-impulse, high-velocity jets are employed (Bartol et al., 2023). For squids, turning tightly in the arms-first orientation is beneficial for steering through complex or uncertain environments, when aligning with prey targets, and during periods of high vigilance, all of which require fine corrections in heading. Alternatively, turning quickly in the tail-first orientation is important for escape, high-speed cruising, vertical migrations, and schooling, when sudden powerful course corrections are required (Bartol et al., 2023). Cuttlefishes have less need for a high-powered tail-first 'mode' because they do not cruise at high speeds, undergo rapid vertical migrations, or school to the extent observed in squids (Hanlon and Messenger, 2018). Indeed, having the capacity to turn with equal proficiency in both orientations is well suited for a cuttlefish's lifestyle, whereby it engages in ambush-style hunting, maneuvers in complex habitats, and escapes from a multitude of predators within a densely populated reef community (Catano et al., 2015; Catano et al., 2016; Rizzari et al., 2014) – behaviors that can all benefit from turning in either orientation. While squids must also hunt and escape, their hunting strategies tend more towards tail-first pursuits before reorienting for striking, and escape jetting is often not constrained as much by a complex habitat, therefore limiting the need for equal performance in both orientations. Furthermore, funnel muscle constraints are thought to contribute to orientation-based performance differences in squids (Bartol et al., 2001a; 2023; Stewart et al., 2010; Kier and Thompson, 2003). Given the lack of significant orientation differences in kinematic or hydrodynamic properties, the radial and longitudinal funnel musculature of cuttlefishes may differ from that of squids, perhaps providing greater force for funnel curvature and aperture control. This is an area of investigation worth exploring further

3.4.3 Jet characteristics

While *S. bandensis* produced a variety of jet wake signatures during turns, the predominant jet pattern was short (L_ω/D_ω of ~2.5) vortex rings (*jet mode I*), often in succession, with this pattern occurring in > 85% of turns. This high reliance on *jet mode I* supports the study's third hypothesis (that *Sepia bandensis* will rely more heavily on *jet mode I* and lower jet velocities than squids). Due to the low number of *jet mode II* flows, it was not possible to accurately determine the transition L_ω/D_ω between *jet mode I* and *II*, i.e., *F* or the physical limit of vortex formation (Gharib et al., 1998; Krueger and Gharib, 2003). However, the observed mean L_ω/D_ω (~2.5) was below the *F* (3-4) reported for other cephalopods (Bartol et al., 2016; Bartol et al., 2022; Bartol et al., 2023), which is consistent with the high prevalence of *jet mode I.* Hatchling *S. bandensis* and *S. officinalis* also show a preference for *jet mode I* during turns (76-82%; Chapter 2). However, this heavy reliance on *jet mode I* differs from patterns observed in adult squids, such as *L. brevis, D. pealeii, and I. illecebrosus*, where a more balanced mix of *jet modes I* and *II* are employed during turns and where mean L_ω/D_ω is >3.3 (Bartol et al., 2023). This difference may occur because the cuttlebone limits relative mantle volumes in cuttlefishes, resulting in shorter overall jet pulses. Indeed, *jet mode I* is observed more often in adult *S. officinalis* (relative to squids) during rectilinear swimming as well (Gladman and Askew, 2023), providing support for this hypothesis. In rectilinear swimming, smaller jets can increase propulsive efficiency, while longer jets are used to maximize power and speed output (Bartol et al., 2008; Bartol et al., 2009a; Bartol et al., 2009b; Bartol et al., 2016; Bartol et al., 2022; Bartol et al., 2023). Thus, greater reliance on *jet mode I* in cuttlefishes may offer improved energy use during turns. Shorter, vectored jets also provide more controlled impulse throughout the turn path (Bartol et al., 2022; 2023), and small jets are beneficial when sneaking up on prey or

avoiding predators because of a reduced flow signature compared to longer jets (e.g., *jet mode II*).

The observed jet velocities (U_{jave} ~14 cm s^{-1}, U_{jmax} ~ 22 cm s^{-1}) are slightly higher than those recorded for some adult squids during turning maneuvers, such as *L. brevis* (U_{jave} ~11 cm s^{-1}, U_{jmax} ~ 17 cm s^{-1}) and *I. illecebrosus* (U_{jave} ~10 cm s^{-1}, U_{jmax} ~ 15 cm s^{-1}), but lower than those reported for other squids, such as *D. pealeii* (U_{jave} ~38 cm s^{-1}, U_{jmax} ~ 62 cm s^{-1}; Bartol et al., 2022, 2023). Along with heavy reliance on *jet mode I,* lower U_j for cuttlefishes was expected (third hypothesis) because cuttlefishes swim slower and rely more heavily on their fins than neritic squids (Hoar et al., 1995). However, our data did not support this, with U_j being fairly similar to *L. brevis* and *I. illecebrosus*. Short but moderately fast jets are advantageous for turning, as they provide focused, repetitive impulses for sustaining and controlling rotation. In contrast to negatively buoyant squids, *S. bandensis* does not need to use its jet to counteract sinking. Rather, it can allocate more jet flow to angular impulse (**A**) to effect the turn. The observed higher $\mathbf{A_{yaw}}$ relative to $\mathbf{A_{roll}}$ and $\mathbf{A_{pitch}}$ is not surprising given that the selected turns were performed primarily in the yaw plane. For the brief squid *L. brevis*, the fins and arms play important roles in $\mathbf{A_{yaw}}$, $\mathbf{A_{roll}}$, and $\mathbf{A_{pitch}}$, contributing angular impulse to effect the turn, stability, and, in the case of the arms, reduced rotational resistance when they are pulled close to the body (Bartol et al., 2022). Fin flows were not easily resolvable in the present study because the fins were small (and transparent) and flows tended to stay close to the brightly lit body, making it difficult to track fin-induced particle fields. The role of the arms in turns was also not quantified. However, the fins were actively undulating during turns and the arms were often curled or extended in a conical shape. Therefore, it is likely that both appendages contribute to turn performance, as is the case with squids. Subsequent studies incorporating flow quantification

techniques that can isolate and track particles superimposed on the body would provide valuable insights on the role of the fins and arms of cuttlefishes during turns.

3.4.4 Other findings

The strong positive relationship between R/L and ω was expected given this relationship has been documented in *S. bandensis* hatchlings (Chapter 2) and in other taxa (Fish, 2002; Fish and Nicastro, 2003; Fish et al., 2003; Fish et al., 2018; Jastrebsky et al., 2016; Maresh et al., 2004; Parson et al., 2011; Rivera et al., 2006; Sutherland et al., 2019a; Chapter 4). This relationship has not been documented consistently in squids, however, possibly because of high behavioral variability (Bartol et al., 2022; Bartol et al., 2023; Jastrebsky et al., 2016; Chapter 4). Relative to hatchlings where $(R/L)_{mean} = 0.67$ and $\omega_{ave} = 38$ deg s^{-1} (Chapter 2), adult *S. bandensis* in the present study turned more tightly (lower R/L) and more quickly (higher ω). Lower ω for *S. bandensis* hatchlings is surprising given smaller animals generally have lower moments of inertia and higher ω than larger swimmers (Fish et al. 2018; Fish and Holzman 2019). Greater agility, i.e., higher ω, and greater maneuverability, i.e., lower R/L, in adults relative to hatchlings may derive from greater muscle development, increased neural control, and more developed fins, which occur at older life stages (Dickel et al., 2006; Kier and Thompson, 2003; Kobayashi et al., 2013; Liu et al., 2017; Thompson and Kier, 2001; Thompson and Kier, 2006).

There were differences in turning performance among individual *S. bandensis*, with two main groups identified in this study: one group that turned with $R/L_{mean} < 0.10$, and another group that turned with $R/L_{mean} > 0.15$, including one cuttlefish (ID #8) that exclusively turned broadly with high angular velocity. Aside from this extremely fast and broad-turning individual,

most cuttlefishes had ω_{max} = 75-150 deg s^{-1}, reflecting their preference for relatively slow routine turns. This makes sense when viewed with an ecological lens, as slow, tight turns are necessary for routine behaviors, such as navigation in challenging environments, tracking prey, and communicating with conspecifics (Bartol et al., 2022; Bartol et al., 2023; Hanlon and Messenger, 1996; Hanlon et al., 2018). Hydrodynamic parameters also varied greatly across individual *S. bandensis*, with each cuttlefish producing a large range of L_ω/D_ω and $\mathbf{A_{yaw}}$. Most cuttlefish produced jets with relatively low U_{jave} and U_{jmax}, including one cuttlefish (ID #1) who had the lowest average minimum turning radius [$(R/L)_{min}$=0.0013] and some of the slowest angular and jet velocities (ω_{ave}=35.15 deg s^{-1}; U_{jave}=2.74 cm s^{-1}). However, one cuttlefish had high jet velocities and still managed to turn relatively tightly. This cuttlefish (ID #3) had U_{jave} > 30 cm s^{-1} and U_{jmax} ~45 cm s^{-1} (Fig 7). The high jet velocities translated to moderately high angular velocities (ω_{ave} ~ 50) and a fairly tight turning radius [$(R/L)_{mean}$ ~0.07], suggesting that short, high-velocity, vectored jets can be effective for controlled, high spin rate turns.

Higher angular velocities for sequences without captured flow fields relative to those with flow fields was unexpected. These differences cannot be easily explained by laser-induced behavioral differences, as laser pulsing was present throughout all data collection periods. However, it is conceivable that the bias toward lower angular velocities (for sequences with captured flow fields) is a product of limitations in detecting higher-velocity jets that are presumably necessary for fast turns. Difficulties in detecting these jets could derive from an insufficiently short Δt or limitations in the 3D particle tracking algorithms. Although missing vectors in the regions of jets were rare and higher jet velocities have been detected using similar equipment and Δt's (Bartol et al., 2023), it is possible that some particle displacements were sufficiently large to go undetected. It also may be that sampling volume size (14 cm x 14 cm x

10 cm) excludes some longer jet wakes used for high angular velocity turns, as only vortex flows that were fully visible and away from sampling volume boundaries were considered. Irrespective of the underlying cause, the observed difference in angular velocity between the datasets suggests that there may be some bias in kinematic data when flow quantification data are collected simultaneously. Indeed, kinematic differences in datasets collected with and without flow field measurements have been reported in prior squids studies as well (e.g., see Bartol et al., 2023, Chapter 4).

3.4.5 Comparison to other nekton

Sepia bandensis turned more tightly (lower *R/L*) than most non-cephalopod swimmers but turned slower (intermediate ω) than most taxa (Table 2). The jet-propelled moon jelly, *Aurelia aurita*, is able to complete turns of relatively high angular velocities (ω_{max} ~400 deg s^{-1}) using asymmetric bell contraction to produce propulsive jets (Costello et al., 2021; Dabiri et al., 2020; Gemmell et al., 2015). Another jet-propelled swimmer, the common siphonophore *Nanomia bijuga*, produces turns with $(R/L)_{mean}$ = 0.15 and reaches average ω_{max} = 215 deg s^{-1} (Sutherland et al., 2019a). While *N. bijuga's* average $(R/L)_{mean}$ is similar to that of *S. bandensis* [$(R/L)_{mean}$ = 0.142], *S. bandensis* achieves tighter turns at its performance extremes [*N bijuga*: minimum $(R/L)_{min}$ = 0.05, *S. bandensis*: minimum $(R/L)_{min}$ = 0.0036; Table 2]. Animals that do not use jet propulsion are also capable of tight turns, including the leopard shark, *Triakis semifasciata*, with average $(R/L)_{min}$ = 0.006 (Porter et al., 2011), which is lower than that reported in the present study for *S. bandensis* [average $(R/L)_{min}$ = 0.0128].

Table 2. Compiled turning metrics for different taxa. Values that were calculated from data presented in the paper are proceeded by "~" and species with an asterisk use jet propulsion. Grey highlighted data is from this chapter.

Species	Average R/L_{mean}	Average R/L_{min}	Minimum R/L_{min}	Average ω_{mean} (deg s^{-1})	Average ω_{max} (deg s^{-1})	Maximum ω_{max} (deg s^{-1})	Study
*Lolliguncula brevis**	0.009	0.0034	0.00042	110.3	268.4	725.8	Jastrebsky et al 2016
Ostracion meleagris	--	--	0.0005	--	--	218.4	Walker 2000
*Sepia bandensis**	0.095	0.0012	0.00013	54.8	160.2	485	Jastrebsky et al 2016
Triakis semifasciata	--	0.006	--	--	~300.2	--	Porter et al 2011
*Sepia bandensis**	0.142	0.0128	0.00036	45.85	100.34	910.5	Present study
Chrysemys picta	--	--	0.0018	--	--	291.6	Rivera et al 2006
*Sepia officinalis**	--	--	--	~115	--	--	Messenger 1968
*Nanomia bijuga**	0.15	---	0.05	104	215	363	Sutherland et al 2019
*Doryteuthis pealeii**	0.16	0.011	---	36.12	82.36	269.66	Ganley et al 2023
*Illex illecebrosus**	0.19	0.015	---	48.19	108.73	255.66	Ganley et al 2023
*Aurelia aurita**	--	--	--	--	~400	--	Dabiri et al 2020
Zalophus californianus	--	0.11	0.09	---	599	690	Fish et al 2003
*Illex illecebrosus**	--	0.5	--	90	--	--	Foyle and O' Dor 1987
Tursiops truncatus	0.21	--	0.08	561	--	1,372	Maresh et al 2004
Thunnus albacares	0.47	--	0.2	--	--	--	Blake et al 1995
Dineutes horni	0.86	--	0.24	1,690.2	--	4,428	Fish and Nicastro 2003

The spotted boxfish, *Ostracion meleagris*, has been observed turning with $(R/L)_{min}$ of 0.0005, which is the tightest length-specific turning radius reported for non-jet propulsors, but is slightly wider than the tightest turns completed by *S. bandensis* and *L. brevis* (Jastrebsky et al., 2016; Walker, 2000). Similarly, the painted turtle, *Chrysemys picta,* has an $(R/L)_{min}$ = 0.0018 at its performance extreme (Rivera et al., 2006), which is significantly larger than the minimum $(R/L)_{min}$ reported in the present study for *S. bandensis*. While *S. bandensis* turns tightly, it does so generally at low angular velocity. With an average ω_{max} of 110 deg s^{-1}, *S. bandensis* turns slower than the jet-propelled siphonophore *N. bijuga* (215 deg s^{-1}), brief squid *L. brevis* (268 deg s^{-1}), the leopard shark *T. semifasciata* (~300 deg s^{-1}), and moon jelly *A. aurita* (~400 deg s^{-1}) (Dabiri et al., 2020; Jastrebsky et al., 2016; Porter et al., 2011; Sutherland et al., 2019). Interestingly, *S. bandensis* in the present study reached higher extreme ω_{max} than all the previously mentioned taxa, indicating that *S. bandensis* is capable of high-speed turns, but does not employ them often. This may be due to their use of crypsis as a first line of defense, which is often successful, eliminating the need for quick escape turns (Bedore et al., 2015; Hanlon and Messenger, 1996). However, both bottlenose dolphins *Tursiops truncatus* (1,372 deg s^{-1}) and whirligig beetles *Dineutes horni* (4,428 deg s^{-1}) reach much higher ω_{max} at their extremes than *S. bandensis*, although these fast-turning species have higher length-specific turning radii (*T. truncatus*: $(R/L)_{mean}$ = 0.21, *D. horni*: $(R/L)_{mean}$ = 0.86; Fish and Nicastro, 2003; Maresh et al., 2004) than *S. bandensis*.

3.4.6 Conclusions

Little is known about the kinematics and hydrodynamics of turning cuttlefishes. The integrated approach (body tracking and 3D flow quantification) used in this study demonstrated

that adult *Sepia bandensis* turn tightly but relatively slowly using short jet pulses, with orientation (arms-first vs tail-first) not having a significant effect on performance or jet properties. Wake patterns were similar to those seen in other jet-propelled animals, but *S. bandensis* relied more heavily on *jet mode I* (>80% of turns), where jet flows rolled up into isolated vortex rings, and produced fewer complex jet signatures than squids. By using short ($L_\omega/D_\omega < 3$), vortex ring-based jets (*jet mode I*) in succession, *S. bandensis* achieved turns with *R/L* as low as 0.00036, which is among the lowest $(R/L)_{min}$ measured to date. These tight turns come with a trade-off, as *S. bandensis* generally completed these turns at low to moderate ω. For broader turns, *S. bandensis* exhibited higher angular velocity, with ω_{max} >900 deg s^{-1}.

CHAPTER 4

FASTER IS NOT ALWAYS BETTER: TURNING PERFORMANCE TRADE-OFFS IN THE INSHORE SQUIDS *DORYTEUTHIS PEALEII* AND *ILLEX ILLECEBROSUS*

PREFACE

The content of this chapter is published in the Journal of Experimental Marine Biology and Ecology April 2023 (https://doi.org/10.1016/j.jembe.2023.151913). Reprinted with permission from Ganley, A.M., Krueger, P.S., and I.K. Bartol. (2023). Faster is not always better: Turning performance trade-offs in the inshore squids Doryteuthis pealeii and Illex illecebrosus. Journal of Experimental Marine Biology and Ecology. 29 May 2023; 565: 10.1016/j.jembe.2023.151913.

4.1 BACKGROUND

Investigations of animal swimming abilities are widespread (Blake and Chan, 2006; Blake et al., 1995; Dabiri et al., 2020; Drucker and Lauder, 2001a; Drucker and Lauder, 2001b; Fountain, 1904; Gray, 1933; Parson et al., 2011; Porter et al., 2011; Rivera et al., 2006; Robinson, 1893; Russell and Steven, 1930; Verrill, 1874). In the marine environment, maneuverability (the ability to turn tightly) and agility (the ability to turn quickly) are critical for predator avoidance, prey capture, movement in complex environments, and even communication (Arnold, 1962; Bartol et al., 2001a; Foyle and O'Dor, 1988; Hanlon and Messenger, 1996; Hanlon et al., 1983; Hanlon et al., 2018; Jastrebsky et al., 2016; Jastrebsky et al., 2017; Messenger, 1968). There is growing interest in turning performance of soft-bodied animals that must rely on directed jets as opposed to fins or flippers, such as jellyfish, siphonophores, and

squids (Bartol et al., 2022; Dabiri et al., 2020; Gemmell et al., 2015; Jastrebsky et al., 2016; Sutherland et al., 2019a).

Described as a three step process, jellyfish turning involves a torque maximizing phase, a moment of inertia minimizing phase, and a final braking phase (Costello et al., 2021; Dabiri et al., 2020). Jellies use a stiffened inner margin of their bell to produce a strong pivot point around which they turn; coupled with enhanced outer margin bending and asynchronous contractions, jellies can produce turns up to ~400 deg s^{-1} (Dabiri et al., 2020; Petie et al., 2011). In contrast, siphonophores rely on division of labor to complete complex maneuvers. Younger nectophores positioned close to the apex of the colony and oriented at an angle, produce significant torque, as their position represents the moment lever extremes in the colony. Older nectophores positioned farther from the apex produce the forward momentum (Costello et al., 2015; Sutherland et al., 2019b). This strategy allows the siphonophore *Nanomia bijuga* to complete turns of 215±90 deg s^{-1} (average maximum angular velocity) with a length specific turning radius of 0.15±0.10 (Sutherland et al., 2019a).

The >800 species of cephalopods have more complex neurocircuitry and morphologies than other jet-propelled invertebrates. Squids, in particular, are incredibly diverse, with slow-moving pelagic forms, such as glass squid (Cranchiids) to fast swimming cruisers like the flying squid (Ommastrephiids) that can reach rectilinear speeds of 11.2 m s^{-1} and even glide in air (Clarke, 1962; Clarke et al., 1979; Hendrickson, 2004; Maciá et al., 2004; Muramatsu et al., 2013; Nigmatullin and Arkhipkin, 1998; O'Dor, 1988; O'Dor, 2002; O'Dor, 2013; O'Dor and Webber, 1991; O'Dor et al., 2013; Stewart et al., 2012; Webber et al., 2000). The ability to use two forms of propulsion (jet and fins) in tandem or alone set squids and cuttlefishes apart from other jet-propelled swimmers. Using this dual mode system, squids and cuttlefishes can hover,

turn tightly, ascend vertically, and even swim forward or backward. This ability to swim forward (oriented arms-first) as well as backward (oriented tail-first) is especially important for hunting because squids and cuttlefishes often use both swimming directions during prey approach, strike, and recoil (Foyle and O'Dor, 1988; Jastrebsky et al., 2017; Kier, 1982; Kier and Van Leeuwen, 1997; Messenger, 1968; Nicol and O'Dor, 1985). The tapered mantle tip together with a streamlined body reduces drag when swimming tail-first, making this orientation more desirable for fast swimming or long distances. However, some squids can also achieve a streamlined shape by holding their arms in a conical configuration while swimming arms-first (Anderson and DeMont, 2005; Bartol et al., 2001b; Bartol et al., 2001a; Bartol et al., 2022), although this likely has an associated muscular cost.

Switching swimming directions is facilitated by the flexible funnel of cephalopods. The funnel, which includes longitudinal, circular, and radial muscles as well as the funnel retractor muscles, can be pointed in any direction underneath the animal for directed jetting (Kier and Thompson, 2003). This allows for jets to be generated at any angle under the animal, leading to propulsion in forward, backward, upward, and sideways directions. In addition, fins can either oscillate or undulate for propulsion, complementing the vectored jet. Squids and cuttlefishes fin morphologies vary greatly with fins of many shapes, sizes, and thicknesses, from thin skirt-like fins to large rhomboidal or lobate fins (Hanlon et al., 2018; Hoar et al., 1994; O'Dor et al., 1995). Many inshore squids decrease fin use with speed, often curling their fins around the mantle at the highest swimming speeds (O'Dor, 1988; Hoar et al., 1994; Bartol et al., 2001b). *Doryteuthis pealeii* (formerly *Loligo pealeii*) demonstrate two fin gaits: a slow-speed gait characterized by undulation and flapping and a fast-speed gait characterized by flapping motion and periods of fin inactivity whereby the fins curl around the mantle (Anderson and DeMont,

2005). *Lolliguncula brevis* exhibits similar fin transitions with speed (Bartol et al., 2001a, b), while also employing more wavelike fin movements during arms-first swimming compared to tail-first swimming (Bartol et al., 2019). Based on hydrodynamic signatures, four distinct fin modes occur in *L. brevis* during tail-first swimming: *fin mode I* where a single vortex is shed on the downstroke, *fin mode II* where undulatory movements create a linked chain of vortices, fin *mode III* in which a vortex is shed on each downstroke and upstroke, and *fin mode IV* where linked double vortices are produced. Only *fin modes II* and *III* occur during arms-first swimming (Stewart et al., 2010).

Little is known quantitatively about the turning dynamics and kinematics of most species of cephalopods. Foyle and O'Dor (1988) reported average angular velocities of 67-139 deg s^{-1} for the shortfin squid, *Illex illecebrosus,* during hunting, and maximum angular velocities of 300 deg s^{-1}. During hunting, dwarf cuttlefish, *Sepia bandensis,* turn at angular velocities ~ 110-120 deg s^{-1} (Messenger 1968). In a more recent study, Jastrebsky et al. (2016) found *S. bandensis* have average angular velocities of 55 deg s^{-1} and mean maximum angular velocities of 160 deg s^{-1} along the yaw axis, with some cuttlefishes reaching angular velocities as high as 485 deg s^{-1}. Squid *Lolliguncula brevis* exceeds *S. bandensis* in agility, exhibiting higher mean angular velocities (110.3 deg s^{-1}), but it is less maneuverable, with minimum length specific turning radii that are twice as large (Jastrebsky et al. 2016). Average minimum length specific turning radii for both *L. brevis* and *S. bandensis* (3.4×10^{-3} and 1.2×10^{-3}, respectively) are among the lowest values reported for any aquatic animal (Jastrebsky et al., 2016).

The longfin squid, *Doryteuthis pealeii,* and shortfin squid, *Illex illecebrosus,* differ ecologically, morphologically, and behaviorally, and they likely employ disparate turning strategies. Both *D. pealeii* and *I. illecebrosus* frequent neritic waters, but *D. pealeii* has a more

southern distribution, residing in waters as far south as the Gulf of Venezuela, and does not venture as far offshore as *I. illecebrosus* (Black et al., 1987; Brodziak and Hendrickson, 1999; Coelho et al., 1994; Dawe et al., 1981; Hendrickson, 2004; Squires, 1967). While both species are negatively buoyant, *I. illecebrosus* is more streamlined, smaller, and has narrower fins than *D. pealeii*. *Doryteuthis pealeii* grows to ~50 cm mantle length (*ML*), while *I. illecebrosus* reaches a maximum length of only ~35 cm *ML*. Weights of smaller *D. pealeii* and *I. illecebrosus* are very similar, with *I. illecebrosus* beginning to outweigh *D. pealeii* at around 20 cm *ML* (Lange and Johnson, 1981). *Doryteuthis pealeii* fins extend ~50% down the mantle and are rounded with low aspect ratios, whereas *I. illecebrosus* fins extend ~25-30% down the mantle and are triangular in shape with high aspect ratios. Triangular, high-aspect ratio fins are thought to be more useful for lift and gliding than maneuverability (Jereb and Roper, 2005; Jereb and Roper, 2010; Roper et al., 1984). In addition, these flexible, dorsally-positioned, triangular fins can be used effectively as rudders, whereas the longer, thinner, lower aspect ratio fins of *D. pealeii* are generally not used for this purpose (Hoar et al., 1994). Finally, *I. illecebrosus* is a faster rectilinear swimmer than *D. pealeii* (O'Dor and Webber, 1991; Webber and O'Dor, 1985). To date, little is known about the turning performance of either of these squids (but see Bartol et al., (2023) for a wake-based analysis of turning).

In this study, the kinematics of turns in *D. pealeii* and *I. illecebrosus* were examined, with the goal of quantifying key metrics like turning radius, angular velocity, fin and jet frequency, and arm angles. The objectives of this study were to investigate whether turning capabilities differ according to species (*D. pealeii* vs *I. illecebrosus*) and swimming direction (arms-first vs tail-first). *Illex illecebrosus* is hypothesized to exhibit higher angular velocities but larger turning radii than *D. pealeii* due to its faster swimming speeds and more streamlined

shape. In addition, turns that are oriented arms-first are predicted to have smaller length-specific turning radii but be slower (lower angular velocities) than tail-first turns. This prediction was based on tight turns being reported for arms-first swimming when approaching prey (Jastrebsky et al, 2017) and overall lower swimming speeds observed for arms-first swimming relative to tail-first swimming (Bartol et al., 2001a; 2016). Indeed, a trade-off between tighter and faster turns is expected, as this pattern is seen in other taxa (Fish and Nicastro, 2003; Sutherland et al., 2019b; Walker, 2000). Finally, tighter turns are predicted to correlate with greater fin activity, as fin motions presumably play important roles in complementing the jet to achieve low length-specific turning radii.

4.2 METHODS

4.2.1 Study species

In this study, 7 *Illex illecebrosus* (Lesueur 1821, Fig. 14A), and 29 *Doryteuthis pealeii* (Lesueur 1821, Fig. 14B) were used. Total length (*L*) of *D. pealeii* ranged from 10.8-28.0 cm, with a mean±s.e.m = 16.4±0.7 cm; *L* for *I. illecebrosus* ranged from 15.1-19.3 cm, with a mean of 17.4±0.6 cm. Squids were caught by jig or cast net in Boothbay Harbor, ME. Squids were kept in a flow-through race-way system (32 ppt and 18°C) at the University of Maine's Darling Marine Center (DMC) in Walpole, ME, and fed a diet of live baitfish caught by seine net (*Luxilus spp., Notropis spp., Pimephales spp.,* and *Semotilus spp.*). Individuals were easily distinguishable by *L* and/or by body markings. All research was conducted under IACUC #21-002.

4.2.2 Data collection

All experiments were performed at the DMC. Squids were placed in a plexiglass experimental chamber (64cm x 64cm x 64cm) filled with aerated and filtered saltwater (32ppt and 18°C). The chamber was illuminated using a series of halogen lights with spectral filters to produce red (>620nm) wavelengths. One Dalsa Falcon camera (Teledyne Dalsa, Inc., Waterloo, ON, Canada; 1400×1200 pixels, 100 frames s^{-1}) was positioned dorsally, and two other Falcons were positioned laterally. The cameras were outfitted with lenses ranging from 9-25 mm.

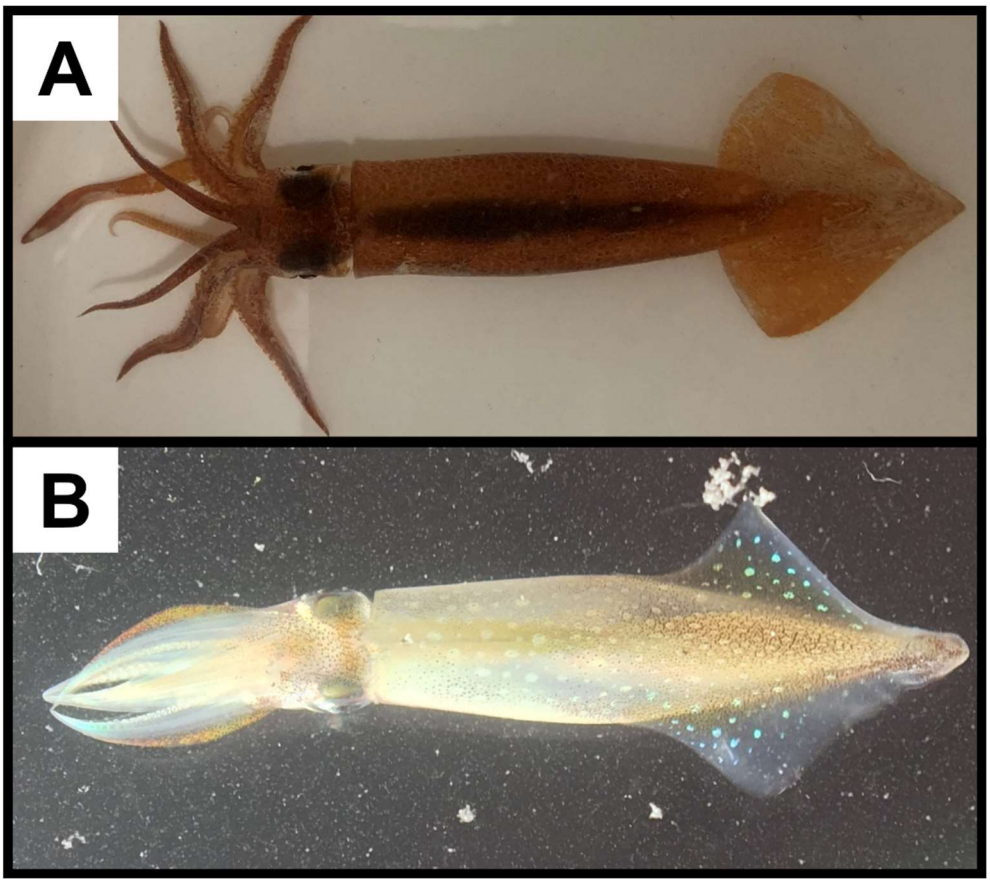

Fig 14. Photos of squids species studied. (A) *Illex illecebrosus*. (B) *Doryteuthis pealeii*. Both squids are oriented with arms on the left and tip of the mantle (tail) on the right. Not to scale.

Squids were recorded in ~1 min sessions (18,000 total frames) using IO industries DVR Express Core2 processor (London, ON, Canada). Squids swam freely in the experimental tank, turning spontaneously. To avoid collisions with tank walls, squids often switched swimming direction, i.e., arms-first to tail-first or vice versa. Each animal was recorded for no more than three hours at a time to avoid exhaustion. Squids were then returned to the holding tank after data collection.

4.2.3 Data analysis

Videoed turns by squids were identified as either arms-first (arms at the leading edge of the turn), or tail-first (posterior tip of the mantle at the leading edge of the turn). Sections of video were selected according to the following criteria: (1) the animal needed to be completely visible in both the dorsal view and one of the side views; (2) the animal needed to be away from tank walls; and (3) total angular displacement had to be >10 deg. Frame-by-frame body tracking was performed using DLTdv digitizing software for turns along the yaw axis (Hedrick 2008). The digitized points in the dorsal perspective included the (1) tail tip, (2) equidistant point between eyes, (3) forward most arm tip, (4) left side of the mantle (region of maximum amplitude), (5) right side of the mantle, (6) left fin tip, and (7) right fin tip (Fig. 2A). Digitized points in the lateral views included the (1) tail tip, (2) eye, (3) arm tip, (4) dorsal funnel edge, (5) ventral funnel edge, and (6) fin tip (Fig. 15B). Points were then smoothed with an in-house MATLAB routine using the Cross-Validation Criterion with a smoothing parameter within 0.1% (Walker, 1998). These tracked points were used to calculate the mean radius of the turn (R_{mean}), the minimum radius of the turn (R_{min}), maximum angular velocity during the turn (ω_{max}), mean angular velocity throughout the turn (ω_{mean}), degree of arm curling (measured by the vertical angular deviation from the mantle, θ_{arms}; Fig. 15C,D), and total angular displacement (θ_{total}).

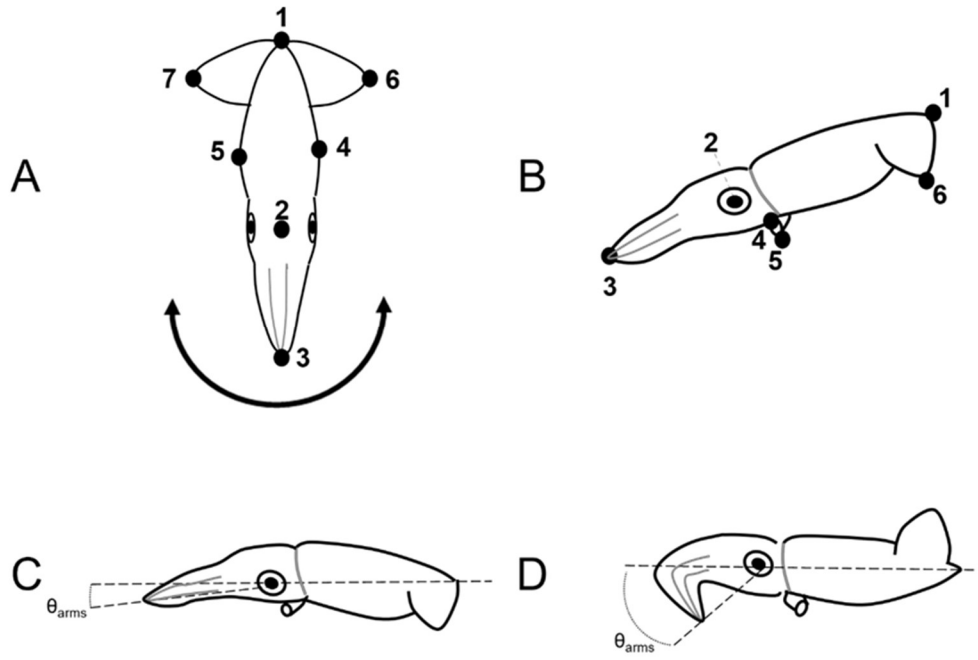

Fig 15. Illustration of points tracked for kinematic measurement in both dorsal and lateral views. (A) For dorsal views, (1) tail tip, (2) point equidistant between eyes, (3) arm tip, (4) left side of mantle (5) right side of mantle (6) left fin tip, (7) right fin tip were digitized. Turning in the yaw plane was measured as depicted with arrow. (B) For lateral views, (1) tail tip, (2) eye, (3) arm tip, (4) funnel edge closest to the body, (5) funnel edge away from body, and (6) fin tip were digitized. (C, D) Illustration of degree of arm curling (θ_{arms}) with a representative small θ_{arms} (C) and large θ_{arms} (D).

These calculations were done using a two-segment approach (one segment from tail tip to the center of the eyes, one segment from eye center to arm tips) similar to the one described in Jastrebsky et al. (2016). Center of Rotation (*COR*) was defined as the point in the dorsal view that moved the least during the turn, and *COR* is generalized in such a way that the points do not need to fall on the body segments themselves, but instead can fall on an angle with respect to those segments. The radius of the turn (*R*) was determined using:

$$(10)\ \frac{1}{R} = \frac{z''}{[1 + (z')^2]^{3/2}}$$

where $z' = dz/dx = \dot{z}/\dot{x}\,, z'' = d^2z/dx^2 = (\dot{x}\ddot{z} - \dot{z}\ddot{x})/\dot{x}^3$, x and z are the coordinates of the *COR* in the dorsal view, t is time, the over dot represents time differentiation, and the derivatives were evaluated using fourth-order accurate finite difference equations. To control for outliers and errors in tracking, the top 10% of values of angular velocity were removed before reporting ω_{max}; for *R*, the bottom 10% were removed to determine R_{min}. *R* values were then normalized by animal total length, and $(R/L)_{mean}$, the average of all *COR* radii comprising the turning path, and $(R/L)_{min}$, the lowest *R/L* after the bottom 10% of *R* were removed, were calculated. Data greater than four standard deviations from the mean were considered outliers and removed, resulting in 3 ω_{max} and 2 R_{min} data points (less than 5% of the data) being removed before analysis.

Fin beats for the inside and outside fins were identified visually (using both lateral and dorsal camera perspectives), with one full upstroke and downstroke constituting a fin beat. The "inside" fin was the fin closest to the center of the turn; the "outside" fin was the fin farthest from the center of the turn. Number of fin beats were then divided by the total time of the turn to determine F_{in} (frequency of inside fin), F_{out} (frequency of outside fin), and F_{ave} (mean of F_{in} and F_{out}). A paired t-test comparing the frequencies of F_{in} and F_{out} was insignificant ($T_{1,127}$=1.2675, p=0.2073), thus all statistics were performed on F_{ave}. Mantle contraction frequency (F_{mantle}) was

determined visually by counting the contractions of the funnel and dividing that by the time of the turn. Fin amplitude (A_{fin}) was calculated by dividing the maximum range of the fin beats during the turn (determined from lateral footage using either the inside or outside fin depending on which had greater amplitude) by the animal's length.

4.2.4 Statistical analysis

A two-way mixed model MANOVA was used to examine the effect of species and swimming direction on turning parameters (IBM SPSS v. 28.0.0.0). The turning parameters (dependent variables) were $(R/L)_{mean}$, $(R/L)_{min}$, ω_{max}, ω_{mean}, θ_{arms}, θ_{total}, F_{mantle}, F_{ave}, and A_{fin}. The Pillai–Bartlett statistic was used for determining significance, as recommended for unequal group sizes by Hand and Taylor (1987). $(R/L)_{mean}$, $(R/L)_{min}$, ω_{max}, and ω_{mean} data were Log_{10} transformed to meet assumptions of normality. θ_{total} was square root transformed, and θ_{arm} was cube root transformed to fit a normal distribution. F_{ave} was transformed to near normal values using the Tukey's Ladder transformation, with resulting lambda value of 0.95 (Tukey, 1977). ANOVAs were used following MANOVA significance to determine which variables were significant. Linear regressions were computed in R using untransformed data using an equation of $y \propto x$. Significance was defined at p-values ≤ 0.05.

4.3 RESULTS

A total of 128 turns (74 turns involving *Doryteuthis pealeii* and 54 turns with *Illex illecebrosus*) were analyzed for this study. Both species (MANOVA, $F_{9,116}=11.340$, $p<0.001$) and swimming direction (MANOVA, $F_{9,116}=2.682$, $p=0.007$) were significant. A species × swimming direction interaction approached significance and warranted further investigation

(MANOVA, $F_{9,116}$=1.987, p=0.074). The interaction derived from *I. illecebrosus* having greater θ_{arms} during arms-first turns than tail-first turns while *D. pealeii* showed no difference between swimming directions (Fig. 16). See Table 3 for a summary of statistical results.

4.3.1 Species comparison

Of the 74 turns recorded for *D. pealeii*, 47.44% were oriented arms-first, and 52.56% were oriented tail first (Fig. 17). Due to the fewer number of *I. illecebrosus* individuals, only 54 turns were analyzed. Of those, 50.91% were oriented arms-first, and 49.09% were oriented tail-first (Fig. 17). The total angular displacement for *D. pealeii* turns ranged from 11.08-142.98 deg, with an average displacement of 52.45±3.74 deg (mean±s.e.m reported). The angular displacement of *I. illecebrosus* ranged from 18.88-96.01 deg and averaged 52.02±2.50 deg.

The mean radius (R_{mean}) of all turns performed by *D. pealeii* was 2.73±0.14 cm, with a range of 0.78-8.50 cm, while the average minimum turning radius (R_{min}) was 0.16±0.017 cm with a minimum *R* across all turns of 0.017 cm. When the radii of the turns were standardized by the body length of the squids, average length specific turning radius of the turns [$(R/L)_{mean}$] was 0.16±0.009 and the average minimum length specific turning radius during turns [$(R/L)_{min}$] was 0.0097±0.0011. The mean radius (R_{mean}) for *I. illecebrosus* turns was 3.42±0.17 cm, with a range of 0.84-7.02 cm with a minimum *R* across all turns of 0.017 cm. When standardized for the length of the animal, $(R/L)_{mean}$ was 0.20±0.011, with a range of 0.05-0.44 for *I. illecebrosus*. $(R/L)_{min}$ during the turns was 0.012±0.0014.

Table 3. Statistical results from ANOVAs performed following significant MANOVA tests.

Asterisks denote significance.

Variable	Turning Metric	DF	F	P
Species	Average length specific turning radius [$(R/L)_{mean}$]	1,124	8.978	0.003**
	Minimum length specific turning radius [$(R/L)_{min}$]	1,124	5.207	0.024*
	Average angular velocity (ω_{ave})	1,124	7.562	0.007**
	Maximum angular velocity (ω_{max})	1,124	12.913	<0.001**
	Average fin flap frequency (F_{ave})	1,124	92.599	<0.001**
	Average fin flap amplitude (A_{fin})	1,124	3.891	0.051
	Average mantle contraction frequency (F_{mantle})	1,124	0.006	0.936
Swim Direction	Average length specific turning radius [$(R/L)_{mean}$]	1,124	5.730	0.018*
	Minimum length specific turning radius [$(R/L)_{min}$]	1,124	0.742	0.391
	Average angular velocity (ω_{ave})	1,124	0.189	0.664
	Maximum angular velocity (ω_{max})	1,124	0.639	0.426
	Average fin flap frequency (F_{ave})	1,124	0.001	0.980
	Average fin flap amplitude (A_{fin})	1,124	0.084	0.772
	Average mantle contraction frequency (F_{mantle})	1,124	0.299	0.585

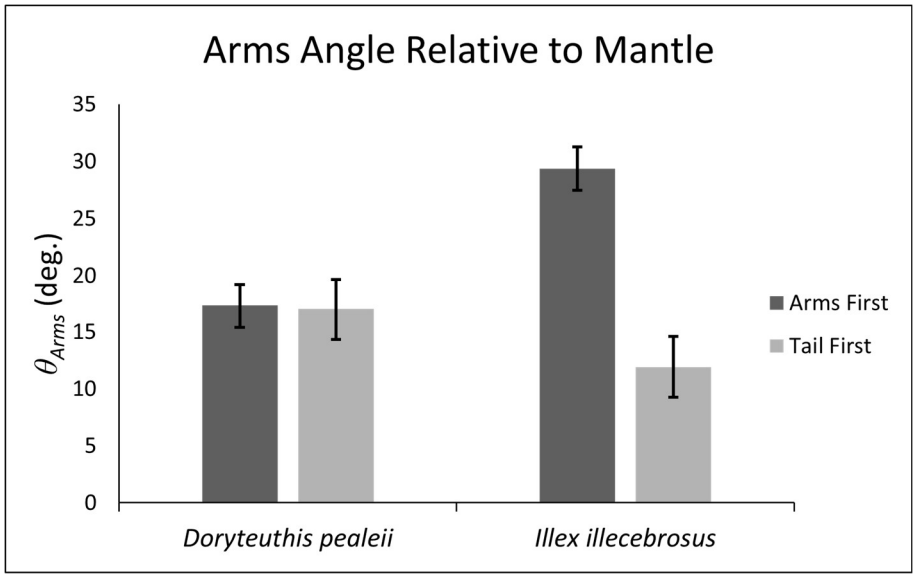

Fig 16. Arm curling (θ_{arms}) for *Illex illecebrosus* and *Doryteuthis pealeii* in the arms-first and tail-first swimming directions. Error bars shown are standard error of the mean.

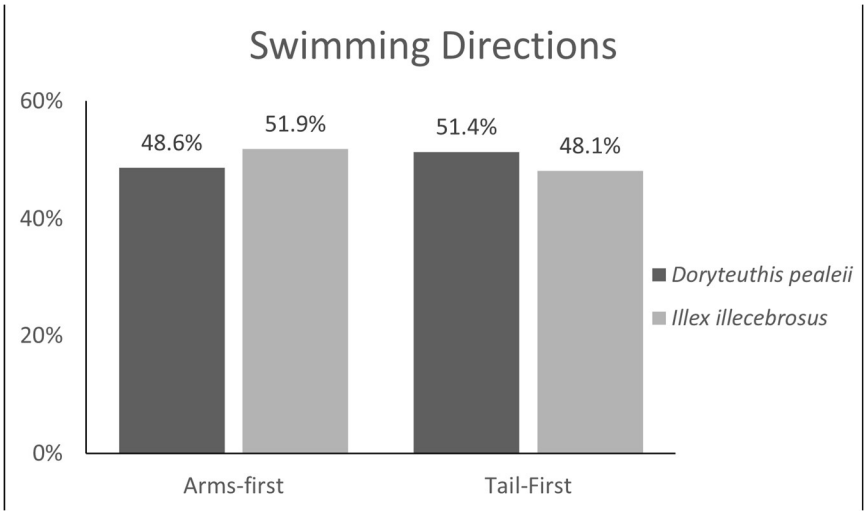

Fig 17. Demographics of swimming directions. Percentages of arms-first and tail-first swimming directions for *Doryteuthis pealeii* and *Illex illecebrosus.*

Both $(R/L)_{mean}$ (ANOVA, $F_{1,124}$=8.978, p=0.003) and $(R/L)_{min}$ ($F_{1,124}$=5.207, p=0.024) were significantly larger for *I. illecebrosus* than *D. pealeii* (Fig. 18A,B). *I. illecebrosus* achieved higher average angular velocity (ω_{ave}; ANOVA, $F_{1,124}$=7.562, p=0.007) and maximum angular velocity (ω_{max}; ANOVA, $F_{1,124}$=12.913, p<0.001) during turns than *D. pealeii* (Fig. 18C,D). The mean angular velocity for *I. illecebrosus* was 46.52±2.87 deg s^{-1} (range: 9.29-101.28 deg s^{-1}) and mean ω_{max} was 108.73±6.59 deg s^{-1}, with the highest ω_{max} = 255.66 deg s^{-1}. For *D. pealeii*, ω_{ave} was 37.66±2.61 deg s^{-1} (range: 6.97-110.07 deg s^{-1}) and mean ω_{max} was 82.36±5.50 deg s^{-1}, with the highest ω_{max} = 269.23 deg s^{-1}.

Doryteuthis pealeii demonstrated higher average fin flap frequency (F_{ave}) than *I. illecebrosus* (ANOVA, $F_{1,124}$=92.599, p<0.001). F_{ave} for *D. pealeii* and *I. illecebrosus* were 2.25±0.10 Hz and 0.79±0.11 Hz, respectively (Fig. 18E). There was also a near significant difference in average fin flap amplitude (A_{fin}) between species, with *D. pealeii* moving their fins over a larger relative area (A_{fin} = 0.179±0.006) than *I. illecebrosus* (A_{fin}= 0.16±0.007; Fig. 18F). There was no significant difference between species in average mantle contraction frequency (F_{mantle}; *D. pealeii* F_{mantle}= 1.75±0.10 Hz, *I. illecebrosus* F_{mantle} = 1.67±0.07 Hz). As mentioned earlier, there is a strong trend showing *I. illecebrosus* curled their arms to a greater degree during arms-first turning (θ_{arms}=29.36±4.09 deg) than during tail-first turning (θ_{arms}=11.93±1.93 deg). However, *D. pealeii* did not exhibit a difference between swimming directions (arms-first θ_{arms}=17.31±3.18 deg, tail-first θ_{arms}=17.00±2.78 deg).

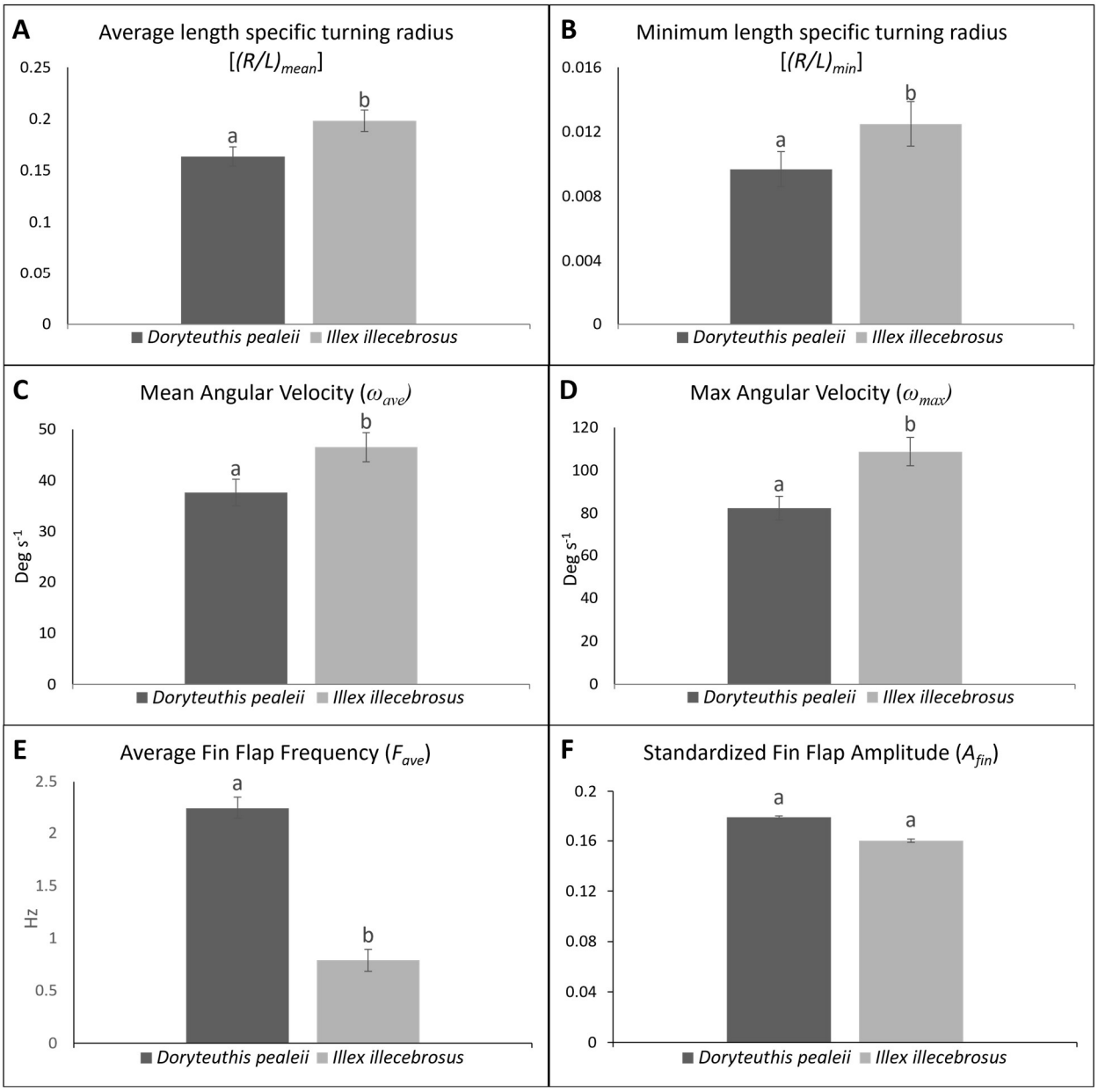

Fig 18. Kinematic measures for *Doryteuthis pealeii* and *Illex illecebrosus*. (A) Average length-specific turning radius $(R/L)_{mean}$, (B) minimum length-specific turning radius $(R/L)_{min}$, (C) average angular velocity (ω_{ave}), (D) maximum angular velocity (ω_{max}), (E) average fin flap frequency of both fins (F_{ave}), and (F) standardized fin flap amplitude (A_{fin}) for *D. pealeii* and *I. illecebrosus*. Different letters denote significant differences; error bars shown are standard error of the mean.

4.3.2 Swimming direction comparison

Arms-first turns had significantly lower $(R/L)_{mean}$ than tail-first, and a trend towards lower $(R/L)_{min}$ (Fig. 19A,B). For arms-first turns, $(R/L)_{mean}$ was 0.162±0.008 and $(R/L)_{min}$ was $9.81x10^{-3}$±$8.80x10^{-4}$. For tail-first turns, $(R/L)_{mean}$ was 0.194±0.012 and $(R/L)_{min}$ was $1.19x10^{-2}$ ±$1.48x10^{-3}$. Arms-first turns had an average ω_{ave} of 41.90±2.81 deg s^{-1}, and ω_{max} was 87.39±4.92 deg s^{-1}, with a range of 21.91-196.27 deg s^{-1}. ω_{ave} for tail-first turns was 40.90±2.78 deg s^{-1}, and ω_{max} was 99.58±7.16 deg s^{-1}, with a range from 15.01-269.23 deg s^{-1}. No significant difference in ω_{ave} or ω_{max} between the turning swimming directions was detected (Fig. 19C,D).

There was no significant difference in fin frequencies or amplitude between swimming directions; as well as no statistical difference in F_{mantle}. Squids turning arms-first had a A_{fin} = 0.172±0.006 (range = 0.072-0.313), F_{ave} = 1.63±0.14 Hz (range = 0-4.375 Hz), and F_{mantle} = 1.79±0.102 Hz (range =0.714-5 Hz). Squids turning tail-first had an A_{fin} = 0.170±0.007 (range = 0.001-0.300), F_{ave} = 1.63±0.134 Hz (range = 0-3.85 Hz), and F_{mantle} = 1.65± 0.08 Hz (range =0.8-5 Hz).

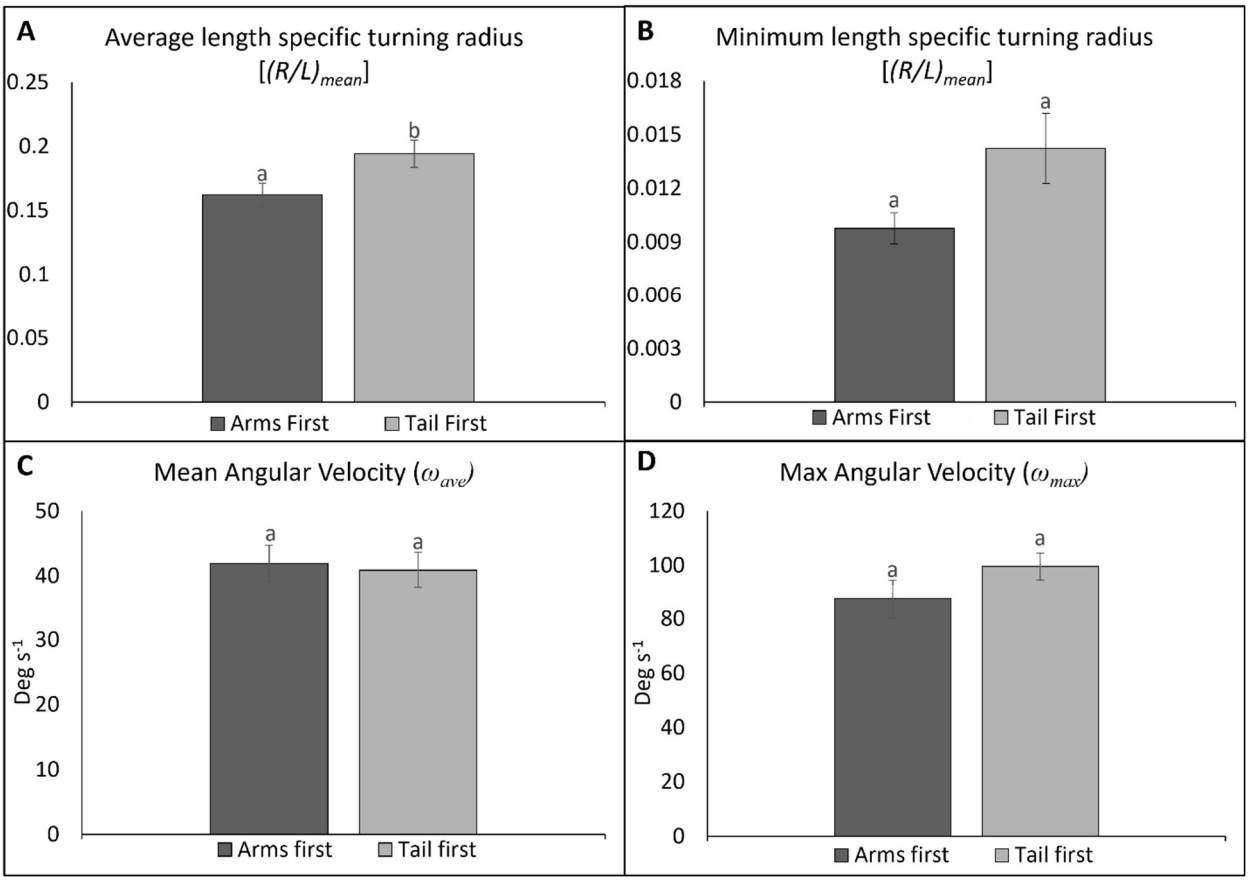

Fig 19. Analysis of kinematic measures by swimming direction. (A) Average length-specific turning radius $(R/L)_{mean}$, (B) minimum length-specific turning radius $(R/L)_{min}$, (C) average angular velocity (ω_{ave}), and (D) maximum angular velocity (ω_{max}) for arms-first oriented turns and tail-first oriented turns. Different letters denote significant differences; error bars shown are standard error of the mean.

4.3.3 Regressions

Linear regressions were computed using untransformed data. As average angular velocity increased, both average and minimum length specific turning radius increased (Fig 20A,B). Similarly, as maximum angular velocities increased, both average and minimum turning radius increased (Fig 20C,D). As the frequency of fin beats decreased, both average angular velocity and length-specific turning radius decreased, although the regressions did not explain a high proportion of the variability given the low R^2 values (Fig 21A,B). As the frequency of fin beats increased, fin beat amplitude also increased, and as the average amplitude of fin beats increased, average turning velocity decreased (Fig 21C,D). *Illex illecebrosus* showed a positive relationship between mantle contraction frequency and average angular velocity and a near significant positive trend between mantle contraction frequency and average length specific turning radius (Fig. 22A,B). *Doryteuthis pealeii* showed no such relationships (Fig. 22C,D).

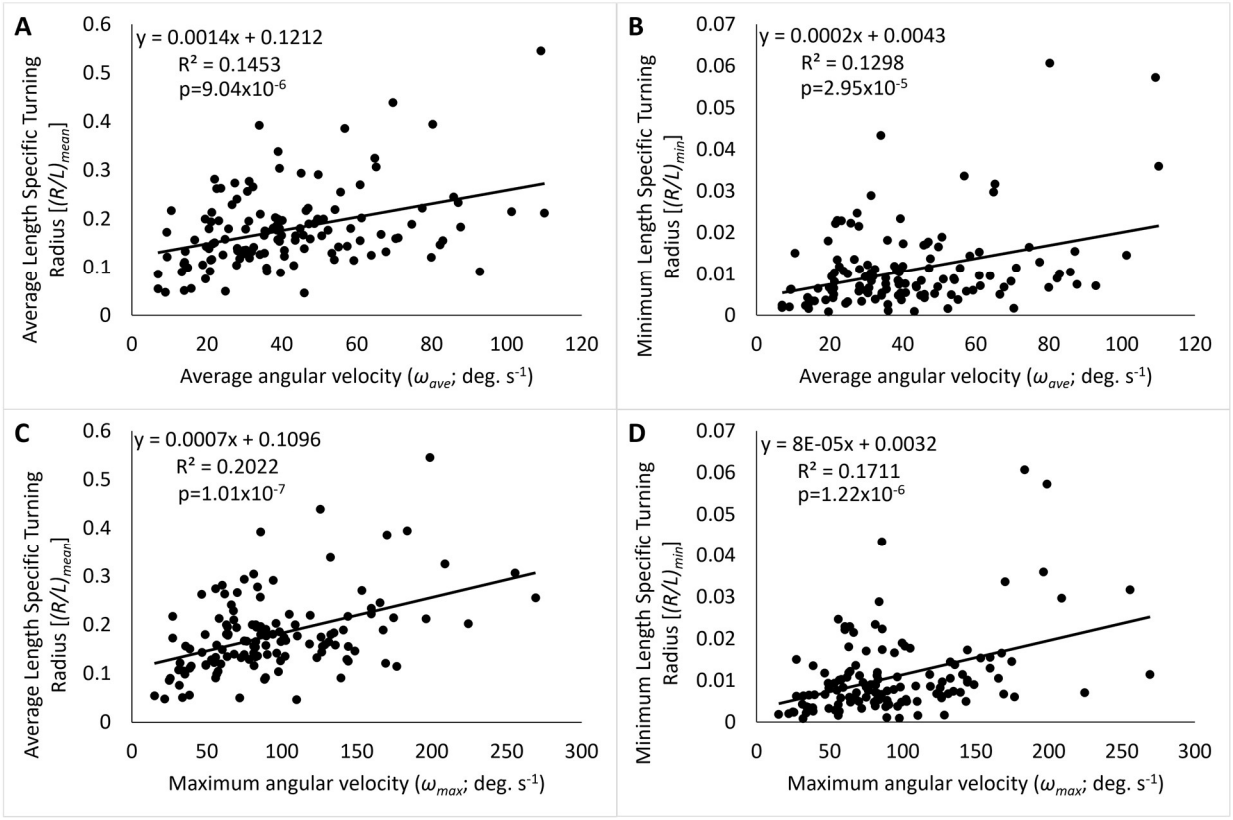

Fig 20: Linear regressions of kinematic measures of turning for *Doryteuthis pealeii* and *Illex illecebrosus*. (A) Average angular velocity (ω_{ave}) and average length specific turning radius [$(R/L)_{mean}$], (B) average angular velocity (ω_{ave}) and minimum length specific turning radius [$(R/L)_{min}$], (C) maximum angular velocity (ω_{max}) and average length specific turning radius [$(R/L)_{mean}$], and (D) maximum angular velocity (ω_{max}) and minimum length specific turning radius [$(R/L)_{min}$]. Regression equations, significance level, and coefficient of determination for each displayed in top left of plot.

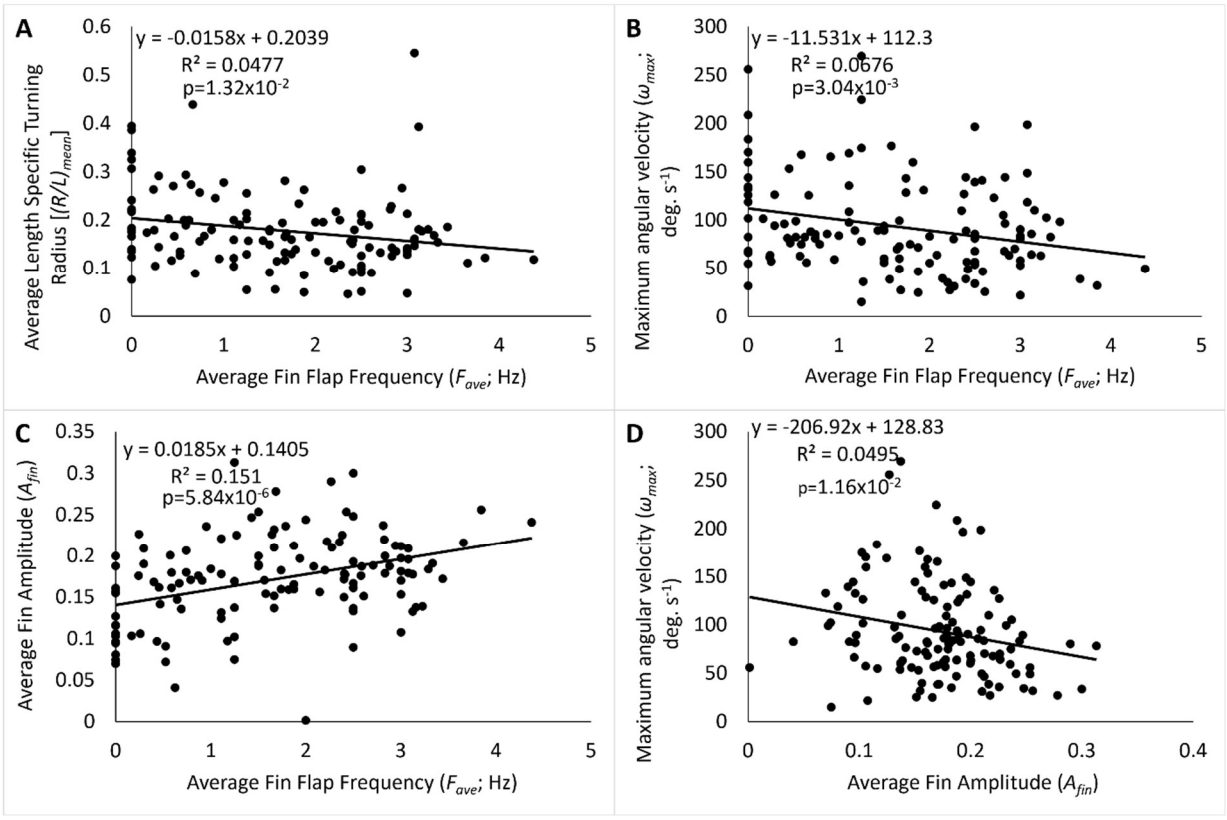

Fig 21. Linear regression analysis of fin movements and various kinematic measures for *Illex illecebrosus* and *Doryteuthis pealeii*. Mean frequency of fin flaps (F_{ave}) during turns and how it relates to (A) average length specific turning radius [$(R/L)_{mean}$], (B) maximum angular velocity during turning (ω_{max}), and (C) standardized fin flap amplitude (A_{fin}). (D) An increase in standardized fin flap amplitude (A_{fin}) relates to maximum angular velocity (ω_{max}). Regression equations, significance level, and coefficient of determination for each displayed in top left of plot.

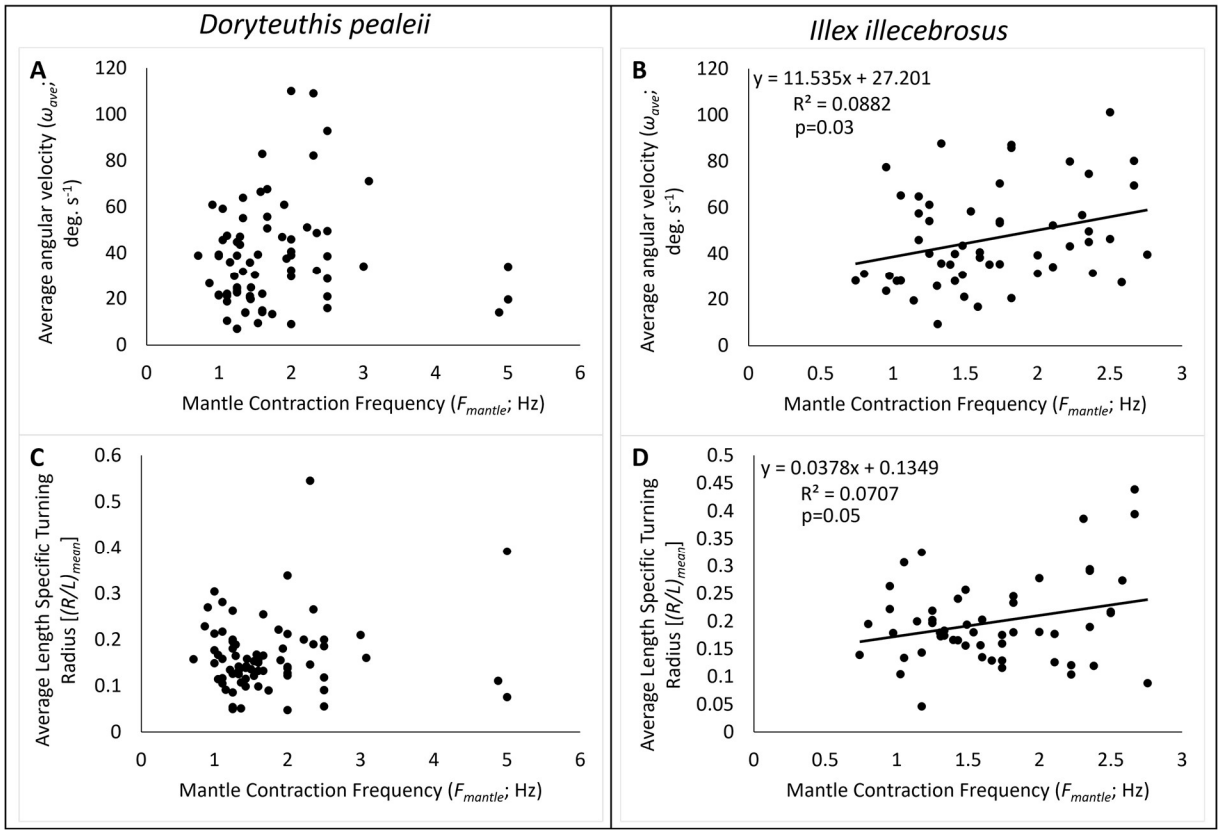

Fig 22: Linear regressions of mantle contraction frequency for *Doryteuthis pealeii* (A,C) **and *Illex illecebrosus*** (B,D). For *D. pealeii*, relationships between mean angular velocity (ω_{ave}) and mantle contraction frequency (F_{mantle}), (A) and average length specific turning radius [$(R/L)_{mean}$] and mantle contraction frequency (F_{mantle}), (C) were not significant. *For I. illecebrosus*, both average angular velocity (ω_{ave}), (B) and normalized mean radius of turns [$(R/L)_{mean}$], (D) had significant relationships with mantle contraction frequency. Regression equations, significance level, and coefficient of determination for each displayed in top left of plot.

4.4 DISCUSSION

Illex illecebrosus exhibited greater agility (faster turns) but less maneuverability (higher turning radii) than *Doryteuthis pealeii*. *Illex illecebrosus'* mean angular velocity was 20% greater than that recorded for *D. pealeii*, but *D. pealeii* achieved significantly lower $(R/L)_{mean}$ and $(R/L)_{min}$ (0.16 and 0.011, respectively) than *I. illecebrosus* (0.19 and 0.013). These differences may be due to disparities in how the arms, fins, and jet are used in the two species. While not significant, there was a strong trend demonstrating that *I. illecebrosus* curled its arms more when turning arms-first than tail-first, but *D. pealeii* showed no difference in arm angle between swimming directions. The high level of arm bending (~30 deg relative to mantle) by *I. illecebrosus* reduced the moment of inertia by bringing mass closer to the center of rotation (like ice skaters pulling arms in close to their bodies to spin faster), resulting in higher angular velocities. *Illex illecebrosus* also flapped its fins less often and with smaller amplitude than *D. pealeii*. In fact, *I. illecebrosus* rarely extended its fin movements beyond the width of the mantle (when viewed laterally), while *D. pealeii* extended its fins more significantly, nearly touching its fins together above and below the body. The increased use of fins during turning presumably aided *D. pealeii* in performing more controlled tighter turns than *I. illecebrosus*, as fin flows have been shown to contribute angular impulse along yaw, pitch, and roll axes (Bartol et al., 2022). In addition to greater fin activity to aid tight turning, fins that extend farther along the mantle, like those in *D. pealeii*, may allow for more control of turning (i.e., lower turning radii) due to greater interaction with the fluid medium (more surface area) and more complex fin movements, such as multiple undulatory waves that are difficult to produce with a shorter fin (Jereb and Roper, 2005; Jereb and Roper, 2010; Roper et al., 1984). Indeed, more undulatory fin movements in *D. pealeii* than *I. illecebrosus* were observed during maneuvers. Reduced fin use

requires greater reliance on the powerful jet, which should contribute to elevated angular velocities (Bartol et al., 2022). This hypothesis is supported by the observed positive relationship between mantle contraction frequency and average angular velocity for *I. illecebrosus* but not *D. pealeii.* Thus, in addition to increased arm curling, *I. illecebrosus'* heavy reliance on its jet likely contributed to its higher angular velocities.

A positive relationship between *R/L* and ω was also found, a pattern seen in other taxa (Fish and Nicastro, 2003; Walker, 2000). This relationship underscores the trade-off between tight and fast turning: as turn speed increases, the ability to complete tighter turns is compromised because inertia increases. Turns of high angular velocity are often driven by long, powerful jet pulses (Bartol et al., 2022), and in the present study, greater *R/L* was observed with higher jet frequency for *I. illecebrosus* In contrast, this study found that greater fin use (i.e., increased fin flap frequency and amplitude) tended to be more strongly related to slower and tighter turns. Due to muscle force limitations, fin use during rectilinear swimming generally decreases with speed, with the fins often curling along the body (O'Dor, 1988; Anderson and Grosenbaugh, 2005; Bartol et al., 2001a; Bartol et al., 2019; Stewart et al., 2010). However, during tight turning, where speed is of lower priority and fin power constraints are less problematic, fin use plays an important role both in effecting the turn and producing lift to counteract negative buoyancy (both *D. pealeii* and *I. illecebrosus* are negatively buoyant). Based on the results of this study, greater fin use facilitated slower but tighter (lower *R/L*) turns and greater jet frequency aided faster (higher ω; in *I. illecebrosus*) but broader turns, highlighting the trade-offs between *R/L* and ω.

For both species, swimming direction had a significant effect on kinematic measures of turning. Arms-first turns were tighter and showed a trend towards lower maximum angular

velocities. Bending of the funnel is a potential limiting factor for arms-first turning, as it requires greater shortening of radial muscles to prevent kinking/funnel constriction and ventral longitudinal muscles to maintain curvature (Bartol et al., 2016; Kier and Thompson, 2003). These muscle requirements can impart force restrictions on jet production, resulting in diminished angular velocities. Although muscle requirements associated with bending presumably limited angular velocity, they did not appear to reduce maneuverability given that tighter turns [lower $(R/L)_{mean}$ and $(R/L)_{min}$] were observed in the arms-first vs the tail-first swimming direction.

The arms-first swimming direction may confer advantages for tight turning, including improved visual perception, as the eyes are closer to the leading edge of the turn than during tail-first turning; improved steering, as forwardly positioned arms can bend in the direction of the turn; and better turn authority as posteriorly located fins can function as rudders. In addition, flow quantification has shown that inshore squids, such as *Lolliguncula brevis*, consistently produce shorter vortex ring flows in the arms-first mode relative to the tail-first mode (Bartol et al., 2016; Bartol et al., 2022). These short vortex rings provide more controlled impulse than longer jets, allowing for shorter turning radii.

From an ecological perspective, tight arms-first turns and fast tail-first turns follow expectations. During prey capture where the squids must orient arms-first to see and capture their target, minute corrections in heading are required to intercept fast moving prey. Therefore, the ability to turn tightly is advantageous for prey interactions, as noted by Jastrebsky et al. (2017), who measured the kinematics of turns by squids that were associated with the capture of shrimp and fish. Tight turns are also important for navigating complex habitats and mating. Often during mating, squids must orient arms-first to allow male squids to deposit a spermatophore into or

onto the female, located behind the arms (Arnold, 1962; Hanlon and Messenger, 1996; Hanlon et al., 1983). This complex behavior requires arms-first swimming from both individuals, as well as precise body positioning. Conversely, escaping from predators and swimming in a group are behaviors that require fast tail-first turning. High speeds and quick changes in direction are useful strategies for avoiding a predator. In addition, *D. pealeii* and *I. illecebrosus* often form schools and shoals (Hanlon et al., 2018). To maintain position in these collective groups, squids must make quick angular adjustments often at high speeds while swimming predominantly in the tail-first swimming direction.

In comparison to other jet-propelled swimmers, both *I. illecebrosus* and *D. pealeii* demonstrate intermediate *R/L* values (Table 4). The lower *R/L* values in Jastrebsky et al. (2017) may be a product of squids being enticed to turn with prey items, resulting in more extreme turns, while the turns in this study were spontaneous and perhaps more reflective of routine movements during non-feeding behavior. Although $(R/L)_{mean}$ for the squids in this study were similar to the common siphonophore, *N. bijuga,* the $(R/L)_{min}$ in this study was lower (Sutherland et al., 2019). This finding together with the lower $(R/L)_{min}$ reported for *S. bandensis* and *L. brevis* in prior studies suggest that cephalopods have the capacity to turn very tightly. The two squids considered in this study turned more slowly than other jet-propelled animals measured to date. This is likely a product of their larger size. For this study, *D. pealeii* and *I. illecebrosus* averaged approximately 16-17 cm in *L*, whereas *L. brevis* and *S. bandensis* averaged ~ 9 cm and 6 cm in *L*, respectively (Jastrebsky et al 2016), the common siphonophore, *N. bijuga*, averaged 1.6 cm in colony length (Sutherland et al 2019), and moon jelly, *A. aurita*, ranged from 1.8-5.4 cm in bell diameter (Dabiri et al 2020). Smaller animals generally have lower moments of inertia than larger animals because their mass is distributed closer to the axis of rotation, allowing them to

achieve higher angular velocities, a trend seen both within and between many other taxa (Fish and Holzman, 2019; Fish et al., 2018).

Compared to non-jetters, *I. illecebrosus* and *D. pealeii* are highly maneuverable. Relatively rigid yellowfin tuna (*Thunnus albacares*) have $(R/L)_{mean} \sim 0.2$, while the flexible California sea lion (*Zalophus californianus*) turns with an $(R/L)_{min} \sim 0.1$ (Blake et al., 1995; Fish et al., 2003). Bottlenose dolphins (*Tursiops truncatus*), angelfish (*Pterophyllum eimekei*), and painted turtle (*Chrysemys picta*) all have $(R/L)_{mean}$ more than double that of *I. illecebrosus* and *D. pealeii* (Blake et al., 1995; Maresh et al., 2004; Rivera et al., 2006). Conversely, only the leopard shark (*Triakis semifasciata*) and spotted boxfish (*Ostracion melegris*) have mean turning radii smaller than the squids examined in this paper (Porter et al., 2011; Walker, 2000). Therefore, the combination of a highly vectorable jet and muscular hydrostatic fins likely facilitates tight turning. Both *D. pealeii* and *I. illecebrosus* demonstrate an intermediate level of agility, turning faster than some fish and most rays. However, other fish and marine mammals can execute turns with nearly double the angular velocity (Domenici and Blake, 1991; Fish et al., 2018; Mayerl et al., 2019; Parson et al., 2011; Rivera et al., 2006). These higher values likely reflect differences in body flexibility, whereby squids have hybrid architectures with rigid (mantle with gladius) and flexible (fins and arms) components while the higher performing fishes and marine mammals have more flexible axial elements to facilitate elevated turning rates (Fish et al., 2018).

Table 4. Kinematic measurements from jet-propelled swimmers. AF refers to measurements of arms-first turns, and TF refers to measurements of tail-first turns. Asterisks refer to measurements that were calculated from data provided in paper.

Species	**$(R/L)_{mean}$**	**$(R/L)_{min}$**	**ω_{ave} (deg s^{-1})**	**ω_{max} (deg s^{-1})**	**θ_{arms} (deg)**	**Study**
*Aurelia aurita**	--	--	--	~400	--	Dabiri et al 2020
Doryteuthis pealeii	0.160	0.011	36.12	82.36	AF: 17.31 TF: 17.00	present study
Illex illecebrosus	0.190	0.015	48.19	108.73	AF: 29.36 TF: 11.93	present study
Illex illecebrosus	--	0.5	90	--	--	Foyle and O'Dor 1987
Lolliguncula brevis	0.009	0.0034	110.3	268.4	--	Jastrebsky et al 2016
Nanomia bijuga	0.150	0.05	104	215	--	Sutherland et al 2019b
Sepia bandensis	0.095	0.0012	54.8	160.2	--	Jastrebsky et al 2016
*Sepia officinalis**	--	--	~115	--	--	Messenger 1968

4.4.1 Concluding thoughts

This study represents the first comparative kinematic turning study of two inshore squids, the shortfin squid, *Illex illecebrosus,* and longfin squid, *Doryteuthis pealeii*. *Doryteuthis pealeii* was found to turn more tightly but more slowly than *I. illecebrosus.* High fin use likely contributed to *D. pealeii's* lower length-specific turning radii, while greater arm curvature, particularly in the arms-first mode, and greater reliance on the powerful jet probably were major factors in *I. illecebrosus'* higher angular velocities. Turning swimming direction (i.e., arms-first or tail-first) played a role in maneuverability and agility, with arms-first turns having significantly lower length-specific radii and tail-first turns exhibiting a trend in higher maximum angular velocity. Tighter turns in the arms-first mode are advantageous for tracking prey and navigating complex habitats, while faster turns in the tail-first mode are useful for escape responses and quick adjustments in schools and shoals. While *I. illecebrosus* and *D. pealeii* have moderate angular velocities, their length-specific turning radii minima are lower than other non-cephalopod swimmers.

CHAPTER 5

CONCLUSIONS

Proficient turning is integral for the ecological success of swimming animals, yet studies specifically addressing turning abilities are uncommon. Cephalopods are of particular interest for turning studies because of their integral role in food web dynamics as both prey and predators, unique propulsive mechanism involving a pulsed jet and oscillatory fins, distinct muscular hydrostatic systems with soft and hard elements, and broad ontogenetic range that spans Reynolds numbers of 1 to 10^8 (Bartol et al., 2008). With the goal of understanding turning in cuttlefishes and squids, three driving questions were explored for this dissertation: (1) what are the turning capabilities of hatchling cuttlefishes, and are there species-specific differences in turning performance during early ontogeny (Chapter 2); (2) how do adult cuttlefishes perform turns and how does adult performance compare with that of conspecific hatchlings (Chapter 3); and (3) how effective are adult neritic squids at turning (Chapter 4)?

In Chapter 2, turning kinematics and flow dynamics were examined in two species of cuttlefish hatchlings, the common cuttlefish *Sepia officinalis* and dwarf cuttlefish *Sepia bandensis*. Hatchlings turned arms-first and tail-first with equal proficiency, and both species turned with similar length-specific turning radii [$(R/L)_{mean} \sim 0.6 – 0.7$]. However, *Sepia officinalis* turned with greater angular velocity ($\omega_{ave} \sim 85$ deg s^{-1}, $\omega_{max} = 250$ deg s^{-1}) than *Sepia bandensis* ($\omega_{ave} \sim 38$ deg s^{-1}, $\omega_{max} = 89$ deg s^{-1}), producing higher jet velocities and impulses. These differences are consistent with their lifestyles, as *S. bandensis* is generally less active than *S. officinalis*, spending more time holding position and even burrowing in the substrate than swimming. Despite higher angular velocities, *S. officinalis* achieved turns of similar tightness to

S. bandensis, which was possible through the use of short, controlled, high-speed jets. *Sepia bandensis* used a similar strategy of frequent, short jets, but employed significantly lower jet velocities (U_{jave} ~ 6 mm s^{-1} vs 9 mm s^{-1} for *S. officinalis*). While both species relied heavily on short pulses that resulted in isolated vortex rings (*jet mode I*), *S. officinalis* had significantly shorter jets (L_ω/D_ω ~ 2.6) than *S. bandensis* (L_ω/D_ω ~ 4.1) with a greater reliance on *jet mode I* (81% vs 75%).

In chapter 3, adult *Sepia bandensis* were found to use similar strategies as hatchling cuttlefishes, relying predominantly on *jet mode I* and turning in both arms-first and tail-first orientations with equal proficiency. While significant variation in turning capabilities was observed, adult *S. bandensis* turned tightly [$(R/L)_{mean}$ ~ 0.14] and relatively slowly [ω_{ave} ~45 deg s^{-1}). These metrics for adult *S. bandensis* reflect higher performance than conspecific hatchlings, though *S. officinalis* hatchlings had higher ω, which was expected given smaller animals have lower moments of inertia than larger animals (Fish et al. 2018; Fish and Holzman 2019). The observed lower ω in hatchling *S. bandensis* could relate to less developed musculature or reduced neural control relative to adults. Jet properties were not consistent predictors of turn performance, as *S. bandensis* relied primarily on short vortex ring jets (L_ω/D_ω ~ 2.5) of moderate velocity (U_{jave} ~14 cm s^{-1}; U_{jmax}~ 22 cm s^{-1}) irrespective of turn type. Compared to other cephalopods, cuttlefishes turned using shorter jets with similar velocity profiles. These results are consistent with *S. bandensis'* residence in complex, benthic habitats, where tight, controlled turns facilitated by short jet pulses and high turning proficiency in either orientation are needed.

In chapter 4, kinematic turning performance of two neritic squids, the shortfin squid *Illex illecebrosus* and longfin squid *Doryteuthis pealeii* was assessed. *Illex illecebrosus* completed faster but broader turns [ω_{ave} ~ 47 deg s^{-1}, $(R/L)_{mean}$ ~ 0.20] than *D. pealeii* [ω_{ave} ~ 38

deg s^{-1}, $(R/L)_{mean}$ ~ 0.16]. *Doryteuthis pealeii* relied more heavily on its fins for turning, with higher fin flap frequencies and amplitudes than *I. illecebrosus*, which likely contributed to *D. pealeii's* lower $(R/L)_{mean}$. Greater arm curvature, particularly in the arms-first mode, and greater reliance on the powerful jet probably were major factors in *I. illecebrosus'* higher angular velocities. Turning orientation (i.e., arms-first or tail-first) played a role in maneuverability and agility, with arms-first turns having significantly lower *R/L* and tail-first turns exhibiting a trend in higher ω_{max}. When compared to the adult cuttlefish *S. bandensis*, adult squid *D. pealeii* and *I. illecebrosus* have similar angular velocities and turning radii, though *I. illecebrosus* turned a bit more broadly [$(R/L)_{mean}$ ~ 0.20 vs $(R/L)_{mean}$ ~ 0.14]. Broader turns in *I. illecebrosus* seem reasonable given it is negatively buoyant and swims at much higher cruising speeds than slower, neutrally buoyant *S. bandensis*, which spends considerable time navigating complex reef systems and making small-scale adjustments for crypsis or ambush hunting (Hanlon and Messenger, 1996; Staudinger et al., 2013). The presence of an orientation effect in squids but not cuttlefishes may also relate to lifestyle differences in the two groups. For squids, having a tail-first turning mode where angular velocity can be maximized through a high-powered jet is important for quick changes in heading during escape, high-speed cruising, vertical migrations, and schooling. Because cuttlefishes do not cruise at high speeds, undergo rapid vertical migrations, or school to the extent observed in squids, a high-powered tail-first mode is less critical. Rather, having the capacity to turn with equal proficiency in both orientations is better suited for blending into habitats and maneuvering in complex reef environments.

Collectively, the dissertation chapters above provide quantitative data on turning kinematics and jet flow dynamics of cuttlefishes and squids, filling important gaps in the understanding of turning performance. Specifically, this dissertation advances our understanding

of how turning changes through ontogeny in cuttlefishes- both in terms of kinematic performance metrics and vortex-wake jet flows- and enhances our understanding of turning performance in squids through consideration of two neritic species that have not been studied to date.

REFERENCES

Anderson, E. J. and DeMont, M. E. (2005). The locomotory function of the fins in the squid *Loligo pealei*. *Mar. Freshw. Behav. Physiol.* **38**, 169–189.

Anderson, E. J. and Grosenbaugh, M. A. (2005). Jet flow in steadily swimming adult squid. *J. Exp. Biol.* **208**, 1125–1146.

Arnold, J. M. (1962). Mating behavior and social structure in *Loligo pealii*. *Biol. Bull.* **123**, 53–57.

Bartol, I. K., Patterson, M. R. and Mann, R. (2001a). Swimming mechanics and behavior of the shallow-water brief squid *Lolliguncula brevis*. *J. Exp. Biol.* **204**, 3655–3682.

Bartol, I. K., Mann, R. and Patterson, M. R. (2001b). Aerobic respiratory costs of swimming in the negatively buoyant brief squid *Lolliguncula brevis*. *J. Exp. Biol.* **204**, 3639–3653.

Bartol, I. K., Gordon, M. S., Gharib, M., Hove, J. R., Webb, P. W. and Weihs, D. (2002). Flow patterns around the carapaces of rigid-bodied, multi-propulsor boxfishes (Teleostei: Ostraciidae). *Integr. Comp. Biol* **24**, 971–980.

Bartol, I. K., Krueger, P. S., Thompson, J. T. and Stewart, W. J. (2008). Swimming dynamics and propulsive efficiency of squids throughout ontogeny. *Integr. Comp. Biol.* **48**, 720–733.

Bartol, I. K., Krueger, P. S., Stewart, W. J. and Thompson, J. T. (2009a). Hydrodynamics of pulsed jetting in juvenile and adult brief squid *Lolliguncula brevis* : evidence of multiple jet 'modes' and their implications for propulsive efficiency. *J. Exp. Biol.* **212**, 1889–1903.

Bartol, I. K., Krueger, P. S., Stewart, W. J. and Thompson, J. T. (2009b). Pulsed jet dynamics of squid hatchlings at intermediate Reynolds numbers. *J. Exp. Biol.* **212**, 1506–1518.

Bartol, I. K., Krueger, P. S., Jastrebsky, R. A., Williams, S. and Thompson, J. T. (2016). Volumetric flow imaging reveals the importance of vortex ring formation in squid swimming tail-first and arms-first. *J. Exp. Biol.* **219**, 392–403.

Bartol, I. K., Krueger, P. S., York, C. A. and Thompson, J. T. (2019). Correction: New approaches for assessing squid fin motions: Coupling proper orthogonal decomposition with volumetric particle tracking velocimetry. *J. Exp. Biol.* **222**, 1–15.

Bartol, I. K., Ganley, A. M., Tumminelli, A. N., Krueger, P. S. and Thompson, J. T. (2022). Vectored jets power arms-first and tail-first turns differently in brief squid with assistance from fins and keeled arms. *J. Exp. Biol.* **225**, 1–15.

Bartol, I. K., Ganley, A. M., Tumminelli, A. N., Bartol, S. M., Thompson, J. T. and Krueger, P. S. (2023). Turning performance and wake dynamics of neritic squids. *Mar. Biol.* **170**, 1–16.

Bedore, C. N., Kajiura, S. M. and Johnsen, S. (2015). Freezing behaviour facilitates bioelectric crypsis in cuttlefish faced with predation risk. *Proc. R. Soc. B Biol. Sci.* **282**, 1–8.

Bettencourt, V. and Guerra, A. (2001). Age studies based on daily growth increments in statoliths and growth lamellae in cuttlebone of cultured *Sepia officinalis*. *Mar. Biol.* **139**, 327–334.

Black, G. A. P., Rowell, T. W. and Dave, E. G. (1987). *Atlas of the biology and distribution of the squids Illex illecebrosus and Loligo pealei in the Northwest Atlantic*. Canadian Special Publication of Fisheries & Aquatic Sciences.

Blake, R. W. and Chan, K. H. S. (2006). Models of the turning and fast-start swimming

dynamics of aquatic vertebrates. *J. Fish Biol.* **69**, 1824–1836.

Blake, R. W., Chatters, L. M. and Domenici, P. (1995). Turning radius of yellowfin tuna (*Thunnus albacares*) in unsteady swimming manoeuvres. *J. Fish Biol.* **46**, 536–538.

Blanchet, M. A., Lydersen, C., Ims, R. A. and Kovacs, K. M. (2016). Making it through the first year: Ontogeny of movement and diving behavior in harbor seals from Svalbard, Norway. *Mar. Mammal Sci.* **32**, 1340–1369.

Bloor, I. S. M., Wearmouth, V. J., Cotterell, S. P., McHugh, M. J., Humphries, N. E., Jackson, E. L., Attrill, M. J. and Sims, D. W. (2013). Movements and behaviour of European common cuttlefish *Sepia officinalis* in English channel inshore waters: First results from acoustic telemetry. *J. Exp. Mar. Bio. Ecol.* **448**, 19–27.

Boletzky, S. Von (1987). Fecundity variation in relation to intermittent or chronis spawning in the cuttlefish, *Sepia officinalis*. *Bull. Mar. Sci.* **40**, 382–388.

Boletzky, S. Von (2003). Biology of early life stages in cephalopod molluscs. *Adv. Mar. Biol.* **44**, 144–204.

Boucaud-Camou, E., Yim, M. and Tresgot, A. (1985). Feeding and digestion of young *Sepia officinalis* during post-hatching devolpment. *Vie Milieu* **35**, 263–266.

Bouchaud, O. (1991). Energy consuption of the cuttlefish *Sepia officinalis* during embryonic development. *Bull. Mar. Sci.* **49**, 333–340.

Boyle, P. R. (1996). Cephalopod populations: Definition and dynamics. *Philos. Trans. R. Soc. B Biol. Sci.* **351**, 985–1002.

Boyle, P. and Rodhouse, P. G. (2005). *Cephalopods: Ecology and Fisheries*. 1st ed. Blackwell Science, Ltd.

Brodziak, J. and Hendrickson, L. (1999). An analysis of environmental effects on survey catches of squids *Loligo pealei* and *Illex illecebrosus* in the northwest Atlantic. *Fish. Bull.* **97**, 9–24.

Budick, S. A. and O'Malley, D. M. (2000). Locomotor repertoire of the larval zebrafish: Swimming, turning and prey capture. *J. Exp. Biol.* **203**, 2565–2579.

Catano, L. B., Gunn, B. K., Kelley, M. C. and Burkepile, D. E. (2015). Predation risk, resource quality, and reef structural complexity shape territoriality in a coral reef herbivore. *PLoS One* **10**, 1–21.

Catano, L. B., Rojas, M. C., Malossi, R. J., Peters, J. R., Heithaus, M. R., Fourqurean, J. W. and Burkepile, D. E. (2016). Reefscapes of fear: Predation risk and reef hetero-geneity interact to shape herbivore foraging behaviour. *J. Anim. Ecol.* **85**, 146–156.

Clarke, M. R. (1962). Respiratory and swimming movements in the cephalopod *Cranchia scabra*. *Nature* **196**, 351–352.

Clarke, M. R., Denton, E. J. and Gilpin-Brown, J. B. (1979). On the use of ammonium for buoyancy in squids. *J. Mar. Biol. Assoc. United Kingdom* **59**, 259–276.

Coelho, M. L., Stobberup, K. A., O'Dor, R. K. and Dawe, E. G. (1994). Life history strategies of the squid, *Illex illecebrosus*, in the Northwest Atlantic. *Aquat. Living Resour.* **7**, 233–246.

Colin, S. P., Costello, J. H., Katija, K., Seymour, J. and Kiefer, K. (2013). Propulsion in Cubomedusae: Mechanisms and Utility. *PLoS One* **8**, 1–12.

Colin, S. P., Costello, J. H., Sutherland, K. R., Gemmell, B. J., Dabiri, J. O. and Du Clos, K. T. (2020). The role of suction thrust in the metachronal paddles of swimming invertebrates. *Sci. Rep.* **10**, 1–8.

Costello, J. H., Colin, S. P., Gemmell, B. J., Dabiri, J. O. and Sutherland, K. R. (2015). Multi-jet propulsion organized by clonal development in a colonial siphonophore. *Nat.*

Commun. **6**, 1–6.
Costello, J. H., Colin, S. P., Dabiri, J. O., Gemmell, B. J., Lucas, K. N. and Sutherland, K. R. (2021). The Hydrodynamics of Jellyfish Swimming. *Ann. Rev. Mar. Sci.* **13**, 375–396.
Coughlin, D. J. (2000). Power production during steady swimming in largemouth bass and rainbow trout. *J. Exp. Biol.* **203**, 617–629.
Coughlin, D. J. and Rome, L. C. (1996). The roles of pink and red muscle in powering steady swimming in scup, stenotomus chrysops. *Am. Zool.* **36**, 666–677.
Dabiri, J. O. (2009). Optimal vortex formation as a unifying principle in biological propulsion. *Annu. Rev. Fluid Mech.* **41**, 17–33.
Dabiri, J. O., Colin, S. P., Costello, J. H. and Gharib, M. (2005). Flow patterns generated by oblate medusan jellyfish: Field measurements and laboratory analyses. *J. Exp. Biol.* **208**, 1257–1265.
Dabiri, J. O., Colin, S. P. and Costello, J. H. (2007). Fluid dynamic constraints on morphology and propulsion of medusae at low Reynolds numbers. In *AGU Fall Meeting Abstracts*, pp. OS54A-04.
Dabiri, J. O., Colin, S. P., Gemmell, B. J., Lucas, K. N., Leftwich, M. C. and Costello, J. H. (2020). Jellyfish and Fish Solve the Challenges of Turning Dynamics Similarly to Achieve High Maneuverability. *Fluids* **5**, 1–13.
Daniel, T. L. (1983). Mechanics and energetics of medusan jet propulsion. *Can. J. Zool.* **61**, 1406–1420.
Daniel, T. L., Jordan, C. and Grunbaum, D. (1992). Hydromechanics of swimming. *Adv. Comp. Environ. Physiol.* **11**, 17–49.
Danos, N. and Lauder, G. V. (2007). The ontogeny of fin function during routine turns in zebrafish *Danio rerio*. *J. Exp. Biol.* **210**, 3374–3386.
Dawe, E. G., Beck, P. C., Drew, H. J. and Winters, G. H. (1981). Long-distance migration of a short-finned squid, *Illex illecebrosus*. *J. Northwest Atl. Fish. Sci.* **2**, 75–76.
Denton, E. J. and Gilpin-Brown, J. B. (1961a). The effect of light on the buoyancy of the cuttlefish. *J. Mar. Biol. Assoc. United Kingdom* **42**, 343–350.
Denton, E. J. and Gilpin-Brown, J. B. (1961b). The buoyancy of the cuttlefish. *J. Mar. biol Ass.* **41**, 319–342.
Dickel, L., Darmaillacq, A. S., Poirier, R., Agin, V., Bellanger, C. and Chichery, R. (2006). Behavioural and neural maturation in the cuttlefish *Sepia officinalis*. *Vie Milieu* **56**, 89–95.
Domenici, P. (2001). The scaling of locomotor performance in predator-prey encounters: From fish to killer whales. *Comp. Biochem. Physiol. - A Mol. Integr. Physiol.* **131**, 169–182.
Domenici, P. and Blake, R. W. (1991). The kinematics and performance of the escape response in the angelfish (*Pterophyllum eimekei*). *J. Exp. Biol.* **156**, 187–205.
Domenici, P. and Blake, R. W. (1997). The kinematics and performance of fish fast-start swimming. *J. Exp. Biol.* **200**, 1165–1178.
Domingues, P. M., Kingston, T., Sykes, A. and Andrade, J. P. (2001). Growth of young cuttlefish, *Sepia officinalis* (Linnaeus 1758) at the upper end of the biological distribution temperature range. *Aquac. Res.* **32**, 923–930.
Drucker, E. G. and Lauder, G. V. (2001a). Wake dynamics and fluid forces of turning maneuvers in sunfish. *J. Exp. Biol.* **204**, 431–442.
Drucker, E. G. and Lauder, G. V. (2001b). Locomotor function of the dorsal fin in teleost fishes: Experimental analysis of wake forces in sunfish. *J. Exp. Biol.* **204**, 2943–2958.
Ellerby, D. J., Spierts, I. L. Y. and Altringham, J. D. (2022). Slow muscle power output of

yellow- and silver-phase european eels (*Anguilla angulla* L.): changes in muscle performance prior to migration. *J. Exp. Biol.* **204,** 1369–1379.

Epps, B. P. and Techet, A. H. (2007). Impulse generated during unsteady maneuvering of swimming fish. *Exp. Fluids* **43**, 691–700.

Finke, E., Pörtner, H. O., Lee, P. G. and Webber, D. M. (1996). Squid (*Lolliguncula brevis*) life in shallow waters: Oxygen limitation of metabolism and swimming performance. *J. Exp. Biol.* **199**, 911–921.

Fish, F. E. (1993). Power output and propulsive efficiency of swimming Bottlenose dolphins (*Tursiops Truncatus*). *J. Exp. Biol.* **185**, 179–193.

Fish, F. E. (1996). Transitions from drag-based to lift-based propulsion in mammalian swimming. *Am. Zool.* **36**, 628–641.

Fish, F. E. (1998). Comparative kinematics and hydrodynamics of odontocete cetaceans: Morphological and ecological correlates with swimming performance. *J. Exp. Biol.* **201**, 2867–2877.

Fish, F. E. (1999). Performance constraints on the maneuverability of flexible and rigid biological systems. *Proc. Elev. Int. Symp. Unmanned Untethered Submers. Technol.* 394–406.

Fish, F. E. (2002). Balancing requirements for stability and maneuverability in cetaceans. *Integr. Comp. Biol.* **42**, 85–93.

Fish, F. E. and Holzman, R. (2019). Swimming turned on its head: Stability and maneuverability of the shrimpfish (*Aeoliscus punctulatus*). *Integr. Org. Biol.* **1**, 85–93.

Fish, F. E. and Hui, C. A. (1991). Dolphin swimming-a review. *Mamm. Rev.* **21**, 181–195.

Fish, F. E. and Nicastro, A. J. (2003). Aquatic turning performance by the whirligig beetle: Constraints on maneuverability by a rigid biological system. *J. Exp. Biol.* **206**, 1649–1656.

Fish, F. E. and Rohr, J. J. (1999). *Review of Dolphin Hydrodynamics and Swimming performance*. SPAWAR Systems Center San Diego, California.

Fish, F. E., Innes, S. and Ronald, K. (1988). Kinematics and estimated thrust production of swimming harp and ringed seals. *J. Exp. Biol.* **137**, 157–173.

Fish, F. E., Hurley, J. and Costa, D. P. (2003). Maneuverability by the sea lion *Zalophus californianus*: Turning performance of an unstable body design. *J. Exp. Biol.* **206**, 667–674.

Fish, F. E., Howle, L. E. and Murray, M. M. (2008). Hydrodynamic flow control in marine mammals. *Integr. Comp. Biol.* **48**, 788–800.

Fish, F. E., Kolpas, A., Crossett, A., Dudas, M. A., Moored, K. W. and Bart-Smith, H. (2018). Kinematics of swimming of the manta ray: Three-dimensional analysis of open-water maneuverability. *J. Exp. Biol.* **221**, 1–10.

Fountain, P. (1904). The swimming powers of animals. *Longman's Mag.* **43**, 326–332.

Foyle, T. P. and O'Dor, R. K. (1988). Predatory strategies of squid (*Illex illecebrosus*) attacking small and large fish. *Mar. Behav. Physiol.* **13**, 155–168.

Fuiman, L. A. and Webb, P. W. (1988). Ontogeny of routine swimming activity and performance in zebra danios (Teleostei: Cyprinidae). *Anim. Behav.* **36**, 250–261.

Ganley, A. M., Krueger, P. S. and Bartol, I. K. (2023). Faster is not always better: Turning performance trade-offs in the inshore squids *Doryteuthis pealeii* and *Illex illecebrosus*. *J. Exp. Mar. Bio. Ecol.* **565**, 1–11.

Gatto, C. R. and Reina, R. D. (2020). The ontogeny of sea turtle hatchling swimming performance. *Biol. J. Linn. Soc.* **131**, 172–182.

Gemmell, B. J., Troolin, D. R., Costello, J. H., Colin, S. P. and Satterlie, R. A. (2015).

Control of vortex rings for manoeuvrability. *J. R. Soc. Interface* **12**, 1–8.
Gemmell, B. J., Colin, S. P., Costello, J. H. and Sutherland, K. R. (2019). A ctenophore (comb jelly) employs vortex rebound dynamics and outperforms other gelatinous swimmers. *R. Soc. Open Sci.* **6**, 1–10.
Gharib, M., Rambod, E. and Shariff, K. (1998). A universal time scale for vortex ring formation. *J. Fluid Mech.* **360**, 121–140.
Gladman, N. W. and Askew, G. N. (2023). The hydrodynamics of jet propulsion swimming in hatchling and juvenile European common cuttlefish *Sepia officinalis*, Linnaeus (1758). *J. Exp. Biol.* **226**, 1–9.
Goff, ronan le and Daguzan, J. (1991). Growth and life cycles of the cuttlefish *Sepia officinalis* in Southern Brittany. *Bull. Mar. Sci.* **49**, 341–348.
Good, J. T., Kendrick, M. R., Podolsky, R. D., Whitaker, J. D. and Kingsley-Smith, P. R. (2023). Life history patterns of the Atlantic brief squid, *Lolliguncula brevis* (Blainville, 1823), in the Charleston Harbor Estuary, South Carolina, USA. *J. Shellfish Res.* **42**, 113–123.
Gray, J. (1933). Studies in animal locomotion. *J. Exp. Biol.* **10**, 88–104.
Guerra, A. (2006). Ecology of *Sepia officinalis*. *Vie Milieu* **56**, 97–107.
Hand, D. J. and Taylor, C. C. (1987). *Multivariate analysis of variance and repeated measures: a practical approach for behavioural scientists*. CRC press.
Hanlon, R. T. and Messenger, J. B. (1996). *Cephalopod Behaviour*. First. New York: Cambridge University Press.
Hanlon, R. T., Hixon, R. F. and Hulet, W. H. (1983). Survival, growth, and behavior of the loliginid squids *Loligo Plei, Loligo Pealei ,* and *Lolliguncula Brevis* (Mollusca: Cephalopoda) in closed sea water systems. *Biol. Bull.* **165**, 637–685.
Hanlon, R. T., Vecchione, M. and Allcock, L. (2018). *Octopus, Squid, and Cuttlefish*. Chicago, Il: Quarto Publishing.
Hedrick, T. L. (2008). Software techniques for two- and three-dimensional kinematic measurements of biological and biomimetic systems. *Bioinspiration and Biomimetics* **3**, 1–6.
Helmer, D., Geurten, B. R. H., Dehnhardt, G. and Hanke, F. D. (2017). Saccadic movement strategy in common cuttlefish (*Sepia officinalis*). *Front. Physiol.* **7**, 1–10.
Hendrickson, L. C. (2004). Population biology of northern shortfin squid (*Illex illecebrosus*) in the Northwest Atlantic Ocean and initial documentation of a spawning area. *ICES J. Mar. Sci.* **61**, 252–266.
Hoar, J. A., Sim, E., Webber, D. M. and O'Dor, R. K. (1994). The role of fins in the competition between squid and fish. *Mech. Physiol. Anim. Swim.*
Jastrebsky, R. A., Bartol, I. K. and Krueger, P. S. (2016). Turning performance in squid and cuttlefish: unique dual-mode, muscular hydrostatic systems. *J. Exp. Biol.* **219**, 1317–1326.
Jastrebsky, R. A., Bartol, I. K. and Krueger, P. S. (2017). Turning performance of brief squid *Lolliguncula brevis* during attacks on shrimp and fish. *J. Exp. Biol.* **220,** 908–919.
Jayne, B. C. and Lauder, G. V. (1995). Are muscle fibers within fish myotomes activated synchronously? Patterns of recruitment within deep myomeric musculature during swimming in largemouth bass. *J. Exp. Biol.* **198**, 805–815.
Jereb, P. and Roper, C. F. E. (2005). *An annotated and illustrated catalogue of species known to date*. Food and Agriculture Organization of the United Nations.
Jereb, P. and Roper, C. F. E. (2010). *Cephalopods of the world-an annotated and illustrated*

catalogue of cephalopod species known to date. Vol 2. Myopsid and oegopsid squids. Food and Agriculture Organization of the United Nations.

Johnsen, S. and Kier, W. M. (1993). Intramuscular crossed connective tissue fibres: skeletal support in the lateral fins of squid and cuttlefish (Mollusca: Cephalopoda). *Zool. Soc. London* **231**, 311–338.

Johnson, T. P., Syme, D. A., Jayne, B. C., Lauder, G. V and Bennett, A. F. (1994). Modeling red muscle power output during steady and unsteady swimming in largemouth bass. *Am. J. Physiol. Integr. Comp. Physiol.* **267**, R481–R488.

Jones, H. D. and Trueman, E. R. (1970). Locomotion of the limpet, *Patella Vulgata* L. *J. Exp. Biol.* **52**, 201–216.

Josef, N., Berenshtein, I., Fiorito, G., Sykes, A. V. and Shashar, N. (2015). Camouflage during movement in the European cuttlefish (*Sepia officinalis*). *J. Exp. Biol.* **218**, 3391–3398.

Katija, K., Colin, S. P., Costello, J. H. and Jiang, H. (2015). Ontogenetic propulsive transitions by *Sarsia tubulosa* medusae. *J. Exp. Biol.* **218**, 2333–2343.

Kier, W. M. (1982). The functional morphology of the musculature of squid arm and tentacles. *J. Morphol.* **172**, 179–192.

Kier, W. M. (1989). The fin musculature of cuttlefish and squid (Mollusca, Cephalopoda): morphology and mechanics. *Zool. Soc. London* **217**, 23–38.

Kier, W. M. and Thompson, J. T. (2003). Muscle arrangement, function and specialization in recent coleoids. *Berliner Paläobiologische Abhandlungen* **3**, 141–162.

Kier, W. M. and Van Leeuwen, J. L. (1997). A kinematic analysis of tentacle extension in the squid *Loligo pealei*. *J. Exp. Biol.* **200**, 41–53.

Kiorboe, T., Jiang, H., Goncalves, R. J., Nielsen, L. T. and Wadhwa, N. (2014). Flow disturbances generated by feeding and swimming zooplankton. *Proc. Natl. Acad. Sci.* **111**, 6–11.

Kobayashi, S., Takayama, C. and Ikeda, Y. (2013). Ontogeny of the brain in oval squid *Sepioteuthis lessoniana* (Cephalopoda: Loliginidae) during the post-hatching phase. *J. Mar. Biol. Assoc. United Kingdom* **93**, 1663–1671.

Krueger, P. S. (2001). The significance of vortex ring formation and nozzle exit over-pressure to pulsatile jet propulsion.

Krueger, P. S. and Gharib, M. (2003). The significance of vortex ring formation to the impulse and thrust of a starting jet. *Phys. Fluids* **15**, 1271–1281.

Lange, A. M. T. and Johnson, K. L. (1981). *Dorsal mantle length total weight relationships of squids Loligo pealei and Illex illecebrosus from the Atlantic coast of the USA*. National Oceanic and Atmospheric Administration, National Marine FIsheries Service.

Langridge, K. V. (2009). Cuttlefish use startle displays, but not against large predators. *Anim. Behav.* **77**, 847–856.

Lauder, G. V. and Drucker, E. G. (2002). Forces, fishes, and fluids: Hydrodynamic mechanisms of aquatic locomotion. *News Physiol. Sci.* **17**, 235–240.

Linden, P. F. and Turner, J. S. (2004). “Optimal” vortex rings and aquatic propulsion mechanisms. *Proc. R. Soc. B Biol. Sci.* **271**, 647–653.

Liu, Y. C., Liu, T. H., Su, C. H. and Chiao, C. C. (2017). Neural organization of the optic lobe changes steadily from late embryonic stage to adulthood in cuttlefish *Sepia pharaonis*. *Front. Physiol.* **8**, 1–16.

Lowe, C. G. (1996). Kinematics and critical swimming speed of juvenile scalloped hammerhead

sharks. *J. Exp. Biol.* **199**, 2605–2610.
Maciá, S., Robinson, M. P., Craze, P., Dalton, R. and Thomas, J. D. (2004). New observations on airborne jet propulsion (flight) in squid, with a review of previous reports. *J. Molluscan Stud.* **70**, 297–299.
Maresh, J. L., Fish, F. E., Nowacek, D. P., Nowacek, S. M. and Wells, R. S. (2004). High performance turning capabilities during foraging by bottlenose dolphins (*Tursiops truncatus*). *Mar. Mammal Sci.* **20**, 498–509.
Martínez, P. and Moltschaniwskyj, N. A. (1999). Description of growth in the tropical cuttlefish *Sepia elliptica* using muscle tissue. *J. Mar. Biol. Assoc. United Kingdom* **79**, 317–321.
Mayerl, C. J., Youngblood, J. P., Rivera, G., Vance, J. T. and Blob, R. W. (2019). Variation in morphology and kinematics underlies variation in swimming stability and turning performance in freshwater turtles. *Integr. Org. Biol.* **1**, 1–12.
McHenry, M. J. and Jed, J. (2003). The ontogenetic scaling of hydrodynamics and swimming performance in jellyfish (*Aurelia aurita*). *J. Exp. Biol.* **206**, 4125–4137.
Messenger, J. B. (1968). Visual attack of cuttlefish *Sepia officinalis*. *Anim. Behav.* **16**, 342–357.
Müller, U. K. and Lentink, D. (2004). Turning on a dime. *Science.* **306**, 1899–1900.
Müller, U. K., Stamhuis, E. J. and Videler, J. J. (2000). Hydrodynamics of unsteady fish swimming and the effects of body size: Comparing the flow fields of fish larvae and adults. *J. Exp. Biol.* **203**, 193–206.
Müller, U. K., Van Den Boogaart, J. G. M. and Van Leeuwen, J. L. (2008). Flow patterns of larval fish: Undulatory swimming in the intermediate flow regime. *J. Exp. Biol.* **211**, 196–205.
Muramatsu, K., Yamamoto, J., Abe, T., Sekiguchi, K., Hoshi, N. and Sakurai, Y. (2013). Oceanic squid do fly. *Mar. Biol.* **160**, 1171–1175.
Nesis, K. N. (1987). *Cephalopods of the World*. T. F. H. Publications.
Nicol, S. and O'Dor, R. K. (1985). Predatory behaviour of squid (*Illex illecebrosus*) feeding on surface swarms of euphausiids. *Can. J. Zool.* **63**, 15–17.
Nigmatullin, C. M. and Arkhipkin, A. I. (1998). A review of the biology of the Diamondback squid, *Thysanoteuthis rhombus* (Oegopsida: Thysanoteuthidae). *Contrib. Pap. to Int. Symp. Large Pelagic Squids.* 155–181.
Nitsche, M. (2006). Vortex Dynamics. In *Encyclopedia of Mathematical Physics: Five-Volume Set* (ed. François, J.-P., Naber, G. L., and Tsun, T. S.), pp. 390–399. Academic Press.
Nixon, M. (1985). Capture of prey, diet, and feeding of *Sepia Officinalis* and *Octopus vulgaris* from hatchling to adut. *Vie Milieu* **35**, 255–261.
Norberg, U. M. and Rayner, J. M. V. (1987). Ecological morphology and flight in bats (Mammalia; Chiroptera): Wing adaptations, flight performance, foraging strategy and echolocation. *Philos. Trans. R. Soc. London* **316**, 335–427.
Norman, M. (2003). *Cephalopods: A world guide*. 2nd ed. Hackenheim, Germany: ConchBooks.
O'Brien, C. E., Mezrai, N., Darmaillacq, A. S. and Dickel, L. (2017). Behavioral development in embryonic and early juvenile cuttlefish (*Sepia officinalis*). *Dev. Psychobiol.* **59**, 145–160.
O'Dor, R. K. (1988). The forces acting on swimming squid. *J. Exp. Biol.* **137**, 421–442.
O'Dor, R. K. (2002). Telemetered cephalopod energetics: Swimming, soaring, and blimping 1. *Integr. Comp. Biol.* **42**, 1065–1070.
O'Dor, R. K. (2013). How squid swim and fly. *Can. J. Zool.* **91**, 413–419.

O'Dor, R. K. and Webber, D. M. (1991). Invertebrate athletes: trade-offs between transport efficiency and power density in cephalopod evolution. *J Exp Biol.* **160**, 93–112.

O'Dor, R. K., Hoar, J. A., Webber, D. M., Carey, F. G., Tanaka, S., Martins, H. R. and Porteiro, F. M. (1995). Squid (*Loligo forbesi*) performance and metabolic rates in nature. *Mar. Freshw. Behav. Physiol.* **25**, 163–177.

O'Dor, R. K., Stewart, J., Gilly, W. F., Payne, J., Borges, T. C. and Thys, T. (2013). Squid rocket science: How squid launch into air. *Deep. Res. Part II Top. Stud. Oceanogr.* **95**, 113–118.

Palacios-Morales, C. and Zenit, R. (2013). Vortex ring formation for low Re numbers. *Acta Mech.* **224**, 383–397.

Parson, J. M., Fish, F. E. and Nicastro, A. J. (2011). Turning performance of batoids: Limitations of a rigid body. *J. Exp. Mar. Bio. Ecol.* **402**, 12–18.

Petie, R., Garm, A. and Nilsson, D. E. (2011). Visual control of steering in the box jellyfish *Tripedalia cystophora*. *J. Exp. Biol.* **214**, 2809–2815.

Porter, M. E., Roque, C. M. and Long, J. H. (2011). Swimming fundamentals: Turning performance of leopard sharks (*Triakis semifasciata*) is predicted by body shape and postural reconfiguration. *Zoology* **114**, 348–359.

Preuss, T., Lebaric, Z. N. and Gilly, W. F. (1997). Post-hatching development of circular mantle muscles in the squid *Loligo opalescens*. *Biol. Bull.* **192**, 375–387.

Rivera, G., Rivera, A. R. V., Dougherty, E. E. and Blob, R. W. (2006). Aquatic turning performance of painted turtles (*Chrysemys picta*) and functional consequences of a rigid body design. *J. Exp. Biol.* **209**, 4203–4213.

Rizzari, J. R., Frisch, A. J., Hoey, A. S. and McCormick, M. I. (2014). Not worth the risk: Apex predators suppress herbivory on coral reefs. *Oikos* **123**, 829–836.

Robin, J.-P., Roberts, M., Zeidberg, L., Bloor, I., Rodriguez, A., Briceño, F., Downey, N., Mascaró, M., Navarro, M., Guerra, A., et al. (2014). Transitions during cephalopod life history: The role of habitat, environment, functional morphology and behaviour. *Adv. Mar. Biol.* **67**, 361–437.

Robinson, L. (1893). Darwinism and swimming: A theory. *Ninet. century* **34**, 721–732.

Rome, L. C., Swank, D. and Corda, D. (1993). How fish power swimming. *Science.* **261**, 340–343.

Roper, C. F. E., Sweeney, M. J. and Nauen, C. (1984). *Cephalopods of the world. An annotated and illustrated catalogue of species of interest to fisheries*. Food and Agriculture Organization of the United Nations..

Russell, F. S. and Steven, G. A. (1930). The swimming of cuttlefish. *Nature* **125**, 893.

Saffman, P. G. (1995). *Vortex dynamics*. Cambridge university press.

Sanchez, G., Setiamarga, D. H. E., Tuanapaya, S., Tongtherm, K., Winkelmann, I. E., Schmidbaur, H., Umino, T., Albertin, C., Allcock, L., Perales-Raya, C., et al. (2018). Genus-level phylogeny of cephalopods using molecular markers: Current status and problematic areas. *PeerJ.* **2018**, 1–19.

Sfakiotakis, M., Lane, D. M. and Davies, J. B. C. (1999). Review of fish swimming modes for aquatic locomotion. *IEEE J. Ocean. Eng.* **24**, 237–252.

Shadwick, R. E. (1994). Animal structures at the marine interface. In *Biomaterials: Cellular Responses to Implanted Materials*, p. 37. Institute for Mechanics and Materials, University of California, San Diego.

Squires, H. J. (1967). Growth and hypothetical age of the Newfoundland bait squid *Illex*

illecebrosus. *J. Fish. Res. Board Canada* **24**, 1209–1217.

Stevens, L. M., Blob, R. W. and Mayerl, C. J. (2018). Ontogeny, morphology and performance: changes in swimming stability and turning performance in the freshwater pleurodire turtle, *Emydura subglobosa*. *Biol. J. Linn. Soc.* **125**, 718–729.

Stewart, W. J., Bartol, I. K. and Krueger, P. S. (2010). Hydrodynamic fin function of brief squid, *Lolliguncula brevis*. *J. Exp. Biol.* **213**, 2009–2024.

Stewart, J. S., Hazen, E. L., Foley, D. G., Bograd, S. J. and Gilly, W. F. (2012). Marine predator migration during range expansion: Humboldt squid *Dosidicus gigas* in the northern California Current System. *Mar. Ecol. Prog. Ser.* **471**, 135–150.

Sutherland, K. R., Gemmell, B. J., Colin, S. P. and Costello, J. H. (2019a). Maneuvering Performance in the Colonial Siphonophore, *Nanomia bijuga*. *Biominetics* **4**, 1–10.

Sutherland, K. R., Gemmell, B. J., Colin, S. P. and Costello, J. H. (2019b). Propulsive design principles in a multi-jet siphonophore. *J. Exp. Biol.* **222**, 1–8.

Thandiackal, R. and Lauder, G. V. (2020). How zebrafish turn: analysis of pressure force dynamics and mechanical work. *J. Exp. Biol.* **223**, 1–15.

Thompson, J. T. and Kier, W. M. (2001). Ontogeny of squid mantle function: Changes in the mechanics of escape-jet locomotion in the oval squid, *Sepioteuthis lessoniana* Lesson, 1830. *Biol. Bull.* **203**, 14–26.

Thompson, J. T. and Kier, W. M. (2006). Ontogeny of mantle musculature and implications for jet locomotion in oval squid *Sepioteuthis lessoniana*. *J. Exp. Biol.* **209**, 433–443.

Thompson, J. T., Bartol, I. K., Baksi, A. E., Li, K. Y. and Krueger, P. S. (2010). The ontogeny of muscle structure and locomotory function in the long-finned squid *Doryteuthis pealeii*. *J. Exp. Biol.* **213**, 1079–1091.

Tukey, J. W. (1977). *Exploratory data analysis*. Reading, MA: Addison-Wesley.

Vecchione, M. and Roper, C. F. E. (1991). Cephalopods observed from submersibles in the Western North Atlantic. *Bull. Mar. Sci.* **49**, 433–445.

Verrill, A. E. (1874). The giant cuttle-fishes of Newfoundland and the common squids of the New England coast. *Am. Nat.* **8**, 167–174.

Vidal, E. A. G., Zeidberg, L. D. and Buskey, E. J. (2018). Development of swimming abilities in squid paralarvae: Behavioral and ecological implications for dispersal. *Front. Physiol.* **9**, 1–17.

Villanueva, R., Vidal, E. A. G., Fernández-Álvarez, F. and Nabhitabhata, J. (2016). Early mode of life and hatchling size in cephalopod molluscs: Influence on the species distributional ranges. *PLoS One* **11**, 1–27.

Vogel, S. (2013). *Comparative Biomechanics: Life's Physical World*. Second. Princeton, New Jersey: Princeton University Press.

Walker, J. A. (1998). Estimating velocities and accelerations of animal locomotion: A simulation experiment comparing numerical differentiation algorithms. *J. Exp. Biol.* **201**, 981–995.

Walker, J. A. (2000). Does a rigid body limit maneuverability? *J. Exp. Biol.* **203**, 3391–3396.

Webb, P. W. (1994). The biology of fish swimming. *Mech. Physiol. Anim. Swim.* **4562**, 45–62.

Webb, P. W. and Fairchild, A. G. (2001). Performance and maneuverability of three species of teleostean fishes. *Can. J. Zool.* **79**, 1866–1877.

Webb, P. W. and Kostecki, P. T. (1984). The effect of size and swimming speed on locomotor kinematics of rainbow trout. *J. Exp. Biol.* **109**, 77–95.

Webber, D. M. and O'Dor, R. K. (1985). Respiration and swimming performance of short-

finned squid (*Illex illecebrosus*). *NAFO Sci. Coun. Stud.* **9**, 133–138.
Webber, D. M., Aitken, J. P. and O'Dor, R. K. (2000). Costs of locomotion and vertic dynamics of cephalopods and fish. *Physiol. Biochem. Zool.* **73**, 651–662.
Weihs, D. (1972). A hydrodynamical analysis of fish turning manoeuvres. *Proc. R. Soc. B Biol. Sci.* **182**, 59–72.
Wu, J.-Z., Ma, H.-Y. and Zhou, M.-D. (2007). *Vorticity and vortex dynamics*. Springer Science & Business Media.
Xu, Z., Lenaghan, S. C., Reese, B. E., Jia, X. and Zhang, M. (2012). Experimental studies and dynamics modeling analysis of the swimming and diving of Whirligig beetles (Coleoptera: Gyrinidae). *PLoS Comput. Biol.* **8**, 1–15.
Yagi, H. and Kawahara, M. (2005). Shape optimization of a body located in low Reynolds number flow. *Int. J. Numer. Methods Fluids* **48**, 819–833.
York, C. A., Bartol, I. K. and Krueger, P. S. (2016). Multiple sensory modalities used by squid in successful predator evasion throughout ontogeny. *J. Exp. Biol.* **219**, 2870–2879.
York, C. A., Bartol, I. K., Krueger, P. S. and Thompson, J. T. (2020). Squids use multiple escape jet patterns throughout ontogeny. *Biol. Open* **9**, 1–9.
Young, R. E. and Harman, R. F. (1988). "Larva," "paralarva" and "subadult" in cephalopod terminology. *Malacologia* **29**, 201–207.

VITA
Alissa Marie Ganley

Education

Old Dominion University; Norfolk, VA 23529; PhD Ecological Sciences; Expected May 2024
Dissertation title: Maneuverability of cuttlefish and squid: an integrated kinematic and hydrodynamic analysis
GPA: 4.0

University of California; Santa Cruz, CA 95064; B.S. Marine Biology; March 2016
GPA: 3.94; Dean's List; Summa cum laude

Presentations

Ganley, A.M, and I.K Bartol. 2023. Turning abilities of *Sepia officinalis* and *Sepia bandensis* hatchlings. Society for Integrative and Comparative Biology Conference, Austin, TX.

Ganley, A.M, and I.K Bartol. 2023. Kinematics of Turning Squid: *Doryteuthis pealeii* and *Illex illecebrosus*. Biology Graduate Student Organization Symposium, ODU, Norfolk, VA.
Fan favorite and runner up for best PhD Presentation.

Ganley, A.M, and I.K Bartol. 2022. Turning kinematics of inshore squid. Society for Integrative and Comparative Biology Conference, Virtual.

Ganley, A.M, and I.K Bartol. 2021. Maneuverability of hatchling *Sepia officinalis*. Society for Integrative and Comparative Biology Conference, Virtual.

Ganley, A.M, and I.K Bartol. 2019. Maneuverability of the common cuttlefish *Sepia officinalis* throughout ontogeny: an integrated kinematic/hydrodynamic analysis. Society for Integrative and Comparative Biology Conference, Tampa, FL.

Publications

Ganley, A.M., Krueger, P.S., and I.K. Bartol. (2023). Faster is not always better: Turning performance trade-offs in the inshore squids *Doryteuthis pealeii* and *Illex illecebrosus*. *Journal of Experimental Marine Biology and Ecology*. 29 May 2023; 565: 10.1016/j.jembe.2023.151913

Bartol, I.K., Ganley, A.M., Tumminelli, A.N., Bartol, S.M., Thompson, J.T., and Paul S. Krueger. (2023). Turning performance and wake dynamics of neritic squids. *Marine Biology*. 12 April 2023; 170 (73): 10.1007/s00227-023-04214-3.

Bartol, I.K., Ganley, A.M., Tumminelli, A.N., Krueger, P.S., and Joseph T. Thompson. (2022). Vectored jets power arms-first and tail-first turns differently in brief squid with assistance from fins and keeled arms. *Journal of Experimental Biology*. 1 August 2022; 225 (15): 10.1242/jeb.24415.